



UNIVERSIDAD DE INVESTIGACIÓN DE TECNOLOGÍA EXPERIMENTAL YACHAY

Escuela de Ciencias Químicas e Ingeniería

**TÍTULO: Synthesis and characterization of ferroelectric
KNN-based ceramics ($\text{K}_{0.5}\text{Na}_{0.5}\text{NbO}_3$)@Cu and
formation of thin films for applications in
photovoltaic cells and supercapacitors**

Trabajo de integración curricular presentado como requisito para
la obtención
del título de Química

Autor:

Estrella Nuñez Jocelyne

Tutor:

PhD. Ávila Sosa Edward

Cotutor:

PhD. Yáñez Limón Martín

Urcuquí, mayo 2020

Urcuquí, 8 de mayo de 2020

SECRETARÍA GENERAL
(Vicerrectorado Académico/Cancillería)
ESCUELA DE CIENCIAS QUÍMICAS E INGENIERÍA
CARRERA DE QUÍMICA
ACTA DE DEFENSA No. UITEY-CHE-2020-00030-AD

A los 8 días del mes de mayo de 2020, a las 16:00 horas, de manera virtual mediante videoconferencia, y ante el Tribunal Calificador, integrado por los docentes:

Presidente Tribunal de Defensa	Dra. GONZALEZ VAZQUEZ, GEMA , Ph.D.
Miembro No Tutor	Dr. TERCICIO THIBAUT , Ph.D.
Tutor	Dr. AVILA SOSA, EDWARD EBNER , Ph.D.

El(la) señor(ita) estudiante **ESTRELLA NUÑEZ, JOCELYNE MARISSA**, con cédula de identidad No. **1723070957**, de la **ESCUELA DE CIENCIAS QUÍMICAS E INGENIERÍA**, de la Carrera de **QUÍMICA**, aprobada por el Consejo de Educación Superior (CES), mediante Resolución **RPC-SO-39-No.456-2014**, realiza a través de videoconferencia, la sustentación de su trabajo de titulación denominado: **Synthesis and characterization of ferroelectric KNN-based ceramics (K0.5Na0.5Nb3)@Cu and formation of thin films for applications in photovoltaic cells and supercapacitor**, previa a la obtención del título de **QUÍMICO/A**.

El citado trabajo de titulación, fue debidamente aprobado por el(los) docente(s):

Tutor	Dr. AVILA SOSA, EDWARD EBNER , Ph.D.
--------------	--------------------------------------

Y recibió las observaciones de los otros miembros del Tribunal Calificador, las mismas que han sido incorporadas por el(la) estudiante.

Previamente cumplidos los requisitos legales y reglamentarios, el trabajo de titulación fue sustentado por el(la) estudiante y examinado por los miembros del Tribunal Calificador. Escuchada la sustentación del trabajo de titulación a través de videoconferencia, que integró la exposición de el(la) estudiante sobre el contenido de la misma y las preguntas formuladas por los miembros del Tribunal, se califica la sustentación del trabajo de titulación con las siguientes calificaciones:

Tipo	Docente	Calificación
Presidente Tribunal De Defensa	Dra. GONZALEZ VAZQUEZ, GEMA , Ph.D.	9,0
Miembro Tribunal De Defensa	Dr. TERCICIO THIBAUT , Ph.D.	10,0
Tutor	Dr. AVILA SOSA, EDWARD EBNER , Ph.D.	10,0

Lo que da un promedio de: **9.7 (Nueve punto Siete)**, sobre 10 (diez), equivalente a: **APROBADO**

Para constancia de lo actuado, firman los miembros del Tribunal Calificador, el/la estudiante y el/la secretario ad-hoc.

Certifico que *en cumplimiento del Decreto Ejecutivo 1017 de 16 de marzo de 2020, la defensa de trabajo de titulación (o examen de grado modalidad teórico práctica) se realizó vía virtual, por lo que las firmas de los miembros del Tribunal de Defensa de Grado, constan en forma digital.*



ESTRELLA NUÑEZ, JOCELYNE MARISSA
Estudiante

Dra. GONZALEZ VAZQUEZ, GEMA , Ph.D.
Presidente Tribunal de Defensa



Firmado electrónicamente por:
GEMA
GONZALEZ

EDWARD EBNER AVILA SOSA
Firmado digitalmente por
EDWARD EBNER AVILA SOSA
Fecha: 2020.05.08 17:11:57
-05'00'

Dr. AVILA SOSA, EDWARD EBNER , Ph.D.

Tutor
**THIBAUT
TERENCIO**

Firmado digitalmente por THIBAUT TERENCIO
DN: cn=THIBAUT TERENCIO c=EC hg=QUITO
o=BANCO CENTRAL DEL ECUADOR
ou=ENTIDAD DE CERTIFICACION DE
INFORMACION-ECIBCE
Módulo: SCS y el submódulo de este documento
Ubicación: Yachay Tech
Fecha: 2020-05-08 17:17:05:00

Dr. TERENCIO THIBAUT , Ph.D.

Miembro No Tutor



Firmado electrónicamente por:

**ANA MARIA
ESCOBAR
LANDAZURI**

ESCOBAR LANDAZURI, ANA MARIA
Secretario Ad-hoc

AUTORÍA

Yo, **JOCELYNE MARISSA ESTRELLA NUÑEZ**, con cédula de identidad 1723070957, declaro que las ideas, juicios, valoraciones, interpretaciones, consultas bibliográficas, definiciones y conceptualizaciones expuestas en el presente trabajo; así cómo, los procedimientos y herramientas utilizadas en la investigación, son de absoluta responsabilidad de el/la autora (a) del trabajo de integración curricular. Así mismo, me acojo a los reglamentos internos de la Universidad de Investigación de Tecnología Experimental Yachay.

Urcuquí, julio del 2020.



Jocelyne Marissa Estrella Nuñez
CI: 1723070957

AUTORIZACIÓN DE PUBLICACIÓN

Yo, **JOCELYNE MARISSA ESTRELLA NUÑEZ**, con cédula de identidad 1723070957, cedo a la Universidad de Investigación de Tecnología Experimental Yachay, los derechos de publicación de la presente obra, sin que deba haber un reconocimiento económico por este concepto. Declaro además que el texto del presente trabajo de titulación no podrá ser cedido a ninguna empresa editorial para su publicación u otros fines, sin contar previamente con la autorización escrita de la Universidad.

Asimismo, autorizo a la Universidad que realice la digitalización y publicación de este trabajo de integración curricular en el repositorio virtual, de conformidad a lo dispuesto en el Art. 144 de la Ley Orgánica de Educación Superior

Urcuquí, Julio del 2020.



Jocelyne Marissa Estrella Nuñez
CI: 1723070957

This research work I would like to dedicate to my parents, and my sister, because I have come to where I am thanks to them and because every triumph of mine is theirs. To Wilmita, for being like a second mother and giving me infinite love. And finally, to Marquito, because from heaven, you live in every memory and in the heart.

Jocelyne Marissa Estrella Nuñwz

Acknowledgements

To God for being my guide, for giving me strength in every step I have taken and for being my refuge at all times.

Thanks to my University Yachay Tech, because I am so proud of be part of this institution, which has allowed me to prepare myself professionally and humanely..

To CINVESTAV, Querétaro for giving me the opportunity to have a research experience with a great research group and make it possible my thesis work.

To my parents, Yoli and Milton, for forming a home full of love and values. For being a great example of perseverance and humility. Thank you for your unconditional support, for urging me to follow my dreams. To May, my sister, who has always been my example, for being my accomplice and friend.

To my second home, Wilmita, Marquito, Marisita, Marc, Gabby, and Evy, thank you because despite the distance, they have been a fundamental pillar in my life.

To my tutor, Dr. Martín Yáñez, thank you for receiving me in your group and allowing me to have my first research experience, for sharing your knowledge with me and for your commitment to your thesis students and research group.

To Karla Moya, for giving me the opportunity to participate in a research environment and live one of the most beautiful experiences.

To my PhD tutor. Edward Ávila, who has dedicated his time and readiness to enrich my research work.

To Osmany García and Chuy, thanks for getting involved and contributing to my research work. Also, for sharing their teachings and challenges. I am very grateful because it has motivated me to continue in this branch of research.

To my family, thank you for always being aware of me, for giving me your love and being a constant support in my life. Thank you for your life teachings, for sharing so many moments of joy and for every word of sincere love.

To my friends from school, because they have been part of the best stage and because they do not need to be constantly seen to know that they are always there for me.

To Iri, Sofi, and Lore, my roommates, friends, sisters, confidants. Thank you for your support, for sharing countless moments and especially for your true friendship.

To my friends at the university, who became a family. To my dear 26, Norto, Mois, Bryan, Jorgito, Papo, Paul, Jonathan, and Chichi. To my dear 19, Paco, Rafa, JD, and Willa. Thank you because you have become brothers for me, thanks for being my confidants, companions both in moments of joy and sadness. Thank you for making my university life one of the most beautiful experiences and because I know they are something constant in my life.

I have to say thanks to Jorge Cárdenas because he has been my best friend during all the career. Thank you for being my partner during this adventure called university.

To my friends in Mexico, for welcoming me and making me feel at home. Thank you for being part of new adventures, for showing me your culture and warmth.

Abstract

Este proyecto estudió la ferroelectricidad de muestras a granel y películas delgadas de $K_{0.5}Na_{0.5}NbO_3$ y el efecto del dopaje con cobre (0.5 y 1 mol%). La síntesis de muestras a granel se realizó por el método cerámico convencional, calcinación, prensado uniaxial y sinterizado a diferentes condiciones. En DRX se observó estructuras perovskitas desde la fase de polvos calcinados. Micrografías SEM de muestras sinterizadas muestran regiones con un tamaño de grano entre 1-2 μ m. A través de curvas de histéresis se observó un comportamiento ferroeléctrico en el KNN puro y KNNCu1%mol, en contraste el KNNCu0.5%mol mostró una fase antiferroeléctrica. Utilizando la espectroscopía de impedancia en función de temperatura, fue posible determinar las temperaturas de transición de las fases ortorrómbico-tetragonal, tetragonal-cúbico y la temperatura de Curie. Para la obtención de películas delgadas, se hicieron blancos de KNN, KNNCu0.5%mol y KNNCu1%mol, siguiendo el mismo proceso de muestras a granel con ciertas modificaciones. Los blancos obtenidos se usaron para el crecimiento de películas delgadas por erosión catódica bajo diferentes condiciones de tiempo, potencia, y sustrato. Se probaron diferentes tratamientos térmicos y se caracterizaron por XRD, histéresis y corriente-voltaje.

PALABRAS CLAVE Cerámicos, Ferroelectricidad, Antiferroelectricidad, Granel, Películas delgadas.

Abstract

This project studied the ferroelectricity of $K_{0.5}Na_{0.5}NbO_3$ bulk samples and thin films and the effect of doping with copper (0.5 and 1 mol%). The synthesis of bulk samples was carried out by the conventional ceramic method, calcination, uniaxial pressing and sintering under different conditions. Perovskite structures were observed in DRX from the calcined powder phase. SEM micrographs of sintered samples show regions with a grain size between 1-2 μ m. Through hysteresis curves, a ferroelectric behavior was observed in the pure KNN and KNNCu1%mol, in contrast, the KNNCu0.5%mol showed an antiferroelectric phase. Using impedance spectroscopy as a function of temperature, it was possible to determine the transition temperatures of the orthorhombic-tetragonal, tetragonal-cubic phases and the Curie temperature. To obtain thin films, KNN, KNNCu0.5%mol and KNNCu1%mol targets were made, following the same process of bulk samples with certain modifications. The targets obtained were used for the growth of thin films by cathodic erosion under different conditions of time, power, and substrate. Different heat treatments were tested and characterized by XRD, hysteresis, and current-voltage.

KEYWORDS

Ceramics, Ferroelectricity, Antiferroelectricity, Bulk, Thin films.

CONTENTS

Contents	vi
List of Figures	viii
1 Introduction	1
1.1 Ferroelectricity	1
1.1.1 Symmetry structure	1
1.2 Polarization	3
1.2.1 Hysteresis loops	8
1.2.2 Electrical Properties	12
1.3 Application of ferroelectric materials	13
2 Conclusion	15
2.1 Recommendations	16

A Crystallite size FWHM estimation figures	18
A.1 KNN, KNNCu0.5%mol, and KNNCu1%mol sintered for 1 hour at 1100°C - Encapsulated	18
A.2 KNN, KNNCu0.5%mol, and KNNCu1%mol sintered for 3 hours at 1100°C - Encapsulated	19
A.3 KNN, KNNCu0.5%mol, and KNNCu1%mol sintered for 4 hours at 1100°C - Without encapsulation	20
B Crystallite Size Plots	21
B.1 KNN Sintered 1 hour at 1100°C - Encapsulated	21
B.2 KNNCu0.5%mol Sintered 1 hour at 1100°C - Encapsulated	22
B.3 KNNCu1%mol Sintered 1 hour at 1100°C - Encapsulated	22
B.4 KNN Sintered 3 hours at 1100°C - Encapsulated	23
B.5 KNNCu0.5%mol Sintered 3 hours at 1100°C - Encapsulated	23
B.6 KNNCu1%mol Sintered 3 hours at 1100°C - Encapsulated	24
B.7 KNN Sintered 4 hours at 1100°C - Without encapsulation	24
B.8 KNNCu0.5%mol Sintered 4 hours at 1100°C - Without encapsulation	25
B.9 KNNCu1%mol Sintered 4 hours at 1100°C - Without encapsulation	25
Bibliography	26

LIST OF FIGURES

1.1	Perovskite structure ABO_3 Ref. [1]	2
1.2	Flow chart of the classification of point groups according its ferroelectric properties BT(Barium titanate), PZT(Lead zirconate titanate), PT(Lead titanate), PLZT(Lead lanthanum zirconate titanate), PMN(Lead magnesium titanate), and KNN(Potassium sodium) [2].	3
1.3	Domain structure after and before of an applied external field.	4
1.4	Dielectric constant vs Temperature showing phase transitions: orthorhombic-tetragonal and tetragonal-cubic phase for KNN and KNN-Cu doped. Ref. [3]	6
1.5	Binary phase diagram $KNbO_3 \sim NaNbO_3$. F_R =rhombohedral, F_O =orthorhombic, F_T =tetragonal, and $F_C = cubic$ Ref. [4]	7
1.6	Dipole orientation for a ferroelectric and antiferroelectric domain.	8
1.7	Commonly hysteresis loop (Polarization vs Electric field) Ref. [5]	9
1.8	Types of hysteresis loops (polarization vs electric field) for dielectric materials: a)Linear dielectric, b)Ferroelectric, c)Relaxor, and d)Antiferroelectric. Ref. [6]	10
1.9	Hard and soft ferroelectric loops Ref. [7]	12
1.10	Applications of ferroelectric materials in bulks and thin films. Ref. [8]	14

B.1	XS estimation for the sample KNN sintered 1 hour at 1100°C - Encapsulated.	21
B.2	XS estimation for the sample KNNCu0.5%mol sintered 1 hour at 1100°C - Encapsulated.	22
B.3	XS estimation for the sample KNNCu1%mol sintered 1 hour at 1100°C - Encapsulated.	22
B.4	Heating ramp for calcination stage, the heating treatment was carried out at 900°C for 4 hours, with a heating rate of 5°C per minute and a cooling rate of 7°C per minute.	23
B.5	XS estimation for the sample KNNCu0.5%mol sintered 3 hours at 1100°C - Encapsulated.	23
B.6	XS estimation for the sample KNNCu1%mol sintered 1 hour at 1100°C - Encapsulated.	24
B.7	XS estimation for the sample KNN sintered 4 hours at 1100°C - Witout encapsulation.	24
B.8	XS estimation for the sample KNNCu0.5%mol sintered 4 hours at 1100°C - Witout encapsulation.	25
B.9	XS estimation for the sample KNNCu1%mol sintered 4 hours at 1100°C - Witout encapsulation.	25

3	Methodology	17
3.1	Methodology for bulk synthesis	17
3.1.1	Stoichiometry Calculation	17
3.1.2	Materials and reagents	19
3.1.3	Methodology bulk synthesis	20
3.1.4	Bulk ceramic synthesis	21
3.2	Target Synthesis	24
3.2.1	Sputtering	27
3.3	Characterization techniques for bulk and thin films	28
3.3.1	Structural characterization	28
3.3.2	Dielectric, Ferroelectric and Band gap properties	31
3.3.3	Band gap characterization	32
4	Results	34
4.1	Bulk characterization	34
4.1.1	Estructural characterization	34
4.1.2	Dielectric, ferroelectric and optical characterization	44
4.2	Thin films characterization	62
4.2.1	KNN	64
4.2.2	KNNCu0.5%mol - Chemical Formula 2	71
4.2.3	KNNCu1%mol - Chemical Formula 2	83
5	Conclusion	92
5.1	Recommendations	93

A Crystallite size FWHM estimation figures	95
A.1 KNN, KNNCu0.5%mol, and KNNCu1%mol sintered for 1 hour at 1100°C - Encapsulated	95
A.2 KNN, KNNCu0.5%mol, and KNNCu1%mol sintered for 3 hours at 1100°C - Encapsulated	96
A.3 KNN, KNNCu0.5%mol, and KNNCu1%mol sintered for 4 hours at 1100°C - Without encapsulation	97
B Crystallite Size Plots	98
B.1 KNN Sintered 1 hour at 1100°C - Encapsulated	98
B.2 KNNCu0.5%mol Sintered 1 hour at 1100°C - Encapsulated	99
B.3 KNNCu1%mol Sintered 1 hour at 1100°C - Encapsulated	99
B.4 KNN Sintered 3 hours at 1100°C - Encapsulated	100
B.5 KNNCu0.5%mol Sintered 3 hours at 1100°C - Encapsulated	100
B.6 KNNCu1%mol Sintered 3 hours at 1100°C - Encapsulated	101
B.7 KNN Sintered 4 hours at 1100°C - Without encapsulation	101
B.8 KNNCu0.5%mol Sintered 4 hours at 1100°C - Without encapsulation . . .	102
B.9 KNNCu1%mol Sintered 4 hours at 1100°C - Without encapsulation . . .	102
Bibliography	103

LIST OF FIGURES

1.1	Perovskite structure ABO_3 Ref. [1]	2
1.2	Flow chart of the classification of point groups according its ferroelectric properties BT(Barium titanate), PZT(Lead zirconate titanate), PT(Lead titanate), PLZT(Lead lanthanum zirconate titanate), PMN(Lead magnesium titanate), and KNN(Potassium sodium) [2].	3
1.3	Domain structure after and before of an applied external field.	4
1.4	Dielectric constant vs Temperature showing phase transitions: orthorhombic-tetragonal and tetragonal-cubic phase for KNN and KNN-Cu doped. Ref. [3]	6
1.5	Binary phase diagram $KNbO_3 \sim NaNbO_3$. F_R =rhombohedral, F_O =orthorhombic, F_T =tetragonal, and $F_C = cubic$ Ref. [4]	7
1.6	Dipole orientation for a ferroelectric and antiferroelectric domain.	8
1.7	Commonly hysteresis loop (Polarization vs Electric field) Ref. [5]	9
1.8	Types of hysteresis loops (polarization vs electric field) for dielectric materials: a)Linear dielectric, b)Ferroelectric, c)Relaxor, and d)Antiferroelectric. Ref. [6]	10
1.9	Hard and soft ferroelectric loops Ref. [7]	12
1.10	Applications of ferroelectric materials in bulks and thin films. Ref. [8]	14

3.1	Heating ramp for calcination stage, the heating treatment was carried out at 900°C for 4 hours, with a heating rate of 5°C per minute and a cooling rate of 7°C per minute.	22
3.2	Heating ramps for the sintering process. T_o (Initial temperature), T_s (Sintering temperature), T_f (final temperature), R_h (heating temperature over time), R_c (cooling temperature over time). The heating treatments carried out are: a)1100°C for 240 minutes with a heating rate of 5°C per minute without encapsulation, b)1100°C for 180 minutes with a heating rate of 5°C per minute with encapsulation (in crucible), and c)1100°C for 60 minutes with a heating rate of 10°C per minute with encapsulation (in crucible).	23
3.3	Flowchart of the samples obtained with their related chemical formula and conditions of temperature treatment in the calcination and sintering.	24
3.4	Target of KNNCu0.5%mol(1) and KNNCu1%mol(2), calcined at 900°C for 4 hours and sintered at 1100°C for 1 hour.	25
3.5	Alternative heating rate based in a sintering at 1000°C per 120 minutes with a heating rate of 10°C per minute.	26
3.6	New targets of KNNCu0.5%mol and KNNCu1%mol obtained with the alternative heating ramp detailed in the Figure 3.5.	26
3.7	Archimedes method for densification measurement. Representation of the measurement in air and in fluid. Ref. [9]	29
4.1	XRD for samples calcinated powders of KNN, and bulk samples of KNNCu0.5%mol and KNNCu1%mol sintered at: a)1100°C for 4 hours without encapsulation, b)1100°C for 1 hour encapsulated, and c)1100°C for 3 hours encapsulated.	36
4.2	Diffractiongram of KNN, KNNCu0.5%mol and KNNCu1%mol in bulk, sintered at 1100°C for 1 hour.	37
4.3	Micrographs of secondary and backscattered electrons for the bulk sample KNN sintered at 1100°C for 1,3 and 4 hours. WE (encapsulated in a crucible), OE (without encapsulation).	40
4.4	Micrographs of secondary and backscattered electrons of KNNCu0.5%mol samples sintered for 4 hours at 1100°C - Formula 1.	41
4.5	Micrographs of secondary and backscattered electrons of KNNCu0.5%mol bulk samples calcined at 900°C for 4 hours and sintered at 1100°C for 4 hours – Formula 2.	42

4.6	Micrographs of secondary and backscattered electrons of KNN ($x=0$), KNNCu0.5%mol ($x=0.005$) and KNNCu1%mol ($x=0.01$) sintered for 1 hour.	44
4.7	P-E loop for the KNN system in bulk sintered at 1100°C for 4 hours without encapsulation and for 3 hours with encapsulation. Measurement carried out at 200Hz for different voltages.	45
4.8	P-E loops for the bulk sample KNNCu0.5%mol, synthesized with the formula 1 and sintered at 1100°C for 4 hours without encapsulation- Frequencies of a(100Hz) and b(200Hz).	46
4.9	P-E loops for the bulk sample KNNCu0.5%mol, synthesized with formula 2 and sintered 4 hours without encapsulation. Frequencies of a(100H) and b(200Hz).	47
4.10	P-E loops for the bulk sample KNNCu0.5%mol synthesized with the chemical formula 1 and sintered at 1100°C for 3 hours with encapsulation – Frequency of 200Hz for different voltages.	48
4.11	P-E loops for the bulk sample KNNCu0.5%mol sintered at 1100°C for 3 hours with encapsulation – Frequencies of 10, 13.3, and 20Hz.	49
4.12	Remnant polarization for the sample of KNNCu0.5%mol, sintered at 1100°C for 3 hours with encapsulation- Measurement carried out at 2500V with a frequency of 200 and 50Hz, respectively.	50
4.13	P-E loops for the sample KNNCu0.5% synthesized with formula 1 and sintered 1-hour with encapsulation. Frequency of 200Hz.	51
4.14	P-E loops of the sample KNNCu0.5%mol sintered 1-hour with encapsulation. 2600V applied at different frequencies.	52
4.15	Normalized capacitance of the sample KNNCu0.5%mol sintered 1-hour with encapsulation. Frequency of 200Hz.	53
4.16	P-E loops of KNNCu0.5%mol sample, sintered 1-hour with encapsulation.	53
4.17	a) Remnant hysteresis at 2600V (20Hz) for KNNCu0.5%mol sintered 1 hour with encapsulation, b) Normalized capacitance for KNNCu0.5%mol sintered 1 hour with encapsulation. Antiferroelectricity behavior at 2600V for 10Hz.	54
4.18	P-E loops of the sample KNNCu1%mol sintered 3 hours with encapsulation. Frequency of 200Hz.	55
4.19	P-E loops for the sample KNNCu1%mol sintered 1-hour with encapsulation. Frequency of 200Hz (a) and 10, 13.3, 20, 40, 200Hz (b).	56

4.20	a) Remnant polarization (2600V-20Hz) and b) Normalized capacitance (2600V-10Hz) of KNNCu1%mol sintered 1 hour with encapsulation.	56
4.21	Relative permittivity and $\tan(\delta)$ vs temperature for sample of KNN sintered at 1100°C for: a) 4 hours with encapsulation, and b) 1 hour without encapsulation.	58
4.22	Relative permittivity and $\tan(\delta)$ vs temperature for samples a) KNNCu0.5%mol sintered 4 hours at 1100°C without encapsulation (Formula 1), b) KNNCu0.5%mol sintered 3 hours at 1100°C with encapsulation (Formula 1), c) of KNNCu0.5%mol sintered 1 hour at 1100°C with encapsulation (Formula 1), and d) KNNCu0.5%mol sintered 4 hours at 1100°C without encapsulation (Formula 2).	59
4.23	Relative permittivity and $\tan(\delta)$ vs temperature for sample of KNNCu0.5%mol sintered 3 hours at 1100°C with encapsulation.	60
4.24	Bandgap calculation by Kubelka-Munk relation-indirect method (explained in the section 3.3.3)	61
4.25	XRD for calcinated powders of KNNCu0.5%mol and KNNCu1%mol at 900°C for 4 hours.	62
4.26	First targets of KNNCu0.5 and KNNCu1, milled 120 minutes in high energy miller, and sintered at 900°C for 4 hours and sintered for 1 hour at 1100°C.	63
4.27	New targets of the systems KNN, KNNCu0.5, and KNNCu1%mol 3.6, milled 30 minutes in a mortar and 90 minutes in high energy miller, calcined 4 hours at 900°C, and sintered 2 hours at 1000°C.	64
4.28	XRD for KNN/ p- type Si, deposited in 5 layers for 10 minutes, with a power of 75W, and sintered at 650°C for 60 minutes in an oxygen atmosphere.	65
4.29	a) 3D Thickness, and b) 3D Roughness for KNN/p- type Si.	66
4.30	Ferroelectric hysteresis for KNN/p- type Si at different frequencies and voltages.	67
4.31	Current-Voltage for KNN/p- type Si.	68
4.32	Film obtained after the heat treatment and XRD for KNN/ITO/glass sample deposited in 5 layers for 10 minutes, with a power of 75W, and sintered at 650°C for 60 minutes in an oxygen atmosphere.	69
4.33	a) 3D Thickness, and b) 3D Roughness for KNN/ITO/glass	69

4.34	Ferroelectric hysteresis for KNN/ITO/glass. The period was 1ms(1000Hz).	70
4.35	Current-Voltage for KNN/ITO/glass.	71
4.36	Film obtained after the heating treatment and XRD for KNNCu0.5%mol/Pt/Si deposited in 90 minutes, with a power of 100W, and sintered at 600°C for 30 minutes in an oxygen atmosphere.	72
4.37	Film obtained after the heating treatment and XRD for KNNCu0.5%mol(1)/ITO/glass deposited for 90 minutes, with a power of 100W, and sintered at 600°C for 30 minutes.	73
4.38	Current-Voltage for KNNCu0.5%mol/ITO/glass.	74
4.39	Film obtained after the heating treatment and XRD for KNNCu0.5%mol(2)/ITO/glass deposited in 5 layers for 10 minutes, with a power of 75W, and sintered at 650°C for 60 minutes in an oxygen atmosphere.	75
4.40	a) 3D Thickness and b) 3D Roughness for KNNCu0.5%mol(2)/ITO/glass.	75
4.41	Ferroelectric hysteresis for KNNCu0.5%mol(2)/ITO/glass.	76
4.42	Current-Voltage for KNNCu0.5%mol/ITO/glass.	77
4.43	Film obtained after the heating treatment and XRD for KNNCu0.5%mol(2)/p-type Si deposited in 5 layers for 10 minutes, with a power of 75W, and sintered at 650°C for 60 minutes in an oxygen atmosphere.	78
4.44	a) 3D Thickness and b) 3D Roughness for KNNCu0.5%mol(2)/p-type Si	78
4.45	Ferroelectric hysteresis for KNNCu0.5%mol(2)/ p- type Si (contact 1). 1ms(1000Hz), 4ms(250Hz), 6ms(166.66Hz), and 10ms(100Hz)	80
4.46	Ferroelectric hysteresis for KNNCu0.5%mol(2)/p- type Si (contact 2).	81
4.47	Current-Voltage for KNNCu0.5%mol(2)/p- type Si and polarized	82
4.48	Film obtained after the heating treatment and XRD for KNNCu1%mol(1)/ITO/glass deposited for 90 minutes, with a power of 100W, and sintered at 650°C for 60 minutes in an oxygen atmosphere.	83
4.49	Ferroelectric hysteresis for KNNCu1%mol(1)/ITO/glass	84
4.50	Current-Voltage for KNNCu1%mol/ITO/glass.	85

4.51	Film obtained after the heating treatment and XRD for KNNCu1%mol(1)/ITO/quartz deposited in 5 layers for 10 minutes, with a power of 50W, and sintered at 650°C for 60 minutes	85
4.52	Thickness 3D image for KNNCu1%mol(1)/ITO/quartz.	86
4.53	Ferroelectric hysteresis for KNNCu1%mol(1)/ITO/quartz. Period: 1ms(1000Hz).	87
4.54	Current-Voltage for KNNCu1%mol(1)/ITO/quartz.	88
4.55	Film obtained after the heating treatment and XRD for KNNCu1%mol(1)/ITO/glass deposited in 5 layers for 10 minutes, with a power of 75W, and sintered at 700°C for 60 minutes.	89
4.56	Thickness 3D image for KNNCu1%mol(1)/ITO/glass.	90
4.57	Thickness 3D image for KNNCu1%mol(1)/ITO/glass.	90
B.1	XS estimation for the sample KNN sintered 1 hour at 1100°C - Encapsulated.	98
B.2	XS estimation for the sample KNNCu0.5%mol sintered 1 hour at 1100°C - Encapsulated.	99
B.3	XS estimation for the sample KNNCu1%mol sintered 1 hour at 1100°C - Encapsulated.	99
B.4	Heating ramp for calcination stage, the heating treatment was carried out at 900°C for 4 hours, with a heating rate of 5°C per minute and a cooling rate of 7°C per minute.	100
B.5	XS estimation for the sample KNNCu0.5%mol sintered 3 hours at 1100°C - Encapsulated.	100
B.6	XS estimation for the sample KNNCu1%mol sintered 1 hour at 1100°C - Encapsulated.	101
B.7	XS estimation for the sample KNN sintered 4 hours at 1100°C - Witout encapsulation.	101
B.8	XS estimation for the sample KNNCu0.5%mol sintered 4 hours at 1100°C - Witout encapsulation.	102
B.9	XS estimation for the sample KNNCu1%mol sintered 4 hours at 1100°C - Witout encapsulation.	102

1.1 Ferroelectricity

Ferroelectricity is defined as the spontaneous alignment of the electrical dipoles of a material [10]. It is a property of dielectric materials, characterized by having a non-zero dipole moment in the absence of an external electric field. This behavior happens below a certain temperature called Curie Temperature, which is the thermal barrier between the ferroelectric and paraelectric state. The phase transitions are associated with structural changes, where the system goes from a centrosymmetric symmetry to a non-centrosymmetric symmetry [11]. Further, the properties can change with the time in the absence of external mechanical or electrical stresses, or temperature changes [12, 13].

1.1.1 Symmetry structure

A certain group of ferroelectric materials are characterized by having a perovskite structure ABO_3 as figure 1.1 shows, where B is associated with a transition metal located in the octahedral sites as Figure 1.1 shows. This kind of crystalline structure is known for its versatility because it allows to combine elements in the same position, giving an aliovalent

substitution [14, 15]. This happens because the perovskite structure allows variations in its composition which can provoke distortions in the unit cell, giving different phases as monoclinic, orthorhombic, tetragonal, and cubic [16]. In the case of $K_{0.5}Na_{0.5}NbO_3$ (KNN), there is a partial substitution of B sites by K and Na atom, the A sites are occupied by Nb^{+5} atoms and the O sites by the oxygen. When the system is doped with copper, the Cu^{+2} atoms substitute the niobium positions. There is a charge disbalance and O^{-2} vacancies are formed to reach charge neutrality [17].

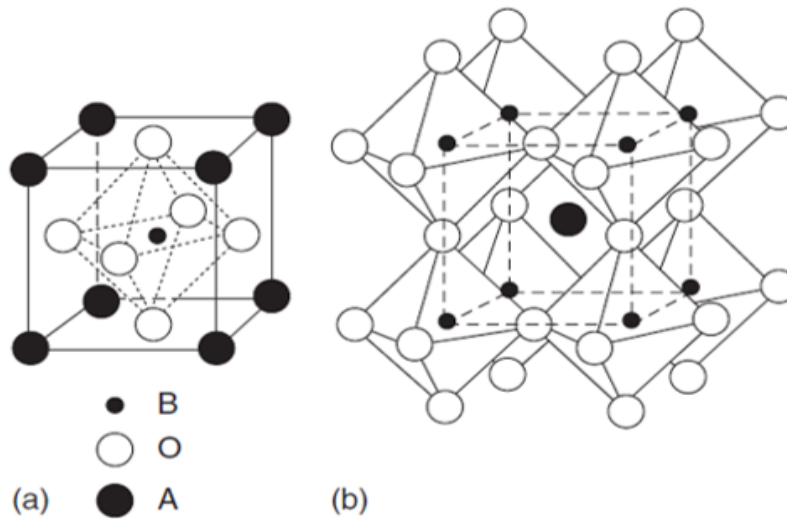


Figure 1.1: Perovskite structure ABO_3 Ref: [1]

1.1.1.1 Classification based on the symmetry

Figure [1.2] presents a scheme of the classification for dielectric materials according to their response to external stimuli. As we can see, their ferroelectric properties have their origin in non-center symmetry and in their piezoelectric and pyroelectric properties, which makes them a promising material. The ferroelectric system of interest in this work is KNN which has a structure with oxygen in an octahedral position (O sites).

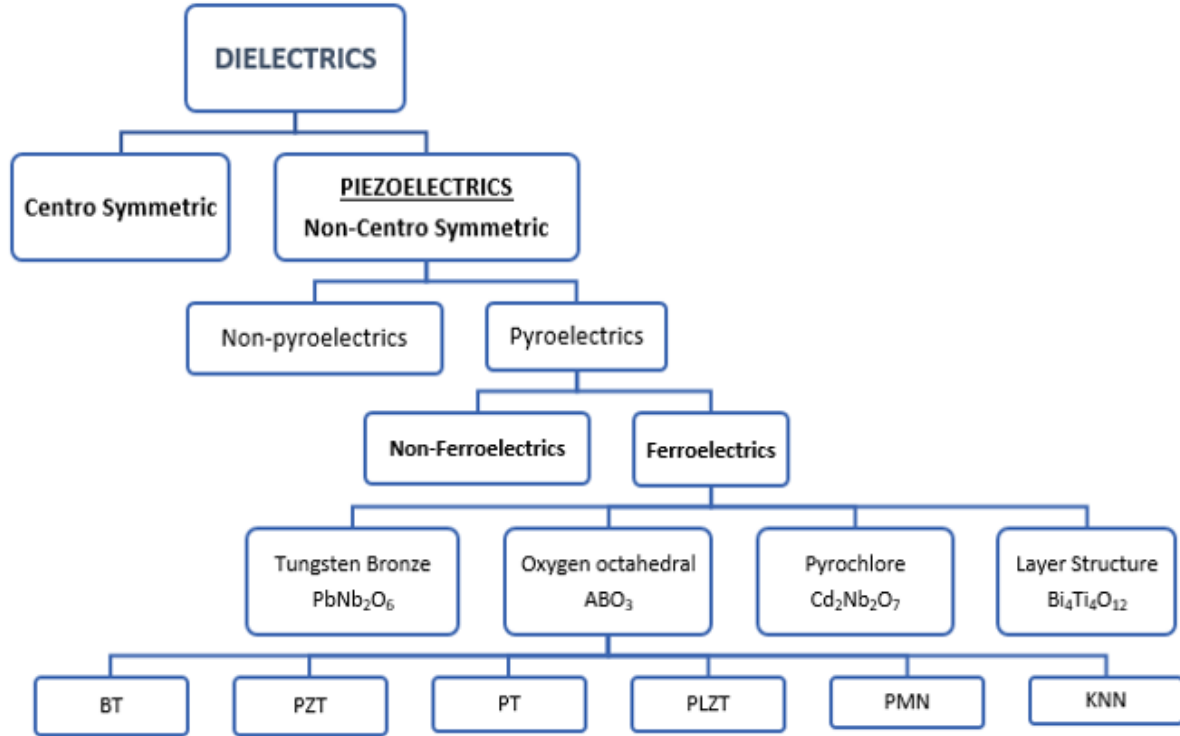


Figure 1.2: Flow chart of the classification of point groups according to its ferroelectric properties BT (Barium titanate), PZT (Lead zirconate titanate), PT (Lead titanate), PLZT (Lead lanthanum zirconate titanate), PMN (Lead magnesium titanate), and KNN (Potassium sodium) [2].

1.2 Polarization

The ferroelectric phenomenon appears by the capacity of the materials to present electric dipoles in its structure, which are susceptible to be reoriented by the application of an external electric field. Based on that, we can define the polarization as the process of dipole alignment in the function of an applied field [18, 19]. As Figure 1.3 illustrates, the dipoles present in a ferroelectric material are organized in domain structures, which are regions with the same dipole orientation which are formed to minimize the potential energy of the system [20, 21]. The directions of these domains are randomly distributed with a resultant polarization equal to zero. The application of an external electric field break

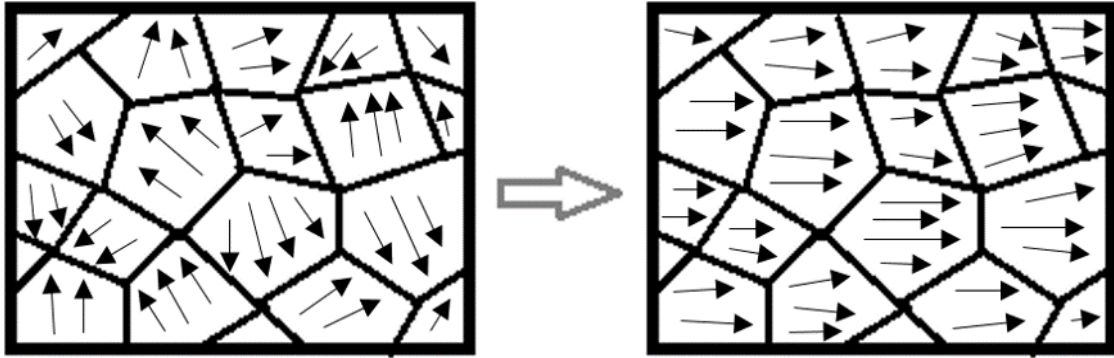


Figure 1.3: Domain structure after and before of an applied external field.

these structures due to the reorientation of the dipoles in the applied field [11].

1.2.0.1 Ferroelectric properties

The ferroelectric response is given by the application of different stresses, which generate an electric field that modifies the polarization and gives rise to the characteristic properties of these materials described below.

Pyroelectricity. - It is a phenomenon through which an electric field is generated by a temperature variation and produces a change in the polarization.

Piezoelectricity. - It is a property in which an electric field is produced by mechanical stress [22, 23].

Although all ferroelectric materials are pyroelectric, however, not all pyroelectric materials are ferroelectric. Below a transition temperature called the Curie temperature ferroelectric and pyroelectric materials are polar and possess a spontaneous polarization or electric dipole moment. However, this polarity can be reoriented or reversed fully or in part through the application of an electric field with ferroelectric materials.

Based on both properties, there are a wide range of application for different devices such as sensors, capacitors, memories, photovoltaic cells, among others [24, 25, 26, 27].

Moreover, the materials development depends on another important factor, that is the dielectric constant (ϵ_r) also known as relative permittivity. This constant is a property of each material, which describes its ability to be polarized and is related to the capacity to store energy [28]. Equation 1.1 relates the relative permittivity (ϵ_r) with the vacuum permittivity (ϵ_0) and the permittivity of the dielectric medium (ϵ) [18, 19]

$$\epsilon_r = \frac{\epsilon}{\epsilon_0} \quad (1.1)$$

1.2.0.2 Ferroelectric transition

Ferroelectric materials suffer a phase transition at a certain temperature called Curie Temperature (T_c). When the temperature is above T_c the material loses the ferroelectric phase and the paraelectric phase appears. There are materials with 2 or more structural transitions, in which T_c point only specifies the ferroelectric-paraelectric phase transition, and the other temperatures are related to the transition to one ferroelectric phase to another ferroelectric phase [24].

The $K_{0.5}Na_{0.5}NbO_3$ (KNN) system has been receiving an important attention due to its high Curie temperature (400-480°C), where ferroelectric properties are lost. As Figure 1.4 illustrates the KNN has two transitions, the first one around 250°C, which corresponds to orthorhombic- tetragonal transition, and the second one around 480°C which is related to the tetragonal-cubic phase transition (Curie temperature). The addition of copper decreases the phase transition temperature [3, 29].

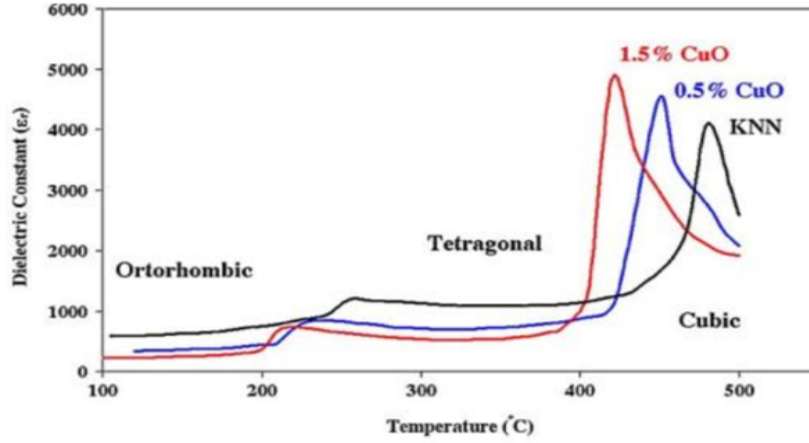


Figure 1.4: Dielectric constant vs Temperature showing phase transitions: orthorhombic-tetragonal and tetragonal-cubic phase for KNN and KNN-Cu doped. Ref. [3]

In [1.4], the peaks of the transition phase are related to values of maximum permittivity, which later experiment a considerable dielectric loss. This behavior is defined by the Curie-Weiss law represented in the Equation [1.2] [30].

$$\varepsilon_r = \frac{A}{T - \Theta_c} \quad (1.2)$$

Where A is a material constant and T is a given temperature above T_c . The value of θ_c is a near point from T_c , which is obtained by the extrapolation of the experimental data [13, 30].

The temperatures at which phase transitions occur can be seen on the binary diagram $KNbO_3 \sim NaNbO_3$ in the figure [1.5]. In this diagram the temperatures at which the composition $K_{0.5}Na_{0.5}NbO_3$ has the following transitions of interest are observed: rhombohedral-ortho-rhombic, ortho-rhombic-tetragonal, and tetragonal-cubic. The Curie point of $K_{0.5}Na_{0.5}NbO_3$ is at about 400°C and the tetragonal phase transforms at about

200°C to orthorhombic. According with the phase diagram the melting temperature for $K_{0.5}Na_{0.5}NbO_3$ are about 1140°C and 1280°C [4].

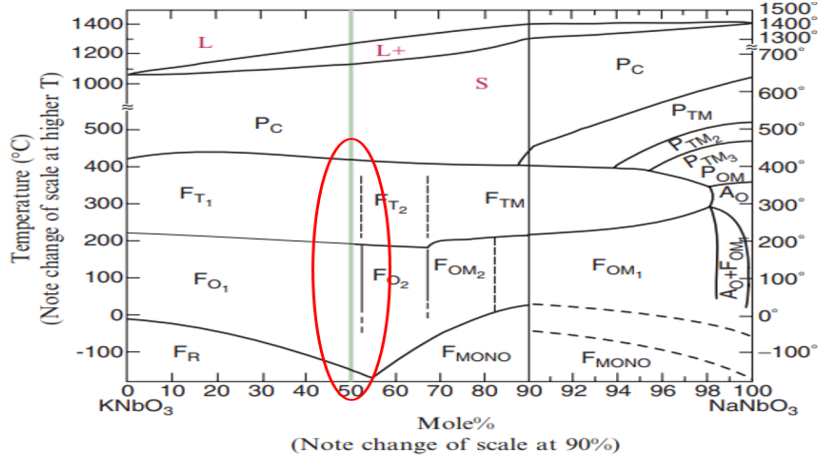


Figure 1.5: Binary phase diagram $KNbO_3 \sim NaNbO_3$. F_R =rhombohedral, F_O =orthorhombic, F_T =tetragonal, and F_C = cubic Ref. [4]

1.2.0.3 Ferroelectric clasification

The application of an external electric field polarizes the adjacent domains with field direction. The orientation of the dipoles determines if a material is ferroelectric or antiferroelectric. Figure [1.6], first shows a ferroelectric behavior characterized by a dipole orientation along. These materials are characterized by the presence of spontaneous polarization and for the reversibility of the polarization caused by an external electric field. Figure [1.6], also contrasts the antiferroelectric behavior, which is defined by the polarization of the dipoles in a opposite direction to the field applied and by a zero net macroscopic remnant polarization [31].

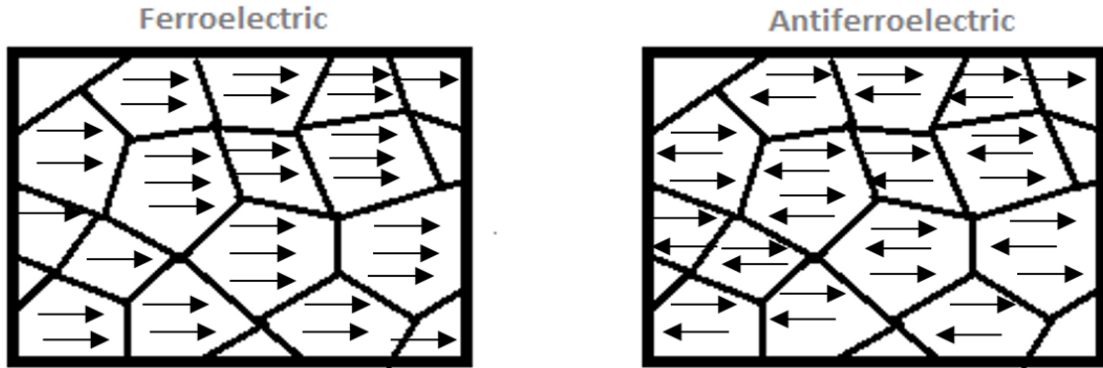


Figure 1.6: Dipole orientation for a ferroelectric and antiferroelectric domain.

1.2.1 Hysteresis loops

The domain arrangement of the materials exhibits a hysteresis loop (polarization versus field), which is characteristic of each material and appears in response to external driving fields. The behavior obtained gives us information about the properties and structures of the material [5]. There are some parameters that could be deduced from hysteresis loops such as: the dischargeable energy which are related to the hatched area (1.8); the dielectric losses which are represented by the area within the hysteresis loop; and the energy storage efficiency though the related ratio of the dischargeable energy and the dielectric losses [6].

Moreover, as Figure 1.7 illustrates, there are other variables that could be determined from hysteresis loops.

Saturation polarization (P_s): It is reached at high electric fields, when the net polarization is maximum and the dipoles are oriented in the field direction, reaching its saturation limit. The value of (P_s) is the polarization related to the maximum applied field in point B of Figure 1.7.

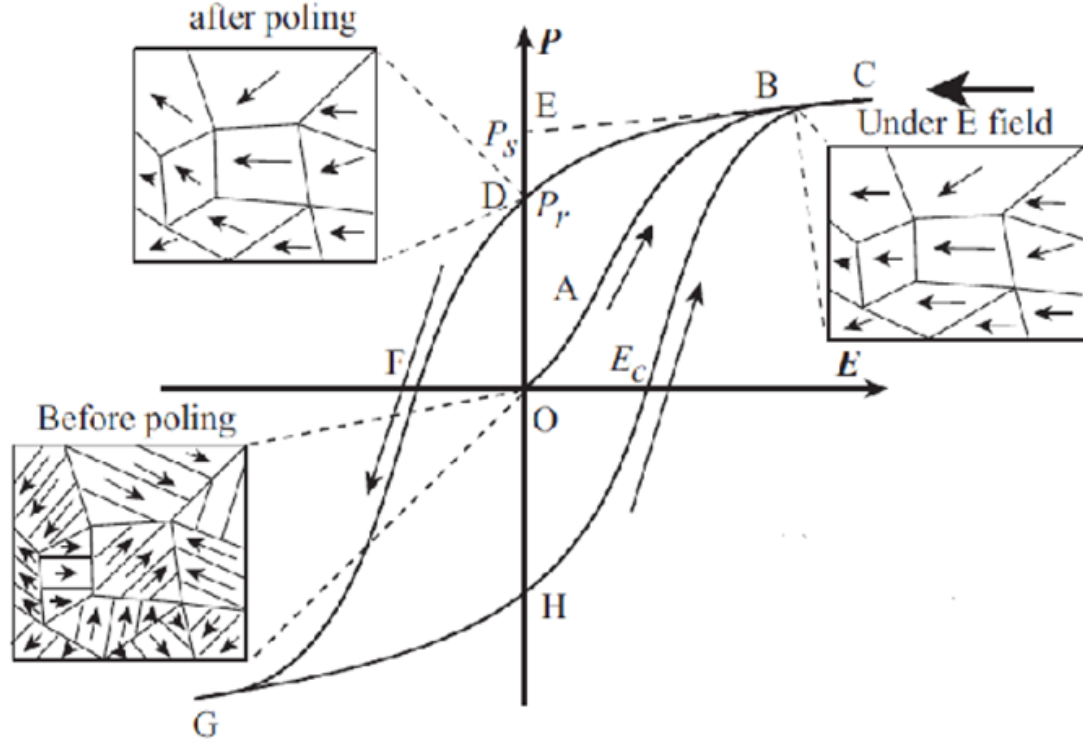


Figure 1.7: Commonly hysteresis loop (Polarization vs Electric field) Ref. [5]

Remnant polarization (P_r): This occurs when a reverse electric field is applied and there is a polarization that remains in a zero field. This parameter corresponds to point D in Figure 1.7 when the system returns to a minimum energy configuration where there is a resultant polarization in the sense of the field. When a negative coercive field is applied a negative remnant polarization ($-P_r$) is achieved and it is related to the point H.

Coercive field (E_c): It makes references to an electric field which is reached a zero-net polarization. It is also known as the required field to revert the orientation of the domains. When the polarization reaches zero, a negative coercive field ($-E_c$) is required to polarize the domain in the opposite direction.

A ferroelectric material is considered ideal when the values of (E_c) and (P_s) are equal. This behavior can be altered by some factors as thickness, composition, thermal treatment, charged defects introduction, mechanical stresses, measurement conditions, among others [32, 18, 11].

1.2.1.1 Classification of hysteresis loops (polarization vs electric field)

According to the morphology features, there are different ferroelectric materials that can be identified in Figure 1.8, a graphical representations of the hysteresis loops (polarization vs field).

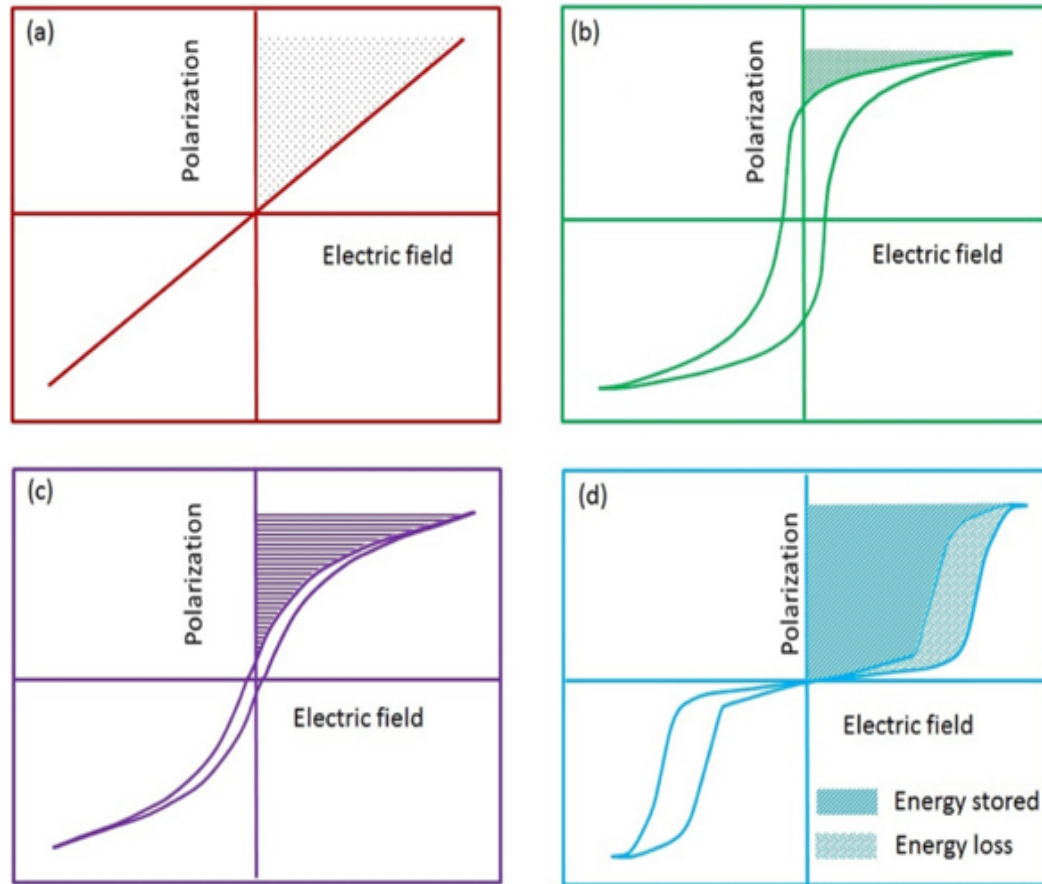


Figure 1.8: Types of hysteresis loops (polarization vs electric field) for dielectric materials: a)Linear dielectric, b)Ferroelectric, c)Relaxor, and d)Antiferroelectric. Ref. [6]

Linear dielectric.- Figure 1.8(a), represents an ideal linear capacitor, which is represented by a straight line in the P-E loops. The polarization is almost proportional to the field applied and the linear behavior is caused by the charge and the voltage are in the same phase. This state is characterized by having a low dielectric constant and high dielectric breakdown strength [32, 6, 5, 33].

Ferroelectric.- Figure 1.8(b), shows a hysteresis loop related to a ferroelectric state. The application of an external electric field produces a variation in the polarization, polarizing most of domains when the coercive field is reached. Once the coercive field is overcome, there is still the alignment of the domains with the field which is attributed to the movement of the domain walls present in the material until the saturation point is obtained. Ferroelectric hysteresis is characterized by a large dielectric constant and lower dielectric breakdown strength [6, 5].

Relaxor ferroelectric.- Figure 1.8(c), shows a typical loop of a relaxor material, which is characterized by a slim loop related to microdomains. The presence of these microdomains provoke a fast response to the electric field applied. These materials do not have a definite ferroelectric hysteresis and are characterized by having a minimum remnant polarization as well as their coercive field [6, 5].

Antiferroelectric.- Figure 1.8(d), illustrates an antiferroelectric hysteresis loop, which is characteristic of non-polar materials with a net polarization of zero before the field is applied. The principal characteristic of this state is related to the opposite orientation of the domains provoked by the external electric field. This state could be identified by a double hysteresis loop. When a high electric field is reached, the antiferroelectric state is reverted to the ferroelectric state. Moreover, the antiferroelectric materials have a higher energy storage and low remnant polarization and coercive field. Antiferroelectric state has been studied in some systems such as BT, PZT, and KNN [6, 8, 5, 33].

Another classification of ferroelectric materials exists based on the thickness of hysteresis loops, which are detailed in Figure 1.9. A ferroelectric material is considered “soft”, when its coercive field strength is low, and the spontaneous polarization is high. Moreover, it is characterized by a low melting temperature, water solubility, and mechanically soft. In contrast, a material is “hard” material, when its coercive field strength is high and its spontaneous polarization is low. This kind of material is mechanically hard, non-water

soluble, and it is related to oxides that are formed at high temperatures [34, 35, 7].

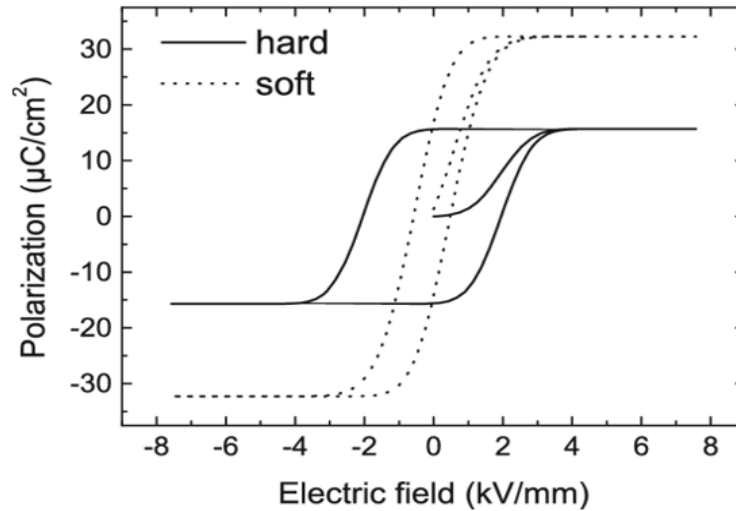


Figure 1.9: Hard and soft ferroelectric loops Ref. [7]

1.2.2 Electrical Properties

There are various stimulus capable of provoking a certain response in solid materials. In this case, an external electric field could modify the ferroelectric properties of the material, which implies directly its area of application. The cations and anions present in the structure own some electric charge and could be carriers to migrating or to diffusing charges when an electric field is applied [19]. The electrical behavior of solid material is based on the Ohm's Law (Equation 1.3), that relates the current (I), the applied voltage (V), and the related resistance (R) of the material through which current passes.

$$V = IR \quad (1.3)$$

The related units of the Ohm's law are volts (J/C) for V, amperes (C/s) for I, and ohms (V/A) for R. The electrical properties of specific material are related to an electrical resistivity (ρ), which is specific of each material. As the equation 1.4 shows, the electrical

resistivity relates the resistance (R) with geometrical parameters as (distance between two points at which the voltage is measured) and the cross-sectional area perpendicular to the direction of the current (A). The related unit of ρ is (Ωm). If we introduce the Ohm's law to the resistivity equation, the equation [1.5](#) results in: [19](#).

$$\rho = \frac{RA}{l} \quad (1.4)$$

$$\rho = \frac{VA}{Il} \quad (1.5)$$

1.2.2.1 Electrical conductivity

The electrical conductivity (σ) is indicative of the capacity of a material to conduce electrical current. The electrical conductivity of each material depends on its bandgap energy (E_g), which is related to the valance and conduction band. The addition of some elements can modify the band structures and hence the conduction properties. As the equation [1.6](#) shows, the electrical conductivity is inversely proportional to the resistivity, so we can call the conductivity as teh amount of electrical current a material can carry, is also known as specific conductance. The final conductivity depends on the concentration of charge carriers, electrons and holes [22](#), [19](#).

$$\sigma = \frac{1}{\rho} \quad (1.6)$$

1.3 Application of ferroelectric materials

Ferroelectric materials can be processed as bulks and thin films by different methods. Each one results in different applications as the Figure [1.10](#) shows.

There is a wide area of technological application which depends on its properties of ferroelectricity, pyroelectricity, and piezoelectricity. The most common ferroelectric devices are sensors, memories, capacitors, generators, and photovoltaic cells [36](#), [37](#). The use of ferroelectric materials as energy storage capacitors has been studied in previous research

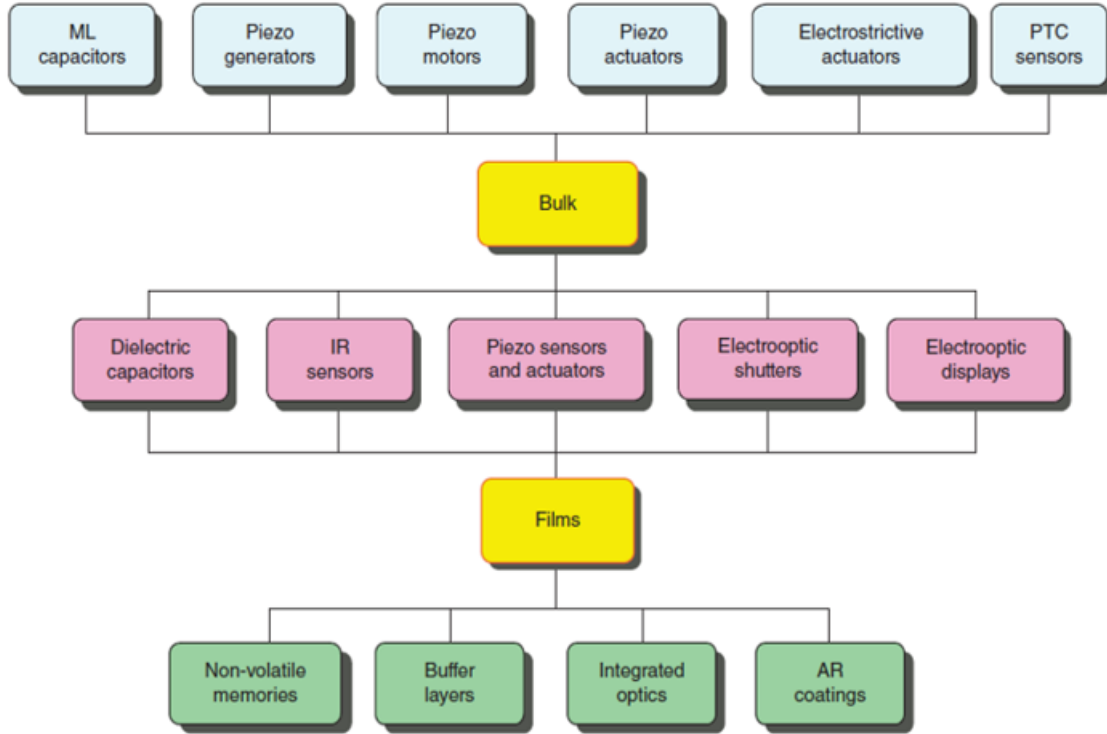


Figure 1.10: Applications of ferroelectric materials in bulks and thin films. Ref. [8]

by its use in power electronic and pulsed power systems [38, 31]. The use of ferroelectric materials in memories has been relevance by its data retention capacity below T_c [39, 40]. On the other hand, the application as sensors has allowed the detection of different thermal or mechanical impulses, which are applicable to industrial systems thanks to their effectiveness and durability [37]. As a thin film, its photovoltaic capacity has been studied as a light absorbing material, with solar cells being its main application [41, 42]. Lead-free ferroelectric systems have great interest in the biological field, for biomedical applications. It can have a promising effect on cell biology, cell bioengineering, cell signaling, biological trapping, cell response modulation, tissue regeneration, and antitumoral action [26, 43],

CHAPTER 2

PROBLEM STATEMENT

Since the discovery of ferroelectric materials with the Rochelle salt, there has been a scientific interest due to their distinctive properties which have been exploited as crystals, ceramics, composites, and thin films. The wide range of technological application includes capacitors with a high-dielectric constant, piezo y pyroelectric devices, transducers, infrared detectors, sensors, filters, and nonvolatile memories [1, 8].

There are numerous ferroelectric systems such as PZT, PBT, PMN, PZLT, BLT, BT, KNN, among others. Most of these materials have lead as one of the substantial elements in their development of ferroelectric materials, which consequently bringing high toxicity for humans and the ecosystem. Based on that precedent, there is an emergent need to develop lead free materials with potential properties. One of the promising materials without lead in its composition is the $K_{0.5}Na_{0.5}NbO_3$ system by its excellent piezoelectric and electromechanical properties, density and high Curie Temperature [44].

The great technological development implies also the need of deepen in the research of new technologies with new materials that improves the properties and have a wide application area in material science, physics and engineering [23]. There are many factors that can be changed to improve the material properties such as the energy storage, energy bandgap,

curie temperature, among others. Between them, the ferroelectric-antiferroelectric properties could produce effects in the electromechanical properties of the ceramics and could be induced by the doping with some elements, for example zirconium in the system $Na_{0.5}Bi_{0.5}TiO_3$, niobium in the system $PbZrTiO_3$, samarium for the system $BiFeO_3$, copper in the system $K_{0.5}Na_{0.5}NbO_3$, among others [45, 46, 47, 48].

In this work, we studied the $K_{0.5}Na_{0.5}NbO_3$ system in bulk and in thin films. Moreover, it was analyzed the effect of doping with copper in two concentrations to see whether it shows a ferroelectric and antiferroelectric phase [3, 46, 17].

2.1 General and Specific objectives

2.1.1 General objective

To synthesize and characterize bulks and thin films of ferroelectric system $K_{0.5}Na_{0.5}NbO_3$ and study the effect of doping the system with copper.

2.1.2 Specific objectives

- To synthesize pure KNN and KNN doped in different concentrations of copper 0.5% and 1%mol to find an antiferroelectric phase.
- To analyse the morphologic, structural, optical and ferroelectric properties of thin films through characterization techniques as Scanning Electron Microscopy, X-Ray Diffraction, hysteresis-loops, and impedance spectroscopy.
- To synthesize a bulk of $KNNCu0.5\%$ mol and $KNNCu1\%$ mol to use in the growth of thin films on ITO by sputtering method.

CHAPTER 3

METHODOLOGY

3.1 Methodology for bulk synthesis

This chapter describes the methodology used during the synthesis and characterization of bulk samples of the system $K_{0.5}Na_{0.5}NbO_3$ doped with Cu.

3.1.1 Stoichiometry Calculation

The ferroelectric system to be synthesized consists of the KNN pure and KNN doped with 0.5%mol and 1%mol of copper.

In the first place it is important to find an stoichiometry formula that could be able to justify the substitution of niobium atoms by copper atoms, guaranteeing the cell neutrality. To develop the base formula of substitution it is primordial to have a mass and charge balance. Both atoms have a similar ionic radio, but the copper atoms substitute an element with different valence.

Balance

$$K_{0.5}^+ + Na_{0.5}^+ + Nb_y^{5+} + Cu_x^{+2} + O_3^{-2} = 0$$

$$0.5 + 0.5 + 5y + 2x = 6$$

$$y = 1 - \frac{2x}{5}$$

$$K_{0.5}Na_{0.5}(Nb_{1-2x/5}Cu_xO_3) \quad (3.1)$$

The Chemical Formula 1 (3.1) was reported in the literature [46]. Analyzing the chemical formula reported, it was observed that of all the added copper, only the 2/5 parts substitute for niobium. It implies that 3/5 parts of copper are not incorporated into the structure and remain free. However, if we consider that all the copper is introduced in the lattice, then there is the production of oxygen vacancies in order to keep the lattice neutral. The copper excess could promote the formation of other phases along with deterioration of purity and system properties.

Based on these considerations, it was proposed a new formula, which considers an adequate treatment of the charge balance.

$$K_{0.5}Na_{0.5}(Nb_{1-x}Cu_xO_{3-\delta})$$

$$K_{0.5}^+ + Na_{0.5}^+ + Nb_{1-x}^{5+} + Cu_x^{+2} + O_{3-\delta}^{-2} = 0$$

$$\delta = \frac{3}{2}x$$

Then, with the value of δ we establish a second formula.

$$K_{0.5}Na_{0.5}(Nb_{1-x}Cu_xO_{3-1.5x}) \quad (3.2)$$

In Chemical Formula 2 (3.2), all of the copper is incorporated in the structure, inducing the formation of vacancies of oxygen to remain the electroneutrality of the cell. The formation of oxygen vacancies results from charge compensation, considering Cu^{2+} and Nb^{5+} .

In the present work, it was studied the influence of both compositions and the resulting different concentration of copper in the synthesis of the system.

3.1.2 Materials and reagents

For the synthesis of the ceramics in bulk the principal reagents used were: Potassium carbonate, sodium carbonate, niobium pentoxide, copper (II) oxide, and ethyl alcohol. In the following Table [3.1](#) the main information about them is detailed.

Niobium (V) oxide	
Brand information	SIGMA-ALDRICH Chemistry Lot # MKCG1252
Chemical formula	Nb ₂ O ₅
Molecular weight	265.81 g/mol
Density	4.47 g/mL at 25°C
Purity	99.9%
Form	powder
Potassium carbonate (Anhydrous)	
Brand information	MEYER Lot # M0911566
Chemical formula	K ₂ CO ₃
Molecular weight	138.21 g/mol
Purity	99.0%
Form	granules
Sodium Carbonate (Anhydrous)	
Brand information	Productos Químicos MONTERREY S.A. Lot # 012325
Chemical formula	Nb ₂ O ₅
Molecular weight	105.99 g/mol
Density	4.47 g/mL at 25°C
Purity	99.8%
Form	Granules
Copper (II) oxide -Anhydrous	
Brand information	GOLDEN BELL Lot # 18051409
Chemical formula	CuO
Molecular weight	79.55 g/mol
Density	4.47 g/mL at 25°C
Purity	99.1%
Form	powder
Ethyl alcohol	
Brand information	CONTYQUIM Lot # BIO096-02150049
Chemical formula	C ₂ H ₅ OH
Molecular weight	46.07 g/mol
Density	4.47 g/mL at 25°C
Purity	96%
Form	liquid

Table 3.1: Chemical compounds used to synthetize the system KNN-Cu doped.

The substrates used for the grown of thin films were indium tin oxide (ITO) glass, indium tin oxide (ITO) quartz, silicon-coated with platinum and p- type Si. For the substrates cleaning, the following reagents where used: C_3H_8O , C_3H_6O (acetone), toluene, xylene, and ionized water.

3.1.3 Methodology bulk synthesis

The synthesis of bulk ceramics must follow the conventinal method from oxides and carbonates powders, followed by a calcination and sintering treatment.

3.1.3.1 Conventional method - milling ball

This technique is based on mechanochemical processing, which involves the deformation and fracturing of particles during repeated collisions with a zirconia ball during high-energy milling. It uses mechanical energy to reduce the particle size distribution and activate chemical reactions and structural changes related to the crystal bonds breaking [49]. The technique uses balls of different size, the number of them depend on the quantity of powder that is going to be ground, and the respective volume of the vial used. During this process it is important to let rest periods to avoid the heating of the sample. The equipment used for this process is the 8000 MIXER/MILL of SPEX-CertiPrep.

Previously to the calcination process, the powders were uniaxially pressed in pellets with a press able to compact ceramic, polymeric and metallic powders. For the calcination, the powders should be compacted in big bulks of 1 inch with a low pression approximately of $25kg/cm^2$.

3.1.3.2 Calcination

The main objective of this step is to obtain a specific crystal phase. During this process, there is the removal of unwanted volatile compounds and the conversion into a more stable

material. For it, the powders were uniaxially pressed in pellets and calcinated without encapsulation. The oven used in this process is a YF-1700 of YIFAN.

3.1.3.3 Sintering

The principal objective of this process is the densification of the material. During this heating process occur some changes in the size and shape of grains and pores. The pores becoming more spherical in shape and smaller in size. These changes are directly related to the porosity, considering the transformation of an originally porous compact to a strong dense ceramic [50]. This process usually occurs in ovens at high temperatures for long periods of time. In this case, the oven used is the same as in the calcination process, a YF-1700 of YIFAN. For all samples, the same heat treatment was used at 900°C for 4 hours.

3.1.4 Bulk ceramic synthesis

Following the previous methodology, it was obtained bulks samples of pure KNN and KNN doped with copper at 0.5% and 1%mol. The last two using chemical formula 1 (3.1) and chemical formula 2 (3.2). For the synthesis, carbonates and oxides were used, the partial and total quantities of each reagent used were calculated according to their equimolar relation and purity. The respective quantities are mixed in a vial Nylamid with balls of 4.98mm and 10.25mm of diameter.

3.1.4.1 Synthesis of KNN

For the synthesis of KNN, powders were milled in a high energy mill for 6 hours in periods of 30 minutes with rests of 20 minutes. After that, the powders obtained were dried directly in the vial for 3 hours at 150°C and then, in a beaker for 2 hours at 200°C. The powders were uniaxially pressed in pellets of ½ inch with an approximate force of 1-ton

equivalent to $25\text{kg}/\text{cm}^2$. The pellets were calcinated for 4 hours at 900°C (Alkoy Papila, 2010) without encapsulation according to the heating ramp of Figure B.9.

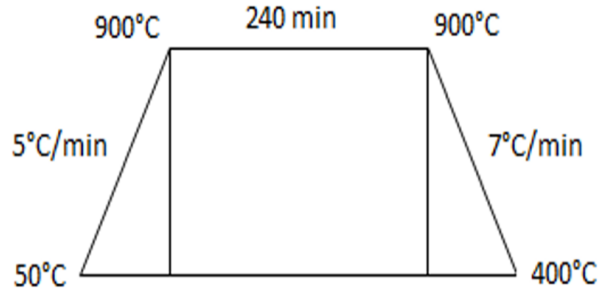


Figure 3.1: Heating ramp for calcination stage, the heating treatment was carried out at 900°C for 4 hours, with a heating rate of 5°C per minute and a cooling rate of 7°C per minute.

The calcinated pellets were milled again in a mortar or in the high energy miller for 15 minutes. The new powders obtained had to be sifted to homogenize the size grain. Again, the powders were uniaxially pressed in pellets of $3/8$ inches with a force of 2.5 tons equivalent to $45\text{kg}/\text{cm}^2$. In the case of the sintering, different times were used: (a) one for 3 hours at 1100°C with encapsulation (in crucible), (b) one for 4 hours at 1100°C without encapsulation, and (c) one for 1 hour at 1100°C with encapsulation (in crucible) as shown Figure 3.2.

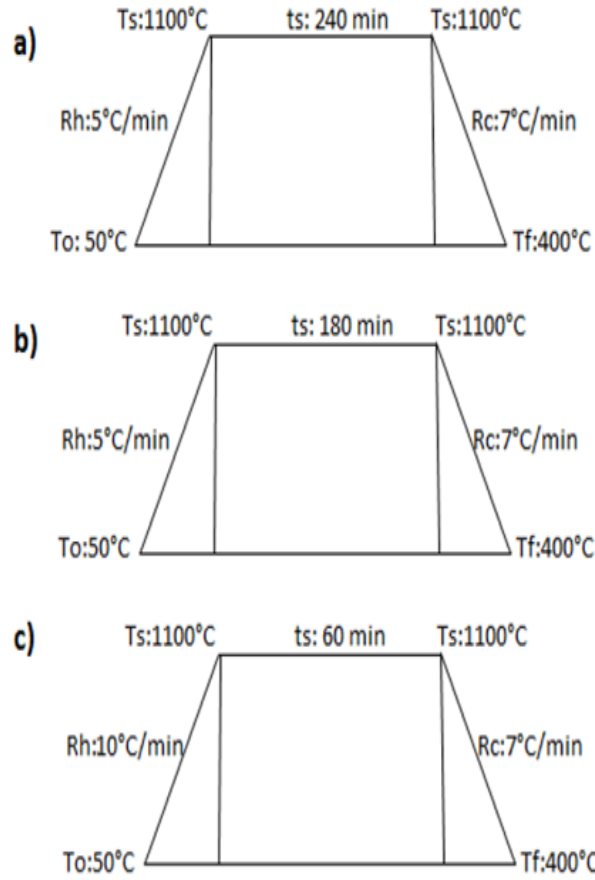


Figure 3.2: Heating ramps for the sintering process. T_o (Initial temperature), T_s (Sintering temperature), T_f (final temperature), R_h (heating temperature over time), R_c (cooling temperature over time). The heating treatments carried out are: a) 1100°C for 240 minutes with a heating rate of 5°C per minute without encapsulation, b) 1100°C for 180 minutes with a heating rate of 5°C per minute with encapsulation (in crucible), and c) 1100°C for 60 minutes with a heating rate of 10°C per minute with encapsulation (in crucible).

3.1.4.2 Synthesis of $\text{KNNCu}0.5\%\text{mol}$ and $\text{KNNCu}1\%\text{mol}$

For the synthesis of the doped systems, it was synthesized KNN doped with copper in concentrations of 0.5% and 1%mol, with both chemical formulas. The procedures of synthesis, calcination, and sintering carried out were the same used for the synthesis

of KNN. For all the calcination and sintering processes, the heating rate used was 5°C per minute, except for the 1-hour sintering at 10°C/min. In the following Figure 3.3, is detailed all the different samples with their related chemical formula and the conditions of calcination and sintering.

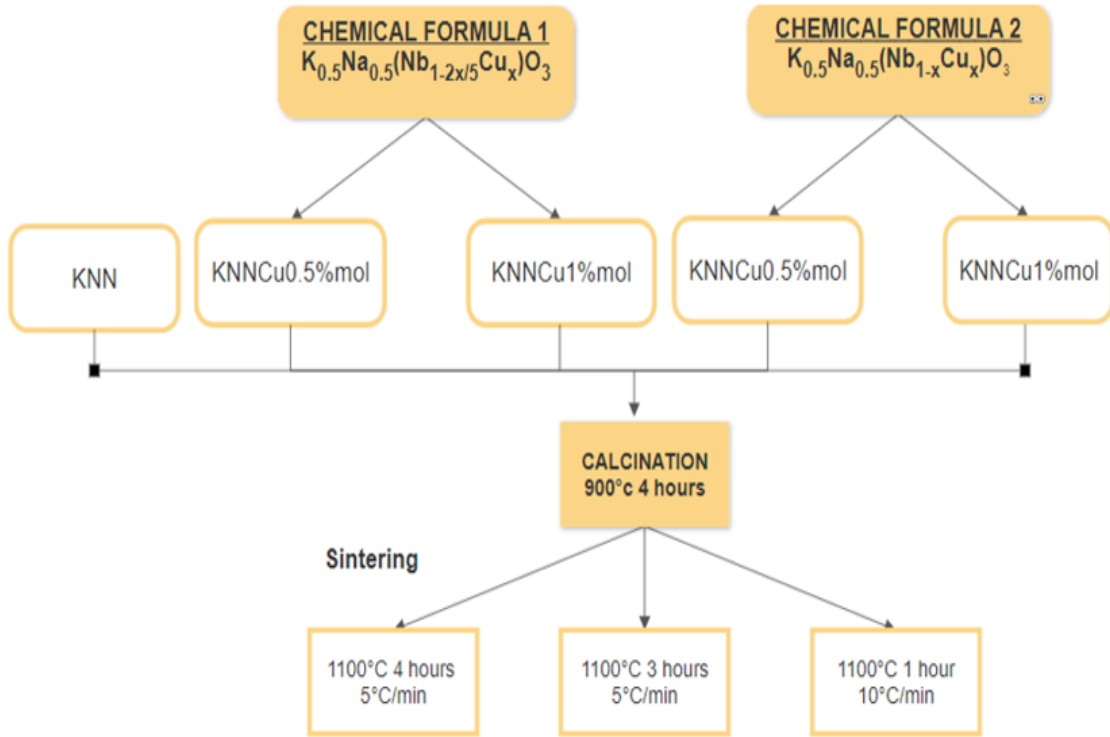


Figure 3.3: Flowchart of the samples obtained with their related chemical formula and conditions of temperature treatment in the calcination and sintering.

3.2 Target Synthesis

For the growth of thin films through sputtering, it is necessary to obtain bulk targets of 2 inches of the material which is going to be sputtered. For it, the materials were obtained through the procedure detailed in section 3.1.3 with some variants. For the targets, it was synthesized around 50 grams for each system. The powders were milled in the high energy miller for 90 minutes. After that, these were pressed in pellets of 1 inch with a pressure of

$25\text{kg}/\text{cm}^2$ and calcinated at 900°C for 4 hours without encapsulation with the heating rate showed in Figure B.9. The pellets obtained were milled again in the high energy miller or in a mortar and sieved to homogenize the grain size. Before the sintering process, the powders were dried in an oven overnight at 80°C . The powders were pressed in a pellet of 2.5 inches with a pressure of $100\text{kg}/\text{cm}^2$ for 10 minutes and these finally, were sintered in a tubular oven YF-1700 of YIFAN at 1100°C for 60 minutes with a heating rate of 10°C per minute. The samples were sintered between bases of platinum and alumina on both sides. It was obtained two targets, one of $\text{KNNCu}0.5\%\text{mol}$ and other of $\text{KNNCu}1\%\text{mol}$, and as a reference was used a bulk of pure KNN obtained in similar conditions. After the heating treatment, the target reduced in diameter from 2.5 inches to 2 inches which is the required diameter to the sputtering process.

As of result of the procedure followed, the targets obtained are illustrated in Figure 3.4. It is notable that both are non-homogeneous, which was solved with a new procedure.



Figure 3.4: Target of $\text{KNNCu}0.5\%\text{mol}$ (1) and $\text{KNNCu}1\%\text{mol}$ (2), calcinated at 900°C for 4 hours and sintered at 1100°C for 1 hour.

The target synthesis was improved, the powders firstly were milled in a mortar for 30 minutes to homogenize. After that, the powders were milled in the high energy miller

SPEX-8000 for 90 minutes. The calcination procedure was carried out for 4 hours at 900°C as the Figure B.9 shows and the sintering process was modified at 1000°C per 2 hours as the Figure 3.5 illustrates.

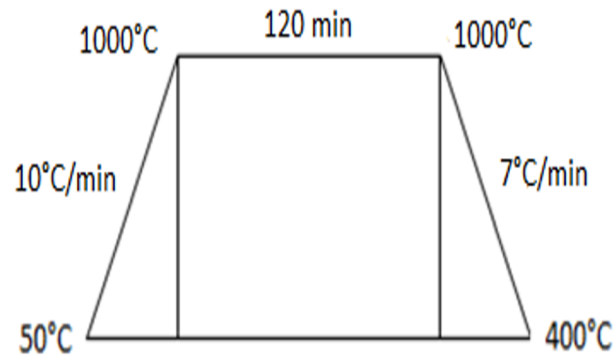


Figure 3.5: Alternative heating rate based in a sintering at 1000°C per 120 minutes with a heating rate of 10°C per minute.

Following the new sintering procedure, the targets obtained are shown in Figure 3.6. In these, it is notable that both are homogeneous compared with the previous ones. In all of the cases, the desired phase is obtained according to the XRD, which is shown in the Figure 4.27.

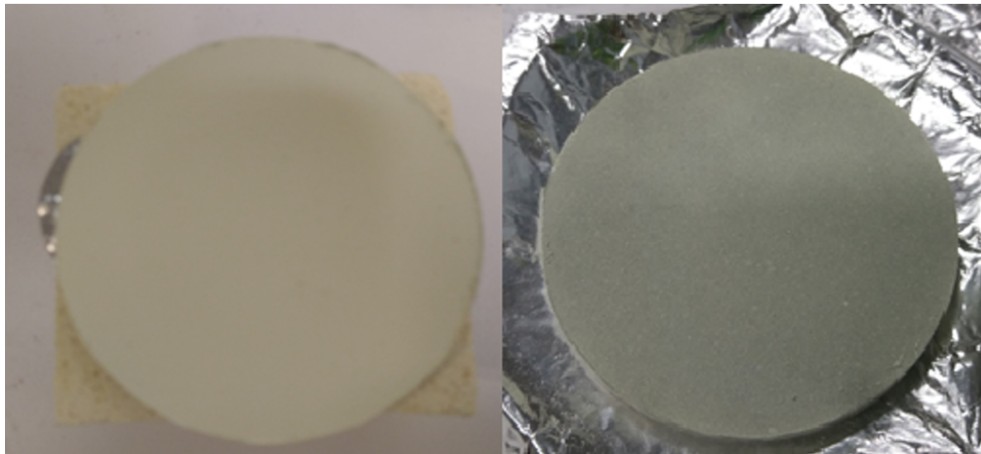


Figure 3.6: New targets of KNNCu0.5\%mol and KNNCu1\%mol obtained with the alternative heating ramp detailed in the Figure 3.5

3.2.1 Sputtering

Cathodic plasma deposition is a high energy deposition process, which is carried out under high vacuum to generate vapor emission from a bombarded target (cathode). In the process is introduced a gas, usually argon, that is ionized when a voltage is applied through a power supply and plasma is formed. The charged ions collide with the target surface and the material is deposited on the substrates [51, 18].

The equipment used for cathodic erosion was INTERCOVAMEX SPUTTERING V3, and the radio frequency power supply was a Dressler CESAR RF Power Generator, with potencies of 50, 75 and 100W. For the growth of thin films, it were used targets of KNN, KNNCu0.5%mol and KNNCu1%mol over substrates of ITO glass, ITO quartz, p- type Si, and Si-Pt coated.

3.2.1.1 Substrate preparation

To perform the sputtering deposition, it was required to follow an adequate cleaning process to remove unwanted particles from the surface, which could affect the correct growth of the films. The process to clean the ITO glass and ITO quartz substrates consists in the use of a solution in equal parts of xylene (J.T. Baker 98.5%), acetone (J.T. Baker 99.70%), and ethylic alcohol (J.T. Baker 99.90%), where the substrates were submerged in an ultrasonic bath for 10 minutes, followed by another ultrasonic bath in ethylic alcohol (J.T. Baker 99.90%) for 10 minutes and finally, rinsed with ionized water and dried with hot air.

For the substrates of p-type Si and Si-Pt coated, the process consists in an ultrasonic bath in ethylic alcohol (J.T. Baker 99.90%) for 5 minutes, followed by an ultrasonic bath in ionized water for 5 minutes and dried with hot air.

3.3 Characterization techniques for bulk and thin films

Different techniques were used to characterize the system $K_{0.5}Na_{0.5}NbO_3$ doped with copper. The properties as bulk and thin film were measured.

3.3.1 Structural characterization

3.3.1.1 Density analysis

The bulk density is known as the mass per unit volume of the particles and interstices. It is important to know the relative densities of the material since the direct dependence of storage capacity on the bulk density. A variation in the particle density could be related to changes in the phase structure, chemical composition or porosity of the ceramic samples [52].

Geometric Method.- This method consists in measuring the thickness and diameter before and after the sintering treatment, to calculate the contraction degree of the material. Considering that the pellet samples have a cylindrical shape, the following equation [3.3] was used to calculate the volume and thus estimate the density reduction percentage.

$$V = \pi * r^2 * h \quad (3.3)$$

$$\rho = \frac{m}{V} \quad (3.4)$$

Where d is the diameter of the pellet and h its thickness. The density reduction percentage was calculated through an evaluation before and after the sintering process.

Archimedes Method.- This method is based on the Archimedes' principle, which states that when an object is immersed in a fluid, it is buoyed up by a force with a magnitude equal to the fluid weight that is displaced by the object. One of the main application is related to the density measurement of an object with an irregular shape [9]. For this method, it was used a density kit, that consists in a graduated beaker filled with water in which firstly, the mass sample is measured suspended outside without contact with the water and then is measured inside the water as Figure 3.7 shows.

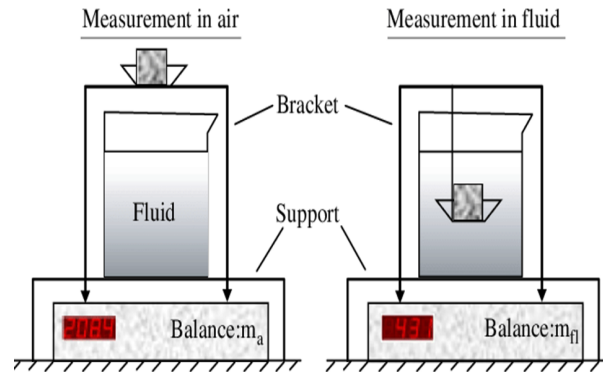


Figure 3.7: Archimedes method for densification measurement. Representation of the measurement in air and in fluid. Ref. [9]

Based on that, the density is calculated with Equation 3.5

$$\rho_p = \frac{m_a}{m_a - m_w} * \rho_w \quad (3.5)$$

Where (ρ_w) is the water density, which has a specific value dependent on the temperature, m_a is the mass of the pellet measured while is suspended in the air and m_w is the mass measured when the sample is immersed in the fluid. To take the mass values it is important to wait a few minutes while the value given by the analytic balance is stabilizing. For this study, the temperature of the water was 22°C and its density 0.9978 g/cm³.

3.3.1.2 X-Ray Diffraction (XRD)

XRD technique gives a structural analysis of materials through the determination of atomic positions, bond lengths and bond angles related to the unit cell. The X-Ray diffraction generates a series of patterns with peaks of different intensities which are used principally to follow the reaction progress and to determine specific phases [53]. For the KNN-Cu system, it was needed to find the perovskite structure, which is related to ferroelectric properties. The patterns obtained were compared with the pattern of the desired phase through the program JADE-Pattern Data Files (PDF).

The equipment used was an X-RAY DIFFRACTOMETER Rigaku, with a voltage of 30kV and current of 20mA.

3.3.1.3 Scanning Electron Microscopy (SEM)

This technique uses high-energy monochromatic electrons, which impact atoms closer to the surface. As a result of this impact, a series of elastic and inelastic signals is generated including back-scattered electrons, secondary electrons, characteristic X-rays, Auger electrons and Cathodo luminescence, each one gives different information and requires specific detectors [53]. The interactions of interest between the electrons and specimen are secondary electrons (inelastic dispersion) and backscattered electrons (elastic dispersion) that derive in images thanks to their respective detectors. Each signal depends on the depth of penetration of the electrons and therefore on the energy of the applied beam, in addition to the morphology, composition, and structure of the target. The micrographs obtained from secondary electrons give topographic information of the sample surface. In contrast, micrographs obtained from backscattered electrons can give information about the composition and structure of the sample. Moreover, it is useful for the identification of different phases on a system thanks to the different light contrasts of each atom [54].

The equipment used for this study was a Phillips XL30 ESEM, which can perform wet modes imaging from 1kV-30kV and 10X-100,000X magnification.

3.3.1.4 Profilometry

This technique provides us with topographies of roughness and thickness of thin films. Surface microtopography, as roughness, profile gives us information about its shape, size, and distribution, that differ according to the deposition processes and treatments applied [55]. Through the software, it is possible to get an average roughness and an average thickness value, which is obtained based on the gradient between the substrate and the thin film .

For this characterization technique, a Bruker Contour GT IN Motion 3D Profiler was used and its respective Bruker's Vision64 Operation and Analysis Software.

3.3.2 Dielectric, Ferroelectric and Band gap properties

3.3.2.1 Ferroelectric hysteresis

Ferroelectric materials are characterized to have an effective electric dipole moment in the absence of an external field, where the dipoles are randomly oriented. The dipoles are grouped in sections called domains, which are affected, when an electric field is applied, and the dipoles are reoriented. As a result of the change of direction of the dipoles, (P-E) hysteresis loops are obtained, where P is polarization ($\mu\text{C}/\text{cm}^2$) and E correspond to the electric field (kV/cm). These cycles present a few points of interest such as (P_s), (P_{sat}), and (E_c) which are useful to determine the ferroelectric properties of the materials. These points are illustrated in the [1.7]. The equipment used was a Precision LCII Ferroelectric Test System with its Vision Data Acquisition and Management System Software. This equipment is ideal for use with thin films and bulk ceramics. The equipment allows to apply a maximum voltage of 4000V in bulk and 4V in thin films.

3.3.2.2 Impedance spectroscopy

Ferroelectric behavior occurs in a specific temperature range, characteristic of each material. This technique allows us to determine the temperatures associated with phase transitions related to structural changes. In addition, it allows obtaining the Curie temperature, at which the spontaneous polarization falls to zero and the materials are no longer ferroelectric and change to paraelectric. Small variations in the perovskite composition could change the Curie temperature significantly [56, 113]. For the measurement, an E4990A Impedance Analyzer KEYSIGHT was used, 20 Hz to 10 MHz.

3.3.2.3 Electrical conductivity

This technique is based on the application of a voltage range over a thin film of substrate/ferroelectric ceramic (KNN)/contact (Au). This characterization test was carried out in the dark, visible light, and ultraviolet light. The measurement consists of the current produced by a variable voltage applied. The objective of this technique is to measure the photocurrent response generated by visible and ultraviolet light [57]. For this technique, the equipment used was KEITHLYE 4200-SCS Semiconductor Characterization System.

3.3.3 Band gap characterization

3.3.3.1 UV-Vis Diffuse Reflectance Spectroscopy

This technique is commonly used to characterize semiconductor materials. It allows us to extract the values of the energy bandgap based on the absorption spectra obtained and the thickness known. By illuminating a particulate material, the radiation is able to penetrate the sample and reflect from the surface. The penetrated light is scattered at various points, which transmit through the particles. The part of the radiation that is returned to the surface is considered as the diffuse reflection [58]. UV-Vis DRS is useful

in powders materials because, it takes advantage of the enhanced scattering phenomenon, where diffuse reflection does not allow the separation of different contributions such as refraction and diffraction. This model works when the particle size is equal to or less than the wavelength of the incident light. The theory which makes possible to use DR spectra is based on the theory of Kubelka-Munk, represented with the equation [3.6](#) [59](#), [60](#).

$$\frac{k}{S} = \frac{(1 - R_{\infty})^2}{2R_{\infty}} \quad \text{[59]} \quad (3.6)$$

K is known as the absorption coefficient equal to 2 and the S value is known as the scattering coefficient. In the Kubelka-Munk theory, the bandgap (E_g) and absorption coefficient are related through the Tauc relation, which are given by the equation [3.7](#) [59](#).

$$(\alpha * h * v)^n = A(hv - E_g) \quad (3.7)$$

A is a constant, and the value of n determine the energy transition process related to conductance and valence band. If n=2 or n=2/3 (indirect method), correspond to a direct allowed and forbidden transitions, respectively. But, if n=1/2 or n=2/3 (direct method) correspond to an indirect allowed and forbidden transitions, respectively [61](#). The plotted curve related to Equation [3.6](#), allows getting the value of the energy bandgap through interpolation with the x-axis. The equipment used was an Ocean Optics Spectrometer and the Analytical Instrument System AIS Model UV-2D.

CHAPTER 4

RESULTS

4.1 Bulk characterization

4.1.1 Estructural characterization

In the following section are showed and discussed the obtained results through the density test, X-Ray Diffraction (XRD), and Scanning Electron Microscopy (SEM) for the bulk samples of the system KNN-Cu doped.

4.1.1.1 Density analysis

Once the bulk pellets were sintered, the thickness and diameter were measured to see the degree of contraction of the material. With this same data, the geometric density was calculated and compared with that obtained by the Archimedes method as shown in Table [4.1](#) shows. All the values of the density obtained by the Archimedes method are greater than 90% taking into account the relative density $4.51g/cm^3$, which shows that all samples have good densification. In previous research, the copper was used to improve the densification of ceramics [\[62\]](#), in this research the densification of the material improves as

well comparing KNN with KNNCu0.5%mol. However, the densification values decrease for the samples of KNNCu1%mol sintered at three different times, but its values keep over 90%, which is a good relation. The effects of 0.5, 1.0, 1.5 and 2 mole% CuO has been studied, and how are related to grain growth and hence with the densification [3, 46, 17].

Sample	Property	4 hours	3 hours	1 hour
KNN	Contraction	9.1%	10.5%	9.8%
	Geometric density	80.5%	93.9%	92.74%
	Archimedes density	91.4%	94.1%	93.4%
KNNCu0.5%M Formula 1	Contraction	10.2%	10.5%	10.5%
	Geometric density	81.5%	93.9%	93.3%
	Archimedes density	94.6%	94.1%	93.9%
KNNCu0.5%M Formula 2	Contraction	12,7%	10%	13.4
	Geometric density	-	71,2%	100.2%
	Archimedes density	93.6%	95.5%	94.4%
KNNCu1%M Formula 1	Contraction	10%	6.9%	9.8%
	Geometric density	90.9%	75.6%	92.4%
	Archimedes density	94.6%	94.0%	92.8%

Table 4.1: Contraction analysis taking into account values from geometric and Archimedes method

4.1.1.2 X-Ray Diffraction

All of the samples crystallized as a pure perovskite. Diffraction patterns are associated with PDF 61-0315 - $K_{0.5}Na_{0.5}NbO_3$ (monoclinic), which was obtained with the database (Pattern Data File) from JADE program . The related cell parameters are: $a=4.00462\text{\AA}$, $b=3.94464\text{\AA}$, $c=4.002\text{\AA}$, $\alpha=90^\circ$, $\beta=90.333^\circ$, and $\gamma=90^\circ$, It is observed in Figure 4.1 that this phase is obtained since the early calcination stage. It is observed that as copper is added a monoclinic phase is obtained.

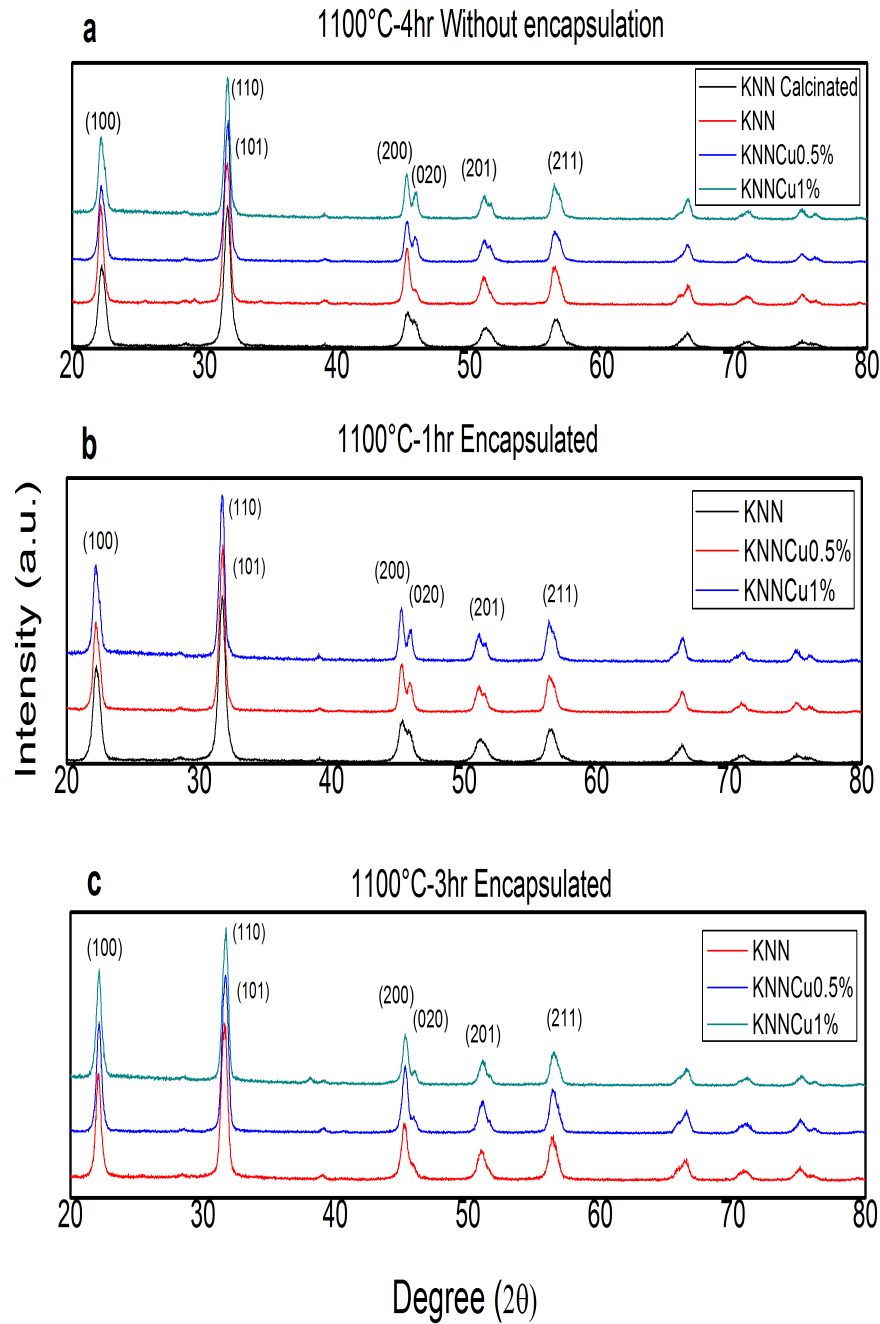


Figure 4.1: XRD for samples calcinated powders of KNN, and bulk samples of KNNCu0.5%mol and KNNCu1%mol sintered at: a)1100°C for 4 hours without encapsulation, b)1100°C for 1 hour encapsulated, and c)1100°C for 3 hours encapsulated.

In order to discuss the sample crystallinity it was considered a region from the three systems to compare the peaks of each one. In the Figure [4.2](#), there is a comparison between diffractograms of the systems: KNN, KNNCu0.5%mol, and KNNCu1%mol in a range of 40° to 55° . Based on the principal peaks, it is notable that the copper doping increases the crystallinity of the sample.

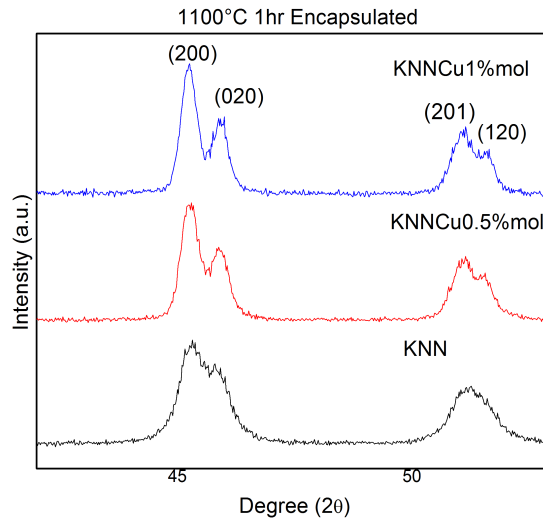


Figure 4.2: Diffractogram of KNN, KNNCu0.5%mol and KNNCu1%mol in bulk, sintered at 1100°C for 1 hour.

The crystallite size obtained for the systems KNN, KNNCu0.5%mol, and KNNCu1%mol were: 141.75\AA , 242.75\AA , 305.75\AA , respectively. These values were obtained as an average of a crystalline size (XS) from a certain crystallographic reflection, which are representative for the sample. The reflections taken into account are detailed in the Table [4.2](#), as we can see the FWHM (Full Width at Half Maximum) values are close in each case, so that the crystalline size is more adequate.

Sample	2θ	hkl	FWHM	XS (Å)
KNN	22.1493	100	0.5230 (0.0059)	247 (4)
	31.6320	110	0.5539 (0.0043)	205 (3)
	45.2188	200	0.5147 (0.0116)	225 (6)
	45.9004	020	0.4719 (0.0323)	262 (19)
KNNCu0.5%mol	22.2237	100	0.6122 (0.0088)	181 (4)
	31.6796	110	0.5483 (0.0061)	208 (3)
	45.2208	200	0.4373 (0.0155)	306 (12)
	45.8614	020	0.4911 (0.0259)	244 (14)
KNNCu1%mol	22.2089	100	0.5783 (0.0037)	200 (2)
	31.6645	110	0.4942 (0.0025)	254 (2)
	45.2089	200	0.3953 (0.0051)	398 (6)
	45.8655	020	0.4145 (0.0081)	347 (8)

Table 4.2: Values of 2θ , FWHM, and XS, for the crystallographic reflections at (100), (110), (200), and (020), for the samples of KNN, KNNCu0.5%mol, and KNNCu1%mol sintered 1 hour at 1100°C.

The peaks present in the patterns and the crystallite size confirm, that as the copper concentration increases, the crystallite size also increases. The same analysis was developed for the systems: KNN, KNNCu0.5%mol, and KNNCu1%mol sintered for 3 and 4 hours in the annexes [5.1](#), where it is notable the same behavior.

Through the FWHM values, it was possible to obtain an average value of the crystallite size for each system, as we can see in the table [4.3](#). It is notable that the one hour sintered samples have superior crystallite growth when copper is added to the system, compared to the 3 and 4 hour sintered samples. In the case of samples sintered for 4 hours, it can be seen that there is no relevant change in crystallite size when doping with copper. Furthermore, in all cases of KNNCu1 mol%, the crystallite size is similar [4.3](#).

Sintering time	KNN	KNNCu0.5%mol	KNNCu1%mol
1 hour	145(1)	192(1)	246(2)
3 hours	186(1)	208(2)	243(2)
4 hours	204(1)	208(1)	246(2)

Table 4.3: Average crystallite values for the samples of KNN, KNNCu0.5%mol, and KNNCu1%mol sintered 1, 3, and 4 hours at 1100°C.

4.1.1.3 Scanning Electron Microscopy

In this section are shown the micrographs of SEM, related to the bulk samples of KNN, KNNCu0.5%mol and KNNCu1%mol with their different sintering conditions of heating time and encapsulation.

KNN

The micrographs of Figure 4.3 represent the samples of KNN sintered at 1100°C for 1 hour with encapsulation, 3 hours with encapsulation and 4 hours without encapsulation. For all the samples it is difficult to define a specific size grain because of the incipient fusion, which increases with the time of sintering. For the samples sintered for extended periods, there are a bimodal grain size formation by the presence of grain size $<1 \mu\text{m}$ and other around $5 \mu\text{m}$ [3]. For 1 and 3 hours of sintering with encapsulation, it is difficult to define a grain size however, for the bulk sample sintered for 4 hours without encapsulation, it is visible the formation of elongated agglomerates of approximately $7 \mu\text{m}$,

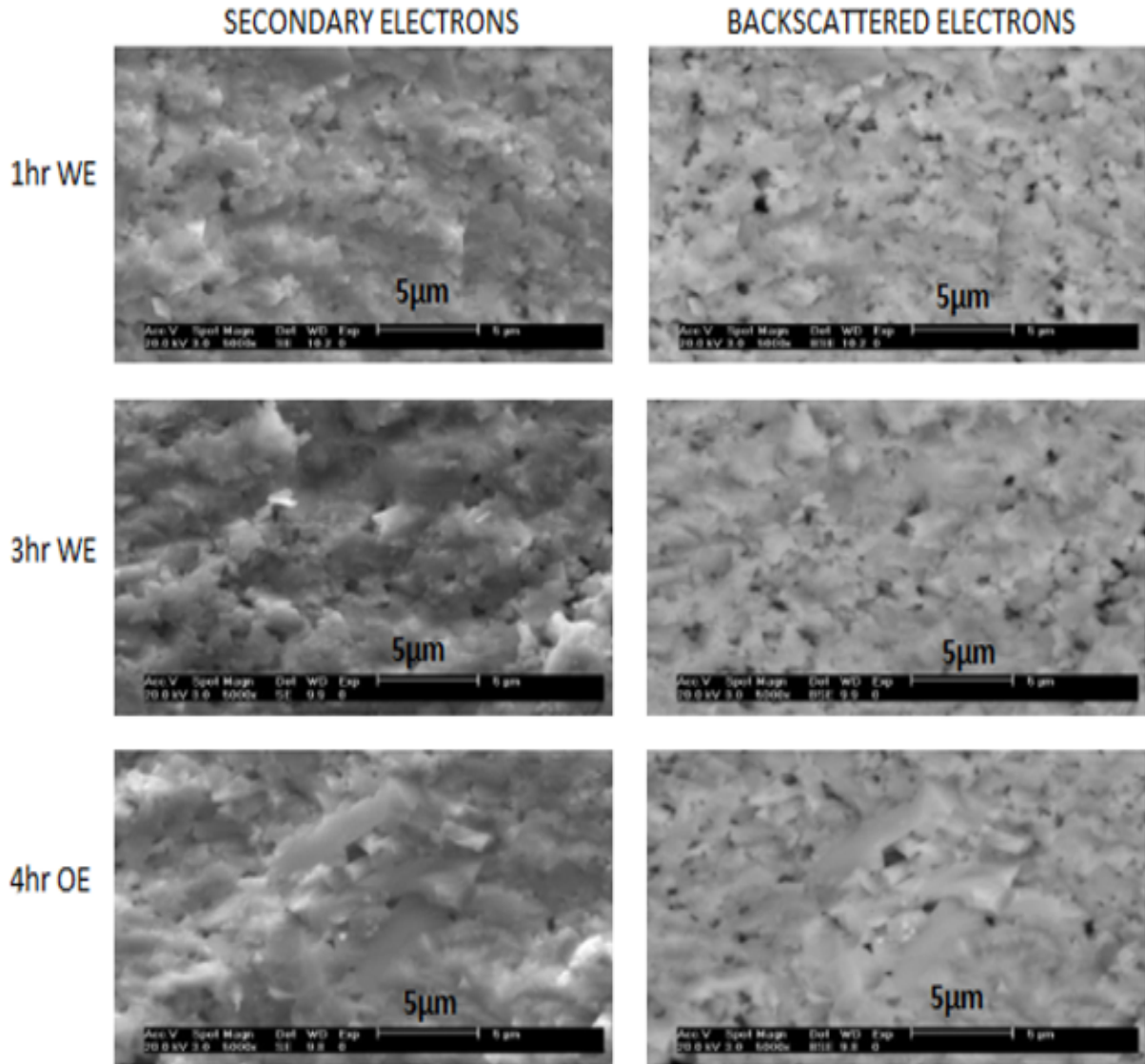


Figure 4.3: Micrographs of secondary and backscattered electrons for the bulk sample KNN sintered at 1100°C for 1,3 and 4 hours. WE (encapsulated in a crucible), OE (without encapsulation).

KNNCu0.5%mol

Below are show micrographs related to samples of KNNCu0.5%mol sintered at the same conditions but prepared with different stoichiometric composition (Chemical formula 1 and chemical formula 2).

Sintered 4 hours(OE) using the chemical formula 1 and 2

In Figure 4.4 and Figure 4.5, there are the micrographs of samples of KNNCu0.5\%mol synthesized with chemical formula 1 and chemical formula 2.

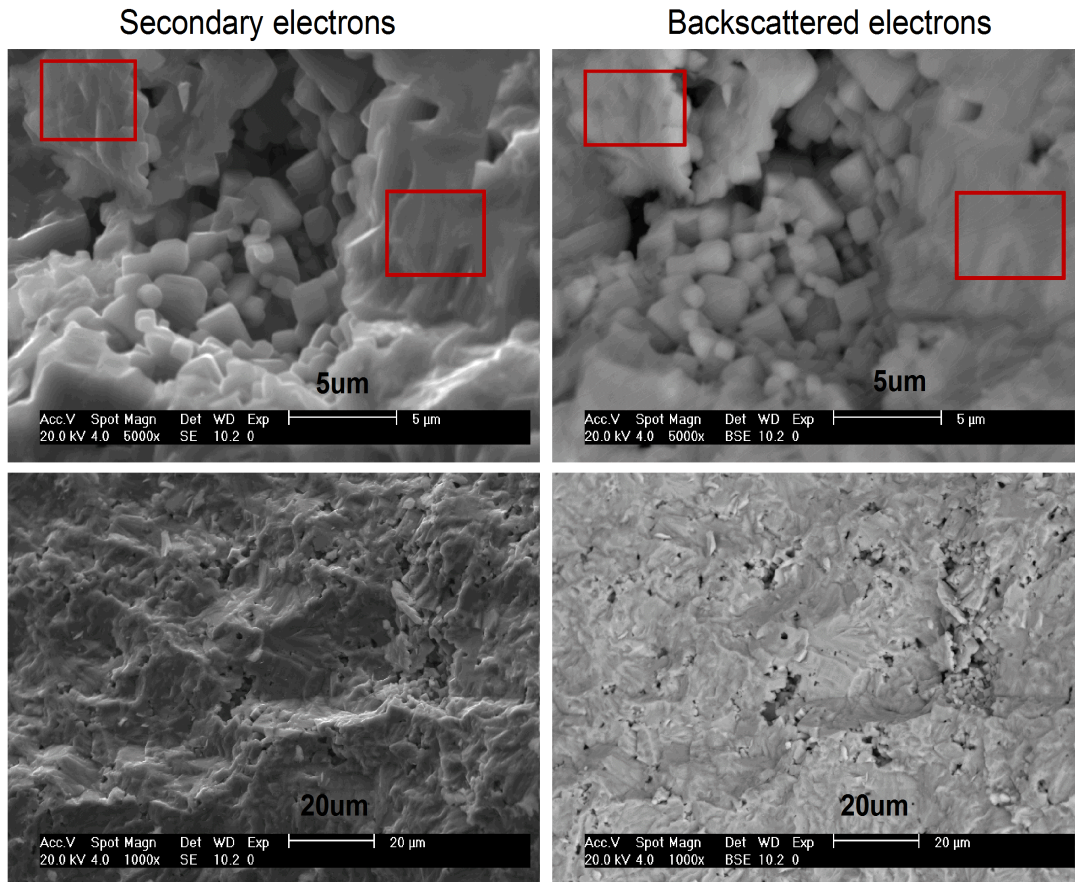


Figure 4.4: Micrographs of secondary and backscattered electrons of KNNCu0.5\%mol samples sintered for 4 hours at 1100°C - Formula 1.

It can be observed in certain zones that there is no homogeneous grain formation with grain boundaries in both of the cases. The SEM micrographs of the sintered samples show

regions with grain size between 1-2 μm , as well as areas with not well-defined grain edges (red zones) probably due to incipient fusion.

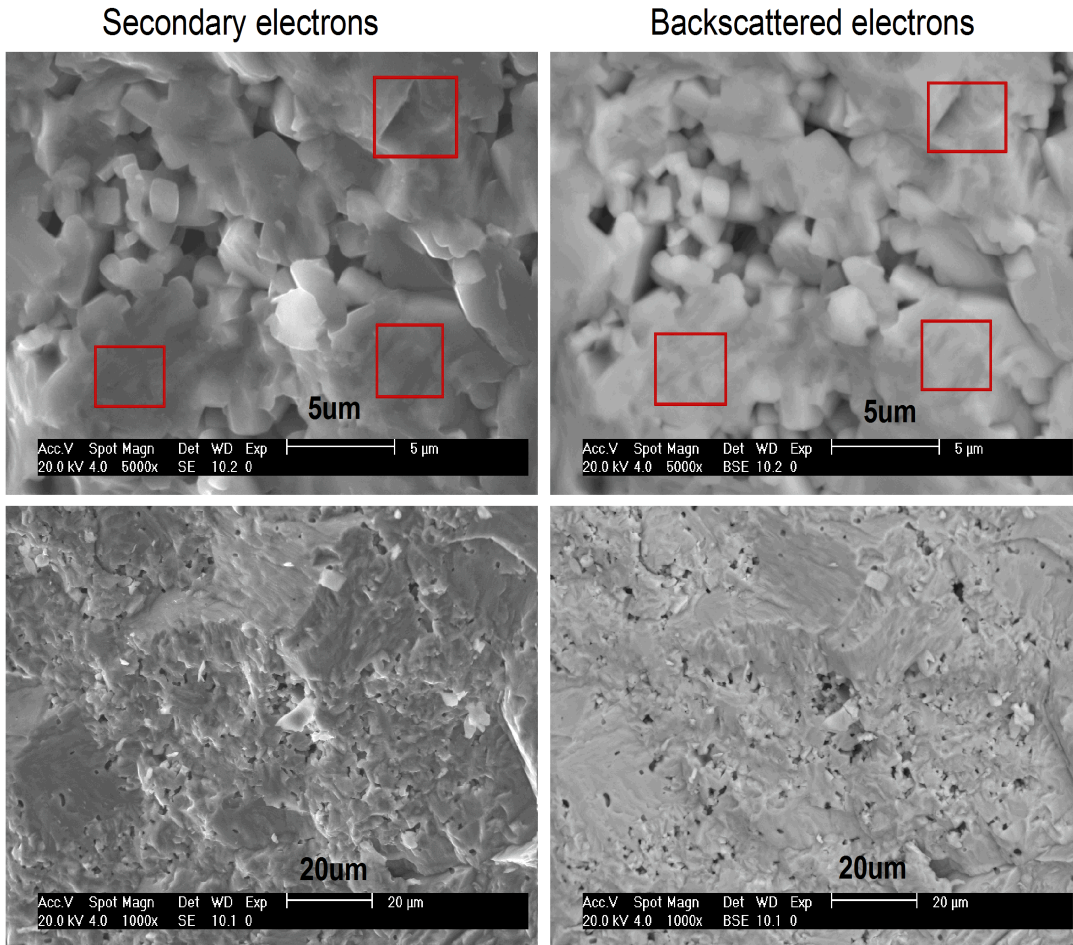


Figure 4.5: Micrographs of secondary and backscattered electrons of KNNCu0.5%mol bulk samples calcined at 900°C for 4 hours and sintered at 1100°C for 4 hours – Formula 2.

As the phase diagram shows in the figure [1.5](#) the melting point is about 1140°C and 1280°C, and the temperature of sintered used in the research was 1100°C. The fact that there is partially grain boundary can be attributed to the long sintering periods, causing

a tendency of the grains to melt or by the addition of copper, which could decrease the melting point. To doping the KNN system with certain elements like copper, lithium or tantalum, has a influence on the melting temperature as has been reported in previous works [30, 63, 64, 3]. Based on these results, experiments were performed sintering the samples with a heating rate of 10°C per minute and reducing the treatment time to 1 hour at the same temperature.

Comparing the micrographs related to formula 1 (4.4) and formula 2 (4.5), it can be seen how there is a smaller proportion of defined grains in the sample developed from formula 2. A greater incorporation of copper into the structure can influence the formation of greater melting zones as we can see in the figure 4.5.

KNNCu_x-WE-1hr-Chemical formula 1

In Figure 4.6, an increase in grain size is shown as the concentration of copper in the structure is increased. In pure KNN micrographs, it is difficult to define the formation of grains and their defined limits. From the KNNCu0.5% mol, an increase amount of grains are observed of 1-2 μ m size are defined. And finally, in the KNNCu1% mol, grains of a specific size between 1-5 μ m are clearly defined without fusion presence. The addition of copper has an influence on the microstructure and promotes a grain coarsening [3]. According to the BSE micrographs, it is visible the presence of a single phase, which is homogeneous mostly in the 3 compositions (KNN, KNNCu0.5%mol, and KNNCu1%mol).

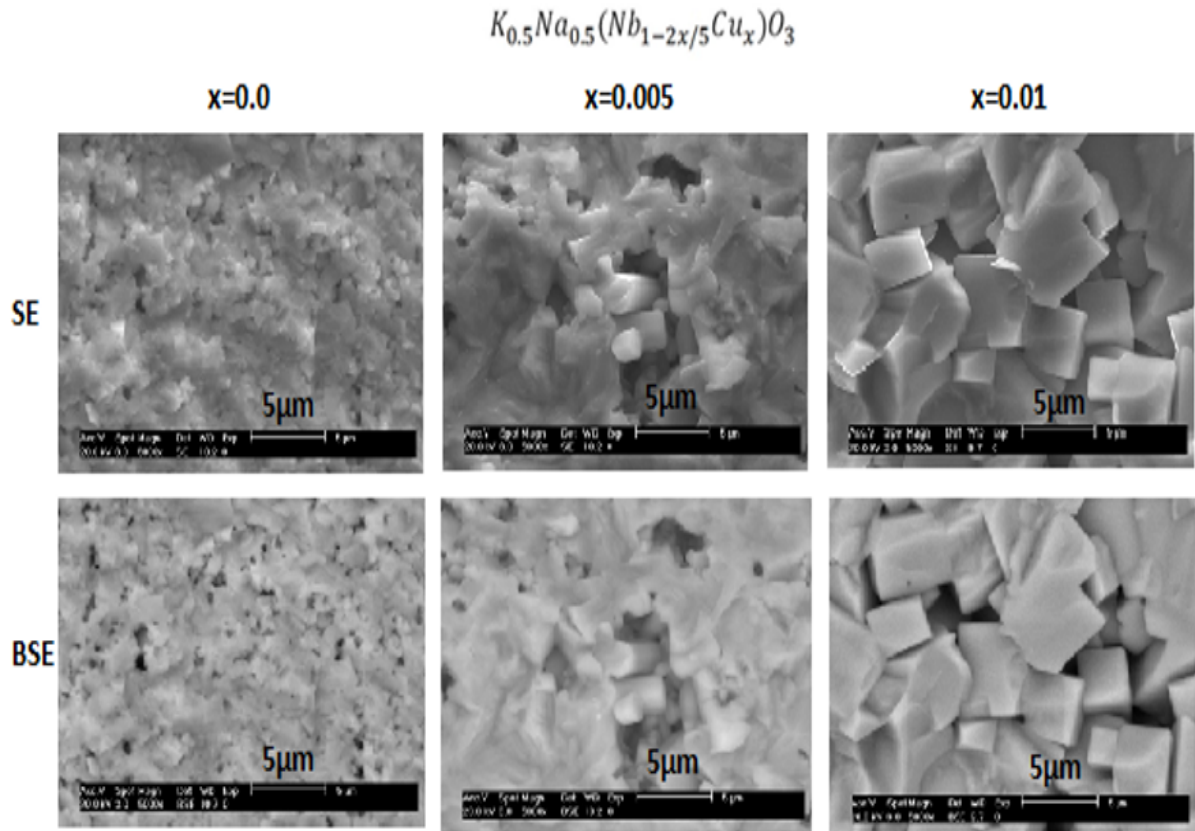


Figure 4.6: Micrographs of secondary and backscattered electrons of KNN ($x=0$), KN-NCu0.5%mol ($x=0.005$) and KNNCu1%mol ($x=0.01$) sintered for 1 hour.

4.1.2 Dielectric, ferroelectric and optical characterization

4.1.2.1 Ferroelectric hysteresis

In this section, the ferroelectric characterization of the systems KNN, KNNCu0.5%mol, and KNNCu1%mol are shown. Specifically, the hysteresis loops were recorded, and, in some samples also normalized capacitance and the remnant hysteresis.

KNN

Figure [4.7](#) illustrates the hysteresis loop for the system KNN sintered for 4 hours without

encapsulation (a) and for 3 hours (b). For the KNN (a), the important values found for the measurement at 3600V for 200Hz are: $P_s = 27.0052\mu C/cm^2$, $P_r \approx 18.451\mu C/cm^2$, and $E_c \approx 22.4621kV/cm$. These values are improved for the KNN sample (b) and measured at 3600V for 200Hz, giving the following values: $P_s = 30.004\mu C/cm^2$, $P_r \approx 21.8804\mu C/cm^2$, and $E_c \approx 21.6463kV/cm$. It is notable, that in both samples there is a ferroelectric behavior, but the encapsulation improves slightly the material properties. The improvement is related to a higher P_s for the encapsulate sample in a crucible, which help to reduce the oxygen flux and to keep a homogeneous temperature over the sample.

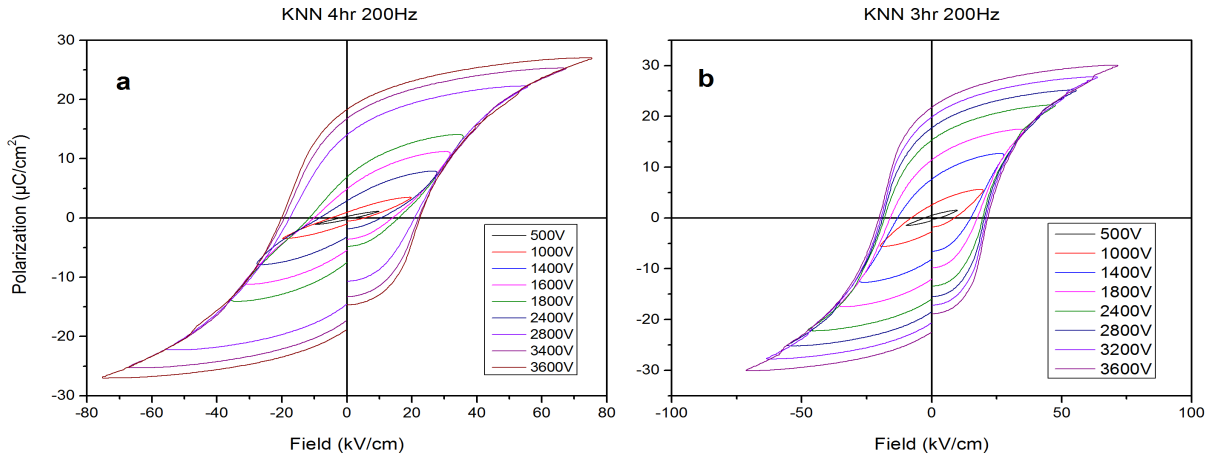


Figure 4.7: P-E loop for the KNN system in bulk sintered at $1100^\circ C$ for 4 hours without encapsulation and for 3 hours with encapsulation. Measurement carried out at 200Hz for different voltages.

KNNCu0.5%mol

Figure 4.8 is related to the sample synthesized with stoichiometry of the Chemical Formula 1 and sintered for 4 hours at $1100^\circ C$ without encapsulation. There are differentiated by the frequencies of the electrical field are applied, which are 100Hz (a) and 200Hz (b), respectively. In both cases, the samples present an antiferroelectric behavior. In the figure, the widening of the loops represents the presence of charge leakage.

On other side, at the higher voltages, a double “pseudo-hysteresis” loops were represented in the Figure 4.8 (a) and (b), showing an open gap in the origin point could be related to

the coexistence of a ferroelectric and antiferroelectric [5]. A saturation polarization is not reached in both periods for any voltage applied and the values of polarization obtained are low compared with the samples of KNN.

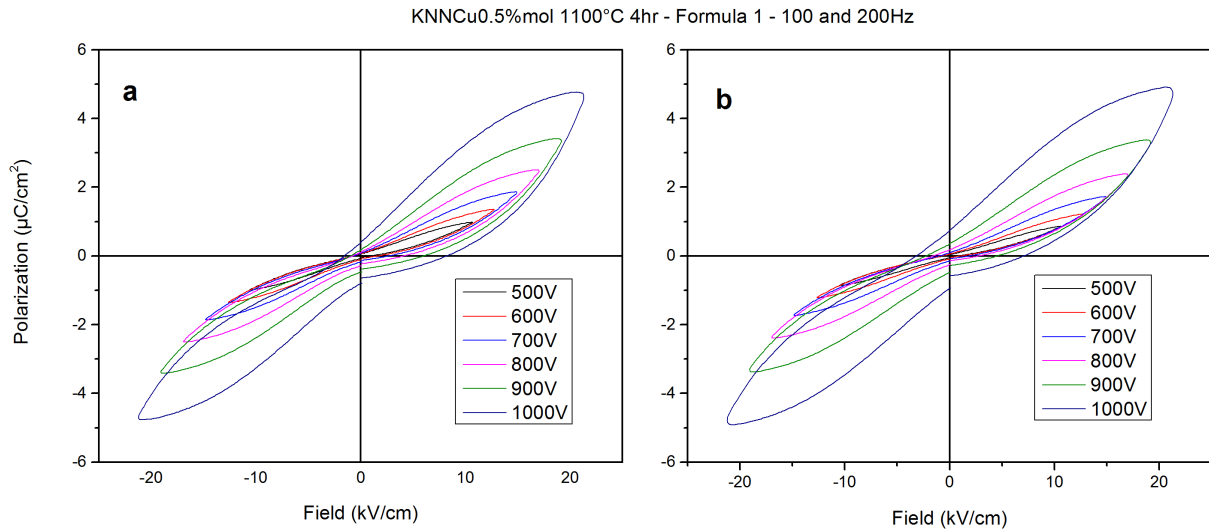


Figure 4.8: P-E loops for the bulk sample KNNCu0.5%mol, synthesized with the formula 1 and sintered at 1100°C for 4 hours without encapsulation- Frequencies of a(100Hz) and b(200Hz).

The sample obtained with the same conditions, but using the stoichiometry deduced from chemical formula 2, presents a similar antiferroelectric behavior as Figure 4.9 shows. It presents a higher value of polarization than the sample obtained with chemical formula 1, but it still been lower than KNN. The presence of charge leakage is still high and the coexistence of a ferroelectric and antiferroelectric phase is also notable.

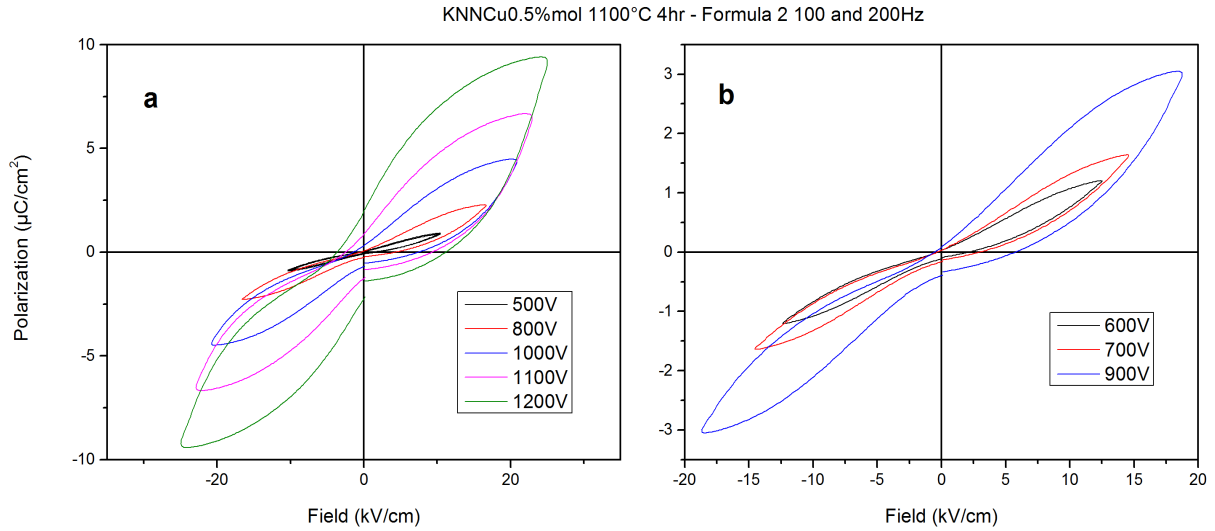


Figure 4.9: P-E loops for the bulk sample KNNCu0.5%mol, synthesized with formula 2 and sintered 4 hours without encapsulation. Frequencies of a(100H) and b(200Hz).

Figure [4.10](#), corresponds to the KNNCu0.5%mol samples sintered for 3 hours with encapsulation. At the maximum applied voltage of 3000V with a frequency of 200Hz, a ferroelectric behaviour is observed. where the following values were reached: $P_s = 27.0098\mu C/cm^2$, $P_r \approx 17.443\mu C/cm^2$, and $E_c \approx 19.1798kV/cm$. At lower electric field applied there is a double loop related to an antiferroelectric phase. As the voltage is increased there is the coexistence of ferroelectric and antiferroelectric properties.

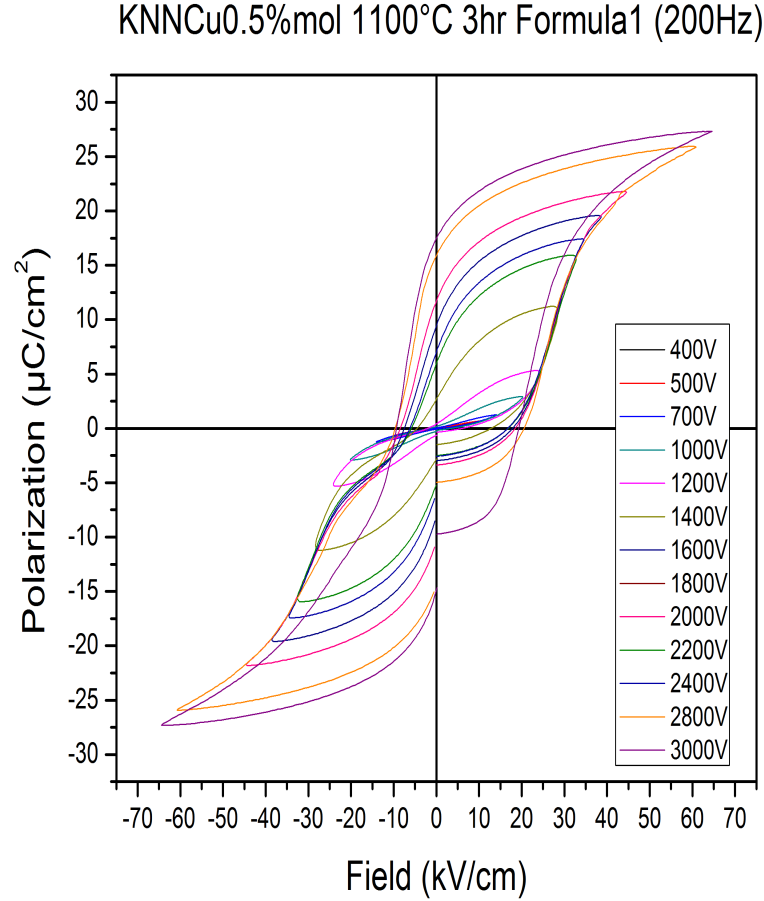


Figure 4.10: P-E loops for the bulk sample KNNCu0.5%mol synthesized with the chemical formula 1 and sintered at 1100°C for 3 hours with encapsulation – Frequency of 200Hz for different voltages.

Figure [4.11](#) shows the same sample with polarization measurements at long period of 100ms, which is equivalent to a frequency of 10Hz. The maximum saturation polarization was $P_s = 30.0063\mu\text{C}/\text{cm}^2$ with a $P_r \approx 20.7373\mu\text{C}/\text{cm}^2$, and $E_c \approx 19.8272\text{kV}/\text{cm}$, which was obtained for 3600V applied with a frequency of 13.3Hz. Therefore, for higher electric field applied the loop corresponds to a ferroelectric phase. The P_s decrease significantly when the frequency increase to 10Hz with the same electric field applied.

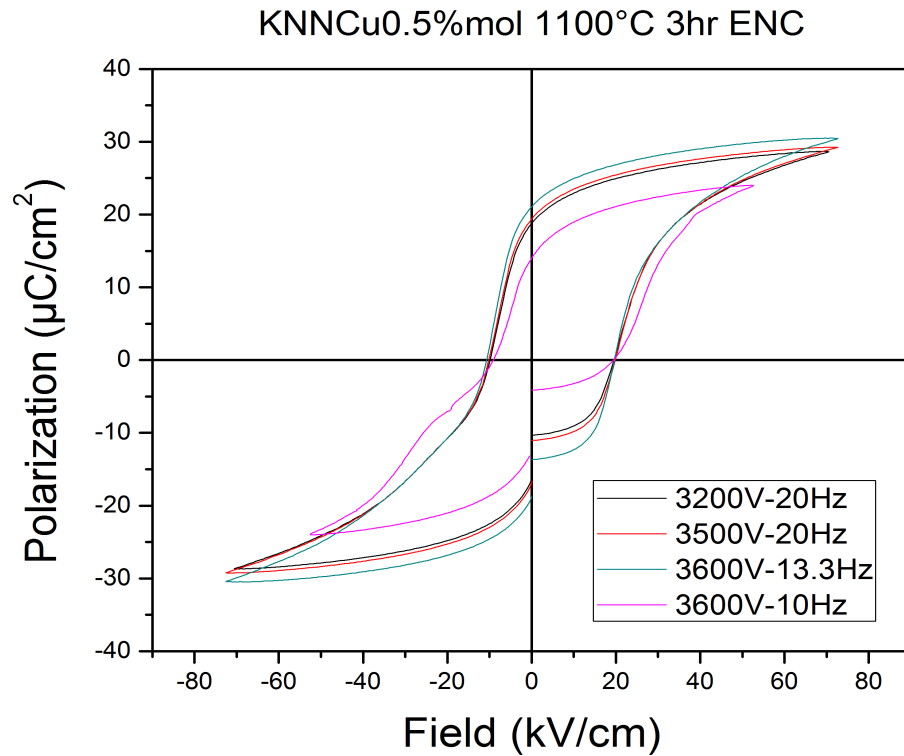


Figure 4.11: P-E loops for the bulk sample KNNCu0.5%mol sintered at 1100°C for 3 hours with encapsulation – Frequencies of 10, 13,3, and 20Hz.

In the Figure [4.12](#) there is a representation of a polarization vs voltage, giving us a “real” hysteresis related to the material, where are discarded the contributions of spatial charges, which could be related to conduction and defects. This behavior is related in the absence of symmetry in the hysteresis curves without a close cycle, which is caused by spatial charges associated with the voltage applied in continuous cycles.

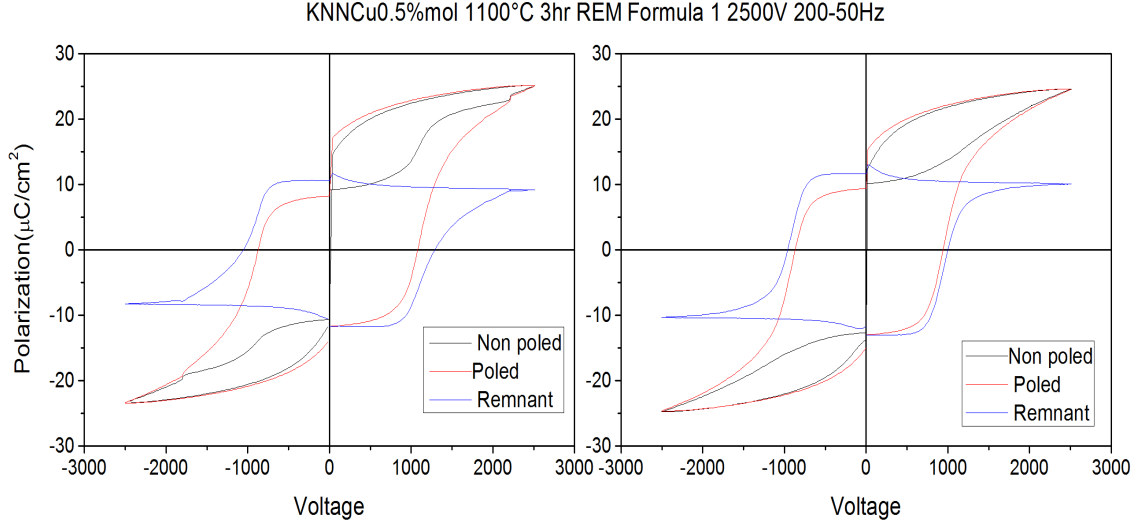


Figure 4.12: Remnant polarization for the sample of KNNCu0.5%mol, sintered at 1100°C for 3 hours with encapsulation- Measurement carried out at 2500V with a frequency of 200 and 50Hz, respectively.

As the sintering time was reduced to 1 hour with encapsulation, the material improves its properties as Figure 4.13 and Figure 4.14 show.

In the first case, for the sample of KNNCu0.5%mol sintered for 1 hour at 1100°C and measured at different voltages, the values obtained were: $P_s \approx 23.1840 \mu C/cm^2$ with a $P_r \approx 9.5073 \mu C/cm^2$, and $E_c \approx 18.1051 kV/cm$. The sample presents a defined double loop characteristic of a antiferroelectric material, with a high value of P_s and absence of charge leakage as we can see in the figure 4.13. In this case, the stoichiometry of the sample was carried out using the chemical formula 1.

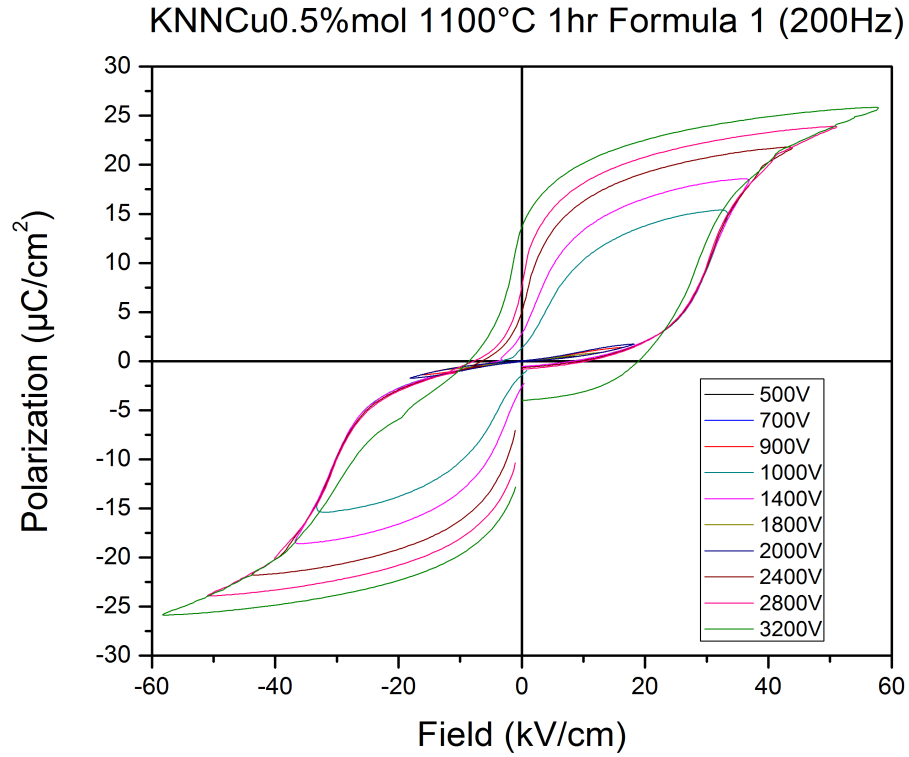


Figure 4.13: P-E loops for the sample KNNCu0.5% synthesized with formula 1 and sintered 1-hour with encapsulation. Frequency of 200Hz.

Figure 4.14 shows the hysteresis loop of the electric field applied for different frequencies in the KNNCu0.5%mol sample, sintered at 1100°C for 1 hour and synthesized with chemical formula 1. A higher polarization is obtained at a frequency of 10Hz, with the following values: $P_s = 24.0316 \mu C/cm^2$ with a $P_r \approx 11.8257 \mu C/cm^2$, and $E_c \approx 17.334 kV/cm$. This sample also has the band in the origin point, which is a signal of the coexistence of the ferroelectric and antiferroelectric phase in the material.

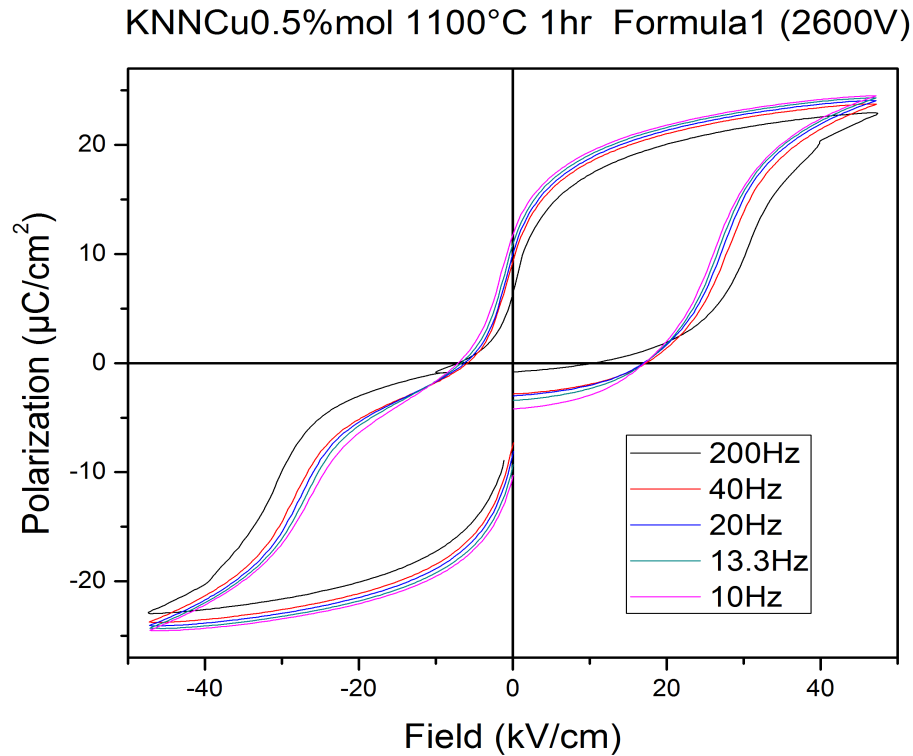


Figure 4.14: P-E loops of the sample KNNCu0.5%mol sintered 1-hour with encapsulation. 2600V applied at different frequencies.

Additional measurements were carried out using alternative options of the Precision LCII Ferroelectric Test System to demonstrate the ferroelectric behavior. Figure 4.15 shows the normalized capacitance where the presence of an antiferroelectric material is confirmed, due to its four peaks (two are overlapping), which describe the minimum energy of this system. These measurements were carried out through alternatives options of the Precision LCII Ferroelectric Test System.

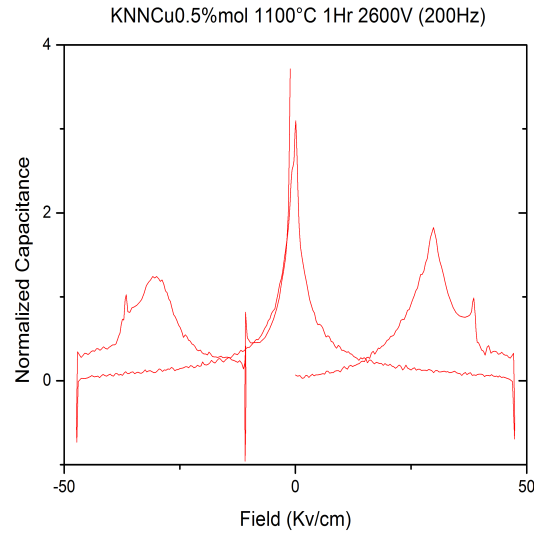


Figure 4.15: Normalized capacitance of the sample KNNCu0.5%mol sintered 1-hour with encapsulation. Frequency of 200Hz

Now, with the hysteresis loops, the following values are obtained at 2200V for a frequency of 200Hz: $P_s = 23.1702\mu C/cm^2$ with a $P_r \approx 9.5073\mu C/cm^2$, and $E_c \approx 18.1051kV/cm$. And for the extended periods of 100ms(10Hz) with 2600V: $P_s = 19.0031\mu C/cm^2$ with a $P_r \approx 3.7456\mu C/cm^2$, and $E_c \approx 9.5309kV/cm$.

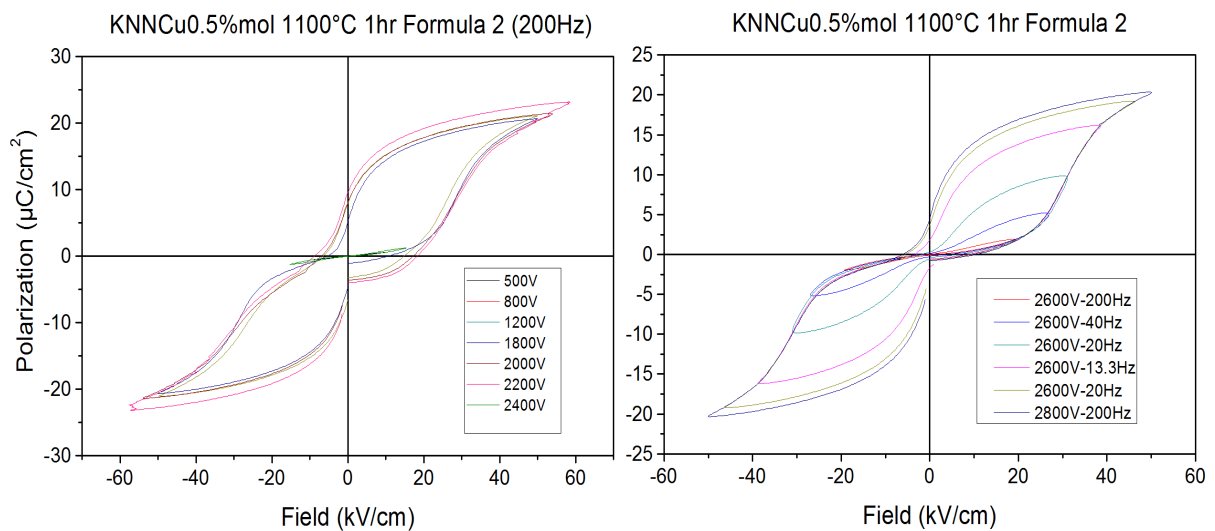


Figure 4.16: P-E loops of KNNCu0.5%mol sample, sintered 1-hour with encapsulation.

Figure 4.16 describes the antiferroelectric behavior of the sample developed with chemical formula 2 and how it supports high voltages for long periods as in the previous sample.

For this case, remnant hysteresis is observed in Figure 4.17(a), where the spatial charge is separated from the polarization to obtain a “real” hysteresis loop is obtained. The normalized capacitance was also performed in Figure 4.17(b), where its antiferroelectric behavior is confirmed, by the presence of the four peaks corresponding to its energy minimum, two of them are overlapping.

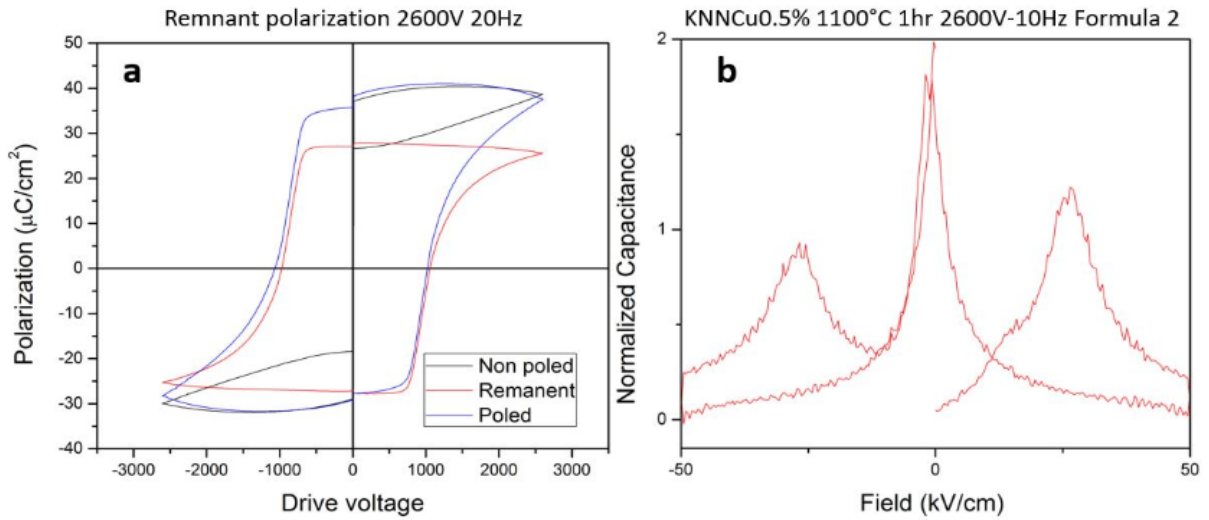


Figure 4.17: a) Remnant hysteresis at 2600V (20Hz) for KNNCu0.5%mol sintered 1 hour with encapsulation, b) Normalized capacitance for KNNCu0.5%mol sintered 1 hour with encapsulation. Antiferroelectricity behavior at 2600V for 10Hz.

KNNCu1%mol

In Figure 4.18 the ferroelectric behavior of the sample using the stoichiometry of chemical formula 1 is observed. At 2400V for a frequency of 200Hz, it was obtained a $P_s = 21.6949 \mu C/cm^2$ with a $P_r \approx 17.2322 \mu C/cm^2$, and $E_c \approx 20.6261 kV/cm$. The P-E loops

show us that when adding more copper, it loses the antiferroelectric behavior and in the same way the remaining polarization decreases.

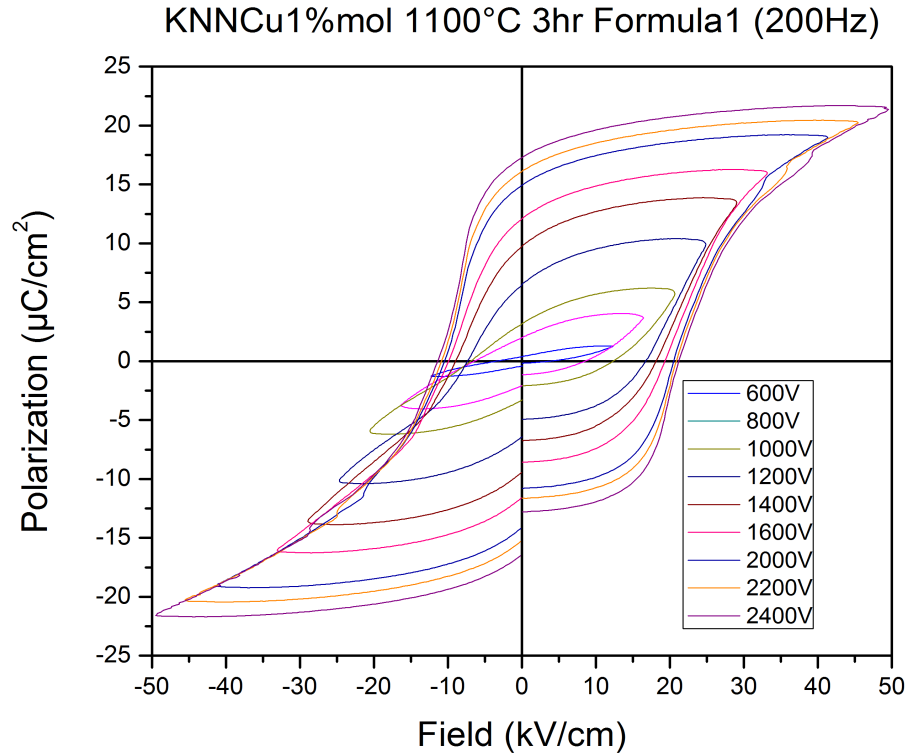


Figure 4.18: P-E loops of the sample KNNCu1%mol sintered 3 hours with encapsulation. Frequency of 200Hz

Now, for the sample synthesized under the stoichiometry of chemical formula 1 but, sintered for 1 hour with encapsulation, the Figure [4.19](#) shows a small concavity change (for high field values), which already indicates the presence of charge leakage when the sample is subjected to long periods of voltage. This is due to the excess of copper, which increases the conductance of the material [\[11\]](#).

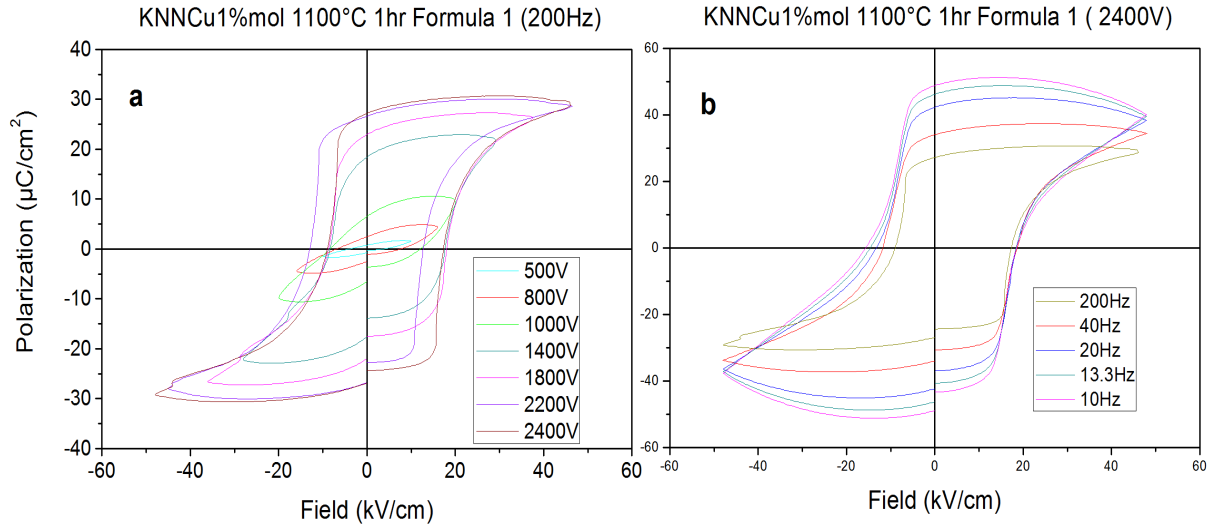


Figure 4.19: P-E loops for the sample KNNCu1%mol sintered 1-hour with encapsulation. Frequency of 200Hz (a) and 10, 13.3, 20, 40, 200Hz (b).

For the same sample, the remnant polarization and normalized capacitance were recorded and the results are shown in Figure 4.20 (a) and (b), respectively. (a) represents a remnant polarization measurement, which allow us to dismiss the polarization cause by spatial charges and shows a “real” behavior of the hysteresis loop. In (b) the graphic of normalized capacitance, presents two peaks which is related to ferroelectric phase presence.

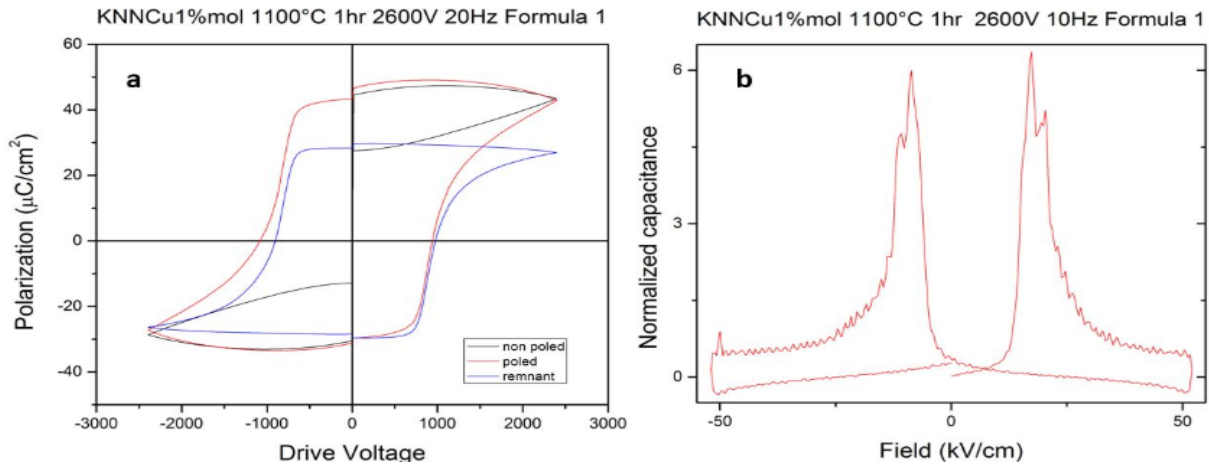


Figure 4.20: a) Remnant polarization (2600V-20Hz) and b) Normalized capacitance (2600V-10Hz) of KNNCu1%mol sintered 1 hour with encapsulation.

Finally, in the Table 4.4, there is a summary of the values of saturation polarization (P_s), remnant polarization (P_r), and coercitive field (E_c) for all of the bulk samples. The KNNCu0.5% mol 1hr (3200V 200Hz) and KNNCu0.5% samples can stand out for their antiferroelectric compartment, with high saturation values and low remnant values.

BULK SAMPLE	P_s ($\mu\text{C}/\text{cm}^2$)	P_r ($\mu\text{C}/\text{cm}^2$)	E_c (kV/cm)	Ferroelectric state
KNN 4 hours (3400V 200Hz)	27.0052	18.451	22.4621	Ferroelectric
KNN 3 hours (3600V 200Hz)	30.004	21.8804	2.6463	Ferroelectric
KNNCu0.5%mol 4 hours (1000V 10Hz) F1	4.7655	3.97	8.2008	Antiferroelectric
KNNCu0.5%mol 4 hours (1200V 100Hz) F2	9.4094	1.98	11.0435	Antiferroelectric
KNNCu0.5%mol 3 hours (3000V 200Hz) F1	27.0098	17.443	19.1798	Antiferroelectric
KNNCu0.5%mol 3 hours (3600V 10Hz) F1	30.0063	20.7373	19.8272	Antiferroelectric
KNNCu0.5%mol 1 hour (3200V 200Hz) F1	23.1840	9.5073	18.1051	Antiferroelectric
KNNCu0.5%mol 1 hour (2600V 10Hz) F1	24.0316	11.8257	17.334	Antiferroelectric
KNNCu0.5%mol 1 hour (2200V 200Hz) F2	23.1702	9.5073	18.1051	Antiferroelectric
KNNCu0.5%mol 1 hour (2600V 10Hz) F2	19.0031	3.7456	9.5309	Antiferroelectric
KNNCu1%mol 3 hours (2400V 200Hz) F1	21.6949	17.2333	20.6261	Ferroelectric
KNNCu1%mol 1 hour (2400V 200Hz) F1	30.6729	27.1174	17.3401	Ferroelectric

Table 4.4: Resume of hysteresis results for bulk samples.

The measurements of hysteresis evidenced how the antiferroelectric properties are more evident in KNNCu0.5%mol, while for samples of KNN, and KNNCu1%mol the behavior is ferroelectric. It was observed how there is a field limit at which the antiferroelectric behavior changes to ferroelectric, and it also observed the coexistence of both phases in the material at certain voltages. Eventually, it was used a normalized capacitance in function of field applied to verify the minimum energy related to ferroelectric (2 peaks) and antiferroelectric phase (4 peaks). Finally, it was illustrated that in almost all samples there is not conductance and charge leakage that influence in the ferroelectric properties.

4.1.2.2 Impedance analysis

KNN

In Figure 4.21, corresponding to the sintered KNN sample for 4 hours without encapsulation (a) and for the sample sintered for 1 hour with encapsulation (b), the relative permittivity behavior is observed as a function of temperature at different frequencies. Two maximum peaks related to phase transitions occur for (a) at 215°C and 410°C, and for (b) at 200°C and 415°C. These temperatures are related to the following phase changes: Orthorhombic-tetragonal-cubic respectively. In addition, the second peak corresponds to the Curie temperature which signals a change from ferroelectric to paraelectric. The measurements at different frequencies show that low frequencies have higher dielectric permittivity and higher dielectric loss.

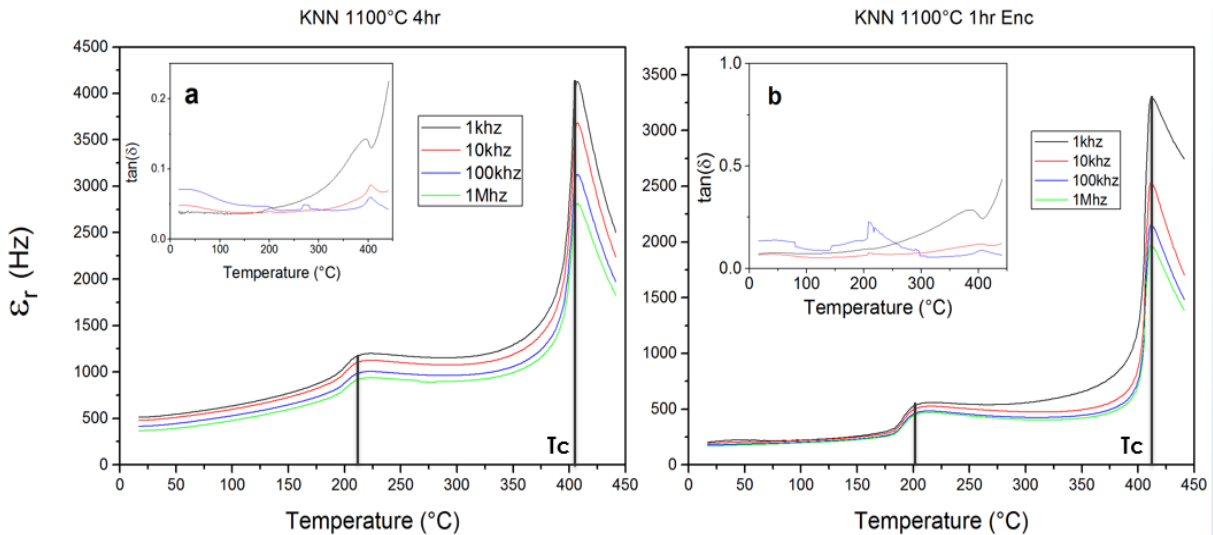


Figure 4.21: Relative permittivity and $\tan(\delta)$ vs temperature for sample of KNN sintered at 1100°C for: a) 4 hours with encapsulation, and b) 1 hour without encapsulation.

KNNCu0.5%mol

Figure 4.22 shows the graphs of permittivity and $\tan(\delta)$ in dependence of the temperature for the samples of KNNCu0.5%mol sintered at 1100°C for 4 hours (without encapsulation), 3 hours (encapsulated), 1 hour (encapsulated), and 4 hours (without encapsulation). For

all of the frequencies, in a, b, c, and d, the transitions related to the system KNN: orthorhombic-tetragonal and tetragonal-cubic occur around 215°C and 415°C respectively. In the case of the dielectric losses, at highest frequency of 1MHz, there are lower dielectric losses.

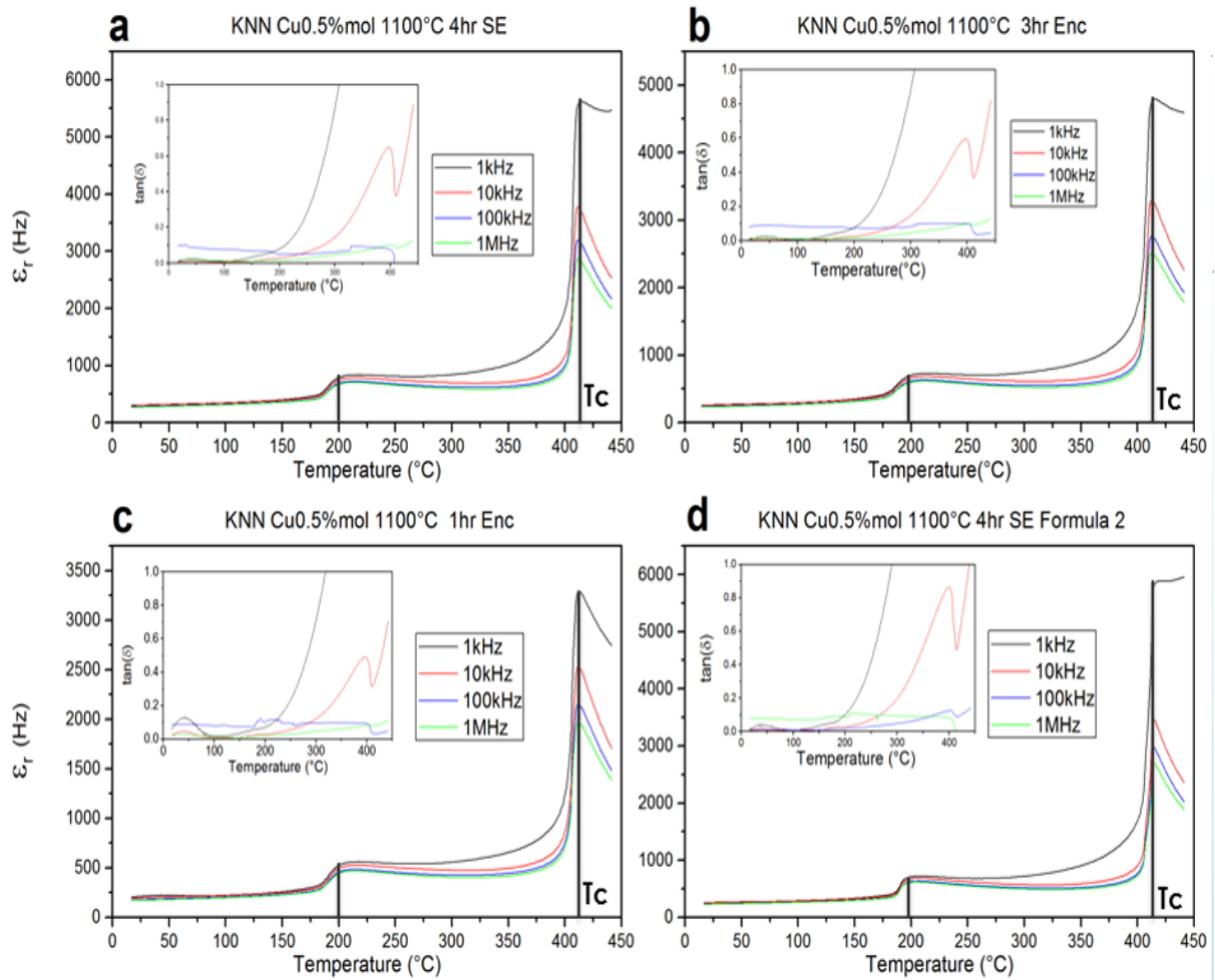


Figure 4.22: Relative permittivity and $\tan(\delta)$ vs temperature for samples a) KNN-Cu0.5%mol sintered 4 hours at 1100°C without encapsulation (Formula 1), b) KNN-Cu0.5%mol sintered 3 hours at 1100°C with encapsulation (Formula 1), c) of KNN-Cu0.5%mol sintered 1 hour at 1100°C with encapsulation (Formula 1), and d) KNN-Cu0.5%mol sintered 4 hours at 1100°C without encapsulation (Formula 2).

KNN1%mol

As Figure 4.23 illustrates, show the impedance test for the KNNCu1%mol sintered at 1100°C for 3 hours (encapsulated). The transition of the orthorhombic-tetragonal phase happens around 180°C and the transition related to the tetragonal-cubic phase occurs around 415°C. The first transitions are related to a lower temperature than the previous samples of KNN(215°C) and KNNCu0.5%mol(215°C), it could be caused by the dopant. It is known that the increase of dopant quantity attenuates the long-range interactions and the temperature at which the permittivity achieves the maximum peak decreases [65].

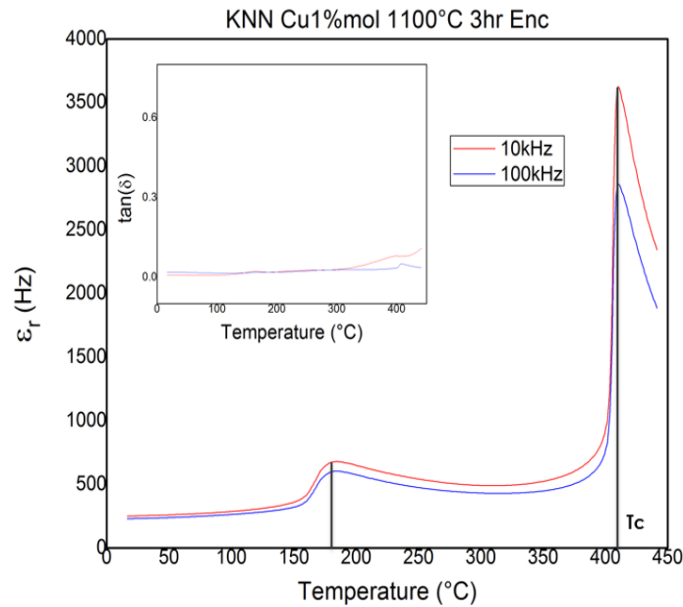


Figure 4.23: Relative permittivity and $\tan(\delta)$ vs temperature for sample of KNNCu0.5%mol sintered 3 hours at 1100°C with encapsulation.

4.1.2.3 UV-Vis Diffuse Reflectance Spectroscopy

UV-Vis Diffuse Reflectance Spectroscopy was performed for the calcined powders of KNN, KNNCu0.5%mol (formula 1, formula 2) and KNNCu1%mol. The energy bandgap is taken from the tangent of the curve.

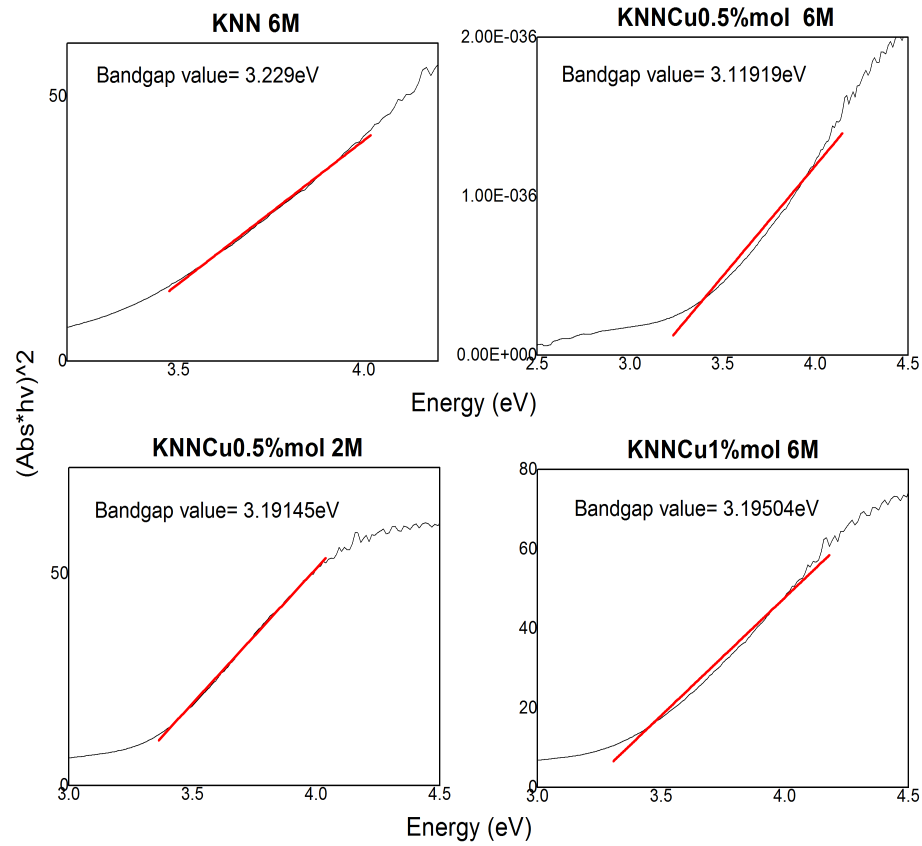


Figure 4.24: Bandgap calculation by Kubelka-Munk relation-indirect method (explained in the section [3.3.3](#))

The spectra obtained from the different samples after the Kubelka-Munk method are shown in Figure [4.24](#). The values of E_g correspond to the intersection between the linear fit and the energy axis, taking into account the indirect bandgap relation.

Table [4.5](#) details the bandgap values obtained by the Kubelka-Munk method. It can be deduced that the bandgap decreases in a minimum proportion when doping the KNN system with copper. Furthermore, it is observed that the use of chemical equation 1 and 2 does not influence the bandgaps obtained.

	Bandgap	Chemical formula
KNN	3.229 eV	1
KNNCu0.5%mol	3.19145 eV	1
KNNCu1%mol	3.11919 eV	2
KNNCu0.5%mol 2M	3.19504 eV	2

Table 4.5: Bandgap values obtained for the samples KNN, KNNCu0.5%mol 2M, KNNCu0.5%mol and KNNCu1%mol.

4.2 Thin films characterization

For the growth of thin films via sputtering, it is necessary to know which crystalline phase have the targets to be used. For this reason, X-ray diffraction of calcined powders and sintered targets based on the chemical formula 2 were performed.

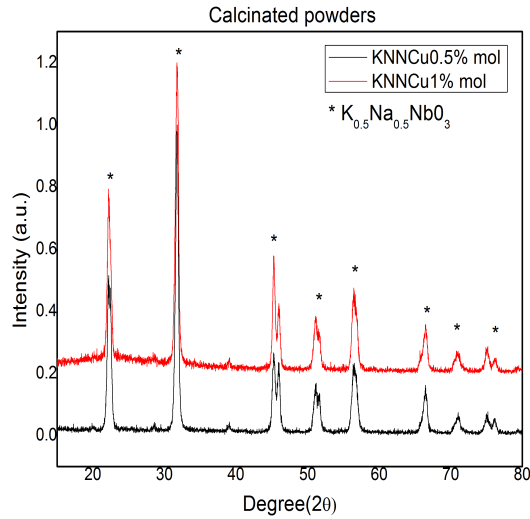


Figure 4.25: XRD for calcined powders of KNNCu0.5%mol and KNNCu1%mol at 900°C for 4 hours.

Figure [4.25](#) shows the diffractogram associated to the calcinated powders for the sys-

tem KNNCu0.5\%mol and KNNCu1\%mol (chemical formula 2). In both cases, it is possible to identify a perovskite structure related to the diffraction pattern PFD 00-061-0.15 $\text{K}_{0.5}\text{Na}_{0.5}\text{NbO}_3$, which has the following lattice parameters: $a=4.00462\text{\AA}$, $b=3.94464\text{\AA}$, $c=4.002\text{\AA}$, $\alpha=90^\circ$, $\beta=90.333^\circ$, and $\gamma=90$, associated to a monoclinic phase. To obtain the desired phase in the early stage of calcination, the diffractograms show that the sintering process does not require a long period of thermal treatment.

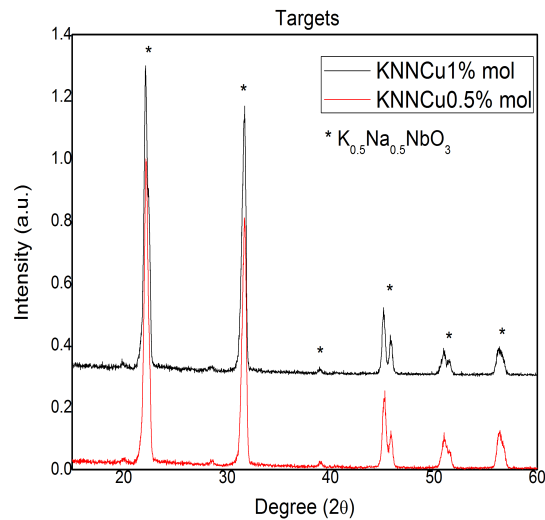


Figure 4.26: First targets of KNNCu0.5 and KNNCu1 , milled 120 minutes in high energy miller, and sintered at 900°C for 4 hours and sintered for 1 hour at 1100°C .

The diffraction pattern of Figure 4.26 shows the phase identification for the first targets 3.4. Even though the targets did not look homogenous to the naked eye, the presence of the monoclinic phase can be observed in both targets.

After making improvements in the process for obtaining the new targets 3.6, targets visually homogeneous were obtained, and in the same way it was verified the presence of a perovskite structure with monoclinic phase as we can see in the Figure 4.27. It is notable a change in the crystallinity and the crystallite size, as it was analyzed previously in 4.2

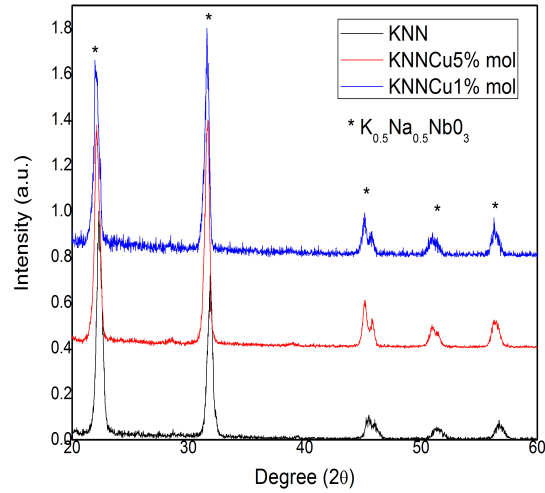


Figure 4.27: New targets of the systems KNN, KNNCu0.5, and KNNCu1%mol [3.6](#), milled 30 minutes in a mortar and 90 minutes in high energy miller, calcined 4 hours at 900°C, and sintered 2 hours at 1000°C.

As diffractograms show in Figure [4.26](#) and Figure [4.27](#), in all of the targets developed, there is the presence of the monoclinic phase PDF 61-0315 $K_{0.5}Na_{0.5}NbO_3$ according to the Powder Data File (PDF) database from Jade 6 program. Once the presence of the desired phase was verified, thin films of the KNN, KNNCu0.5% mol and KNNCu1% mol systems were grown over different substrates, which are described below.

4.2.1 KNN

As reference, it was used the pure KNN system to contrast with the systems doped with copper. In this case, the grown was developed on p-type Si and ITO/glass substrates, with the respective conditions of the sputtering and thermal treatment described below.

4.2.1.1 KNN(2)/p-type Si-75W 10min(x5)-650°C 60min O₂

In both cases, as a product of the growth in layers by sputtering and a subsequent heat treatment in an oxygen atmosphere, a fairly uniform film was obtained. The color changes are related to different thicknesses as we can see in Figure 4.28. Through XRD, the main phase was identified as $K_{0.5}Na_{0.5}NbO_3$ (monoclinic) with a minimal secondary phase of $K_3Nb_7O_{19}$ (Triclinic). Besides, in correlation with the target, the presence of the desired phase can be confirmed.

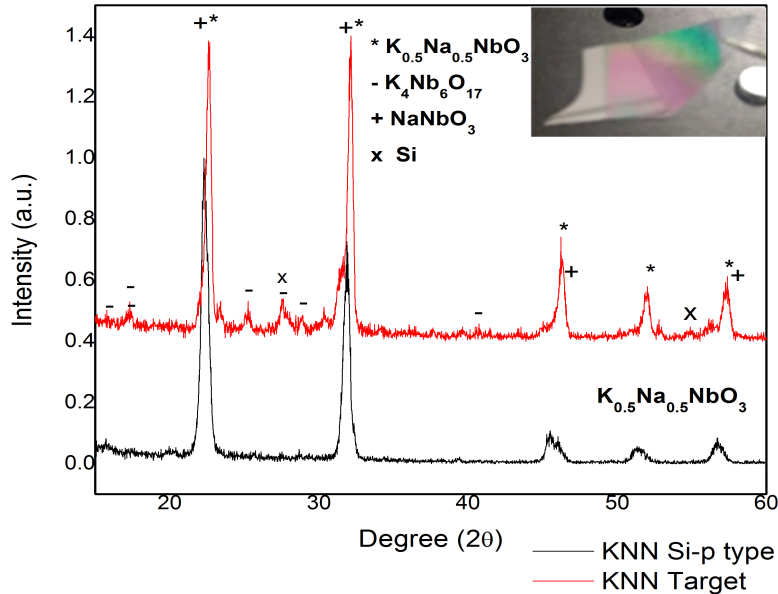


Figure 4.28: XRD for KNN/ p- type Si, deposited in 5 layers for 10 minutes, with a power of 75W, and sintered at 650°C for 60 minutes in an oxygen atmosphere.

Through profilometry it was obtained Figure 4.29, where (a) shows a 3D image of the thickness of the KNN/p- type Si film. A thickness of 90 nm was measured taking as reference the difference between the substrate and the thickness of the film. The region of higher growth in (a) have been due to the Kapton tape used during sputtering growth. The average roughness obtained was $0.23\mu\text{m}$. In (b) there is a 3D image of the roughness

associated with the KNN/p- type Si film, where it is notable a film mostly homogeneous with the presence of certain peaks.

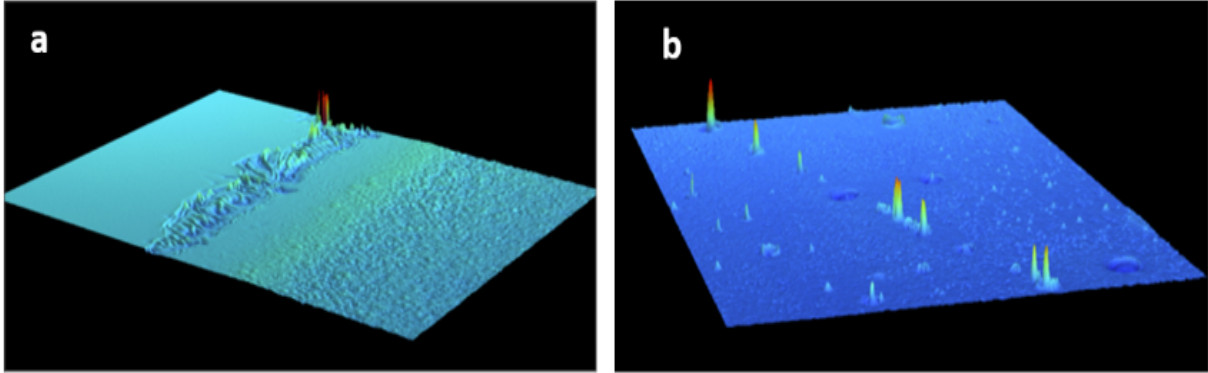


Figure 4.29: a)3D Thickness, and b)3D Roughness for KNN/p- type Si.

In Figure [4.30](#), the KNN/p- type Si film initially (1V-1kHz) does not show a ferroelectric behavior, so a double polarization cycle was induced slightly, which resulted in the tendency to a ferroelectric behavior (5V-1kHz) and with the presence of certain initial carriers (conductance). The maximum supported voltage was 9V for 200Hz after that a conductive behavior was seen.

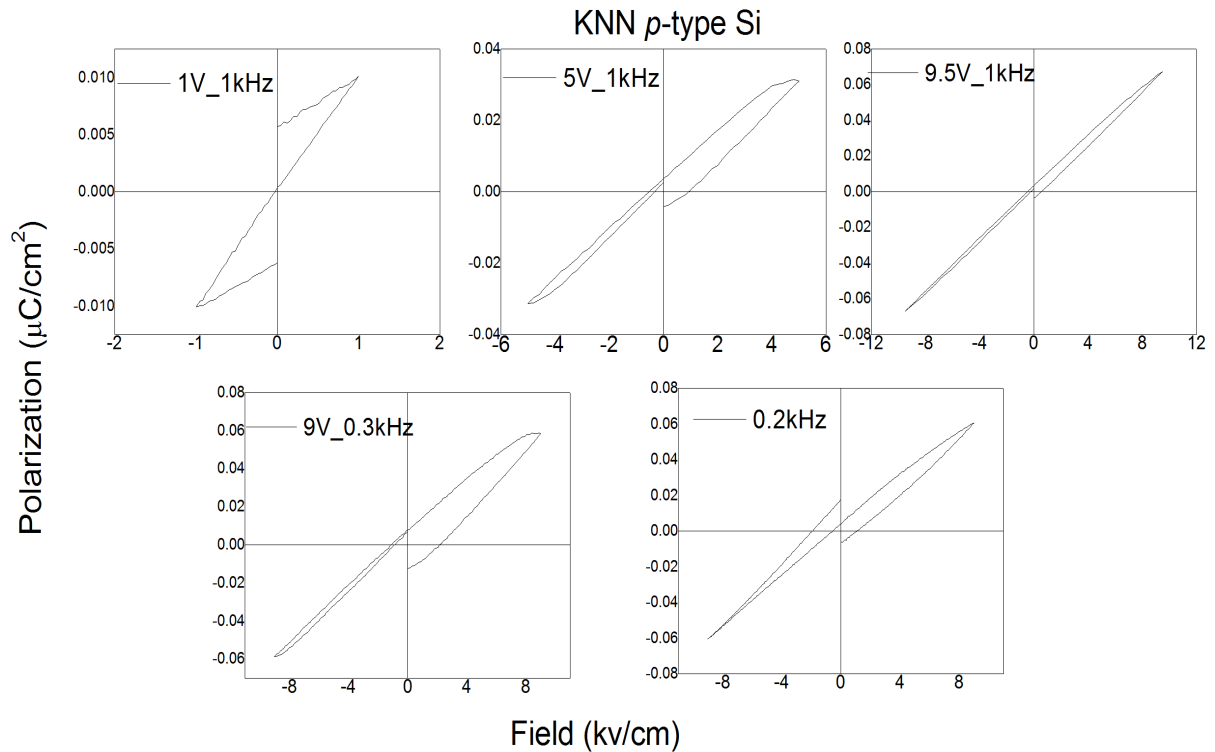


Figure 4.30: Ferroelectric hysteresis for KNN/p- type Si at different frequencies and voltages.

Figure [4.31](#) displays the relation between the $\ln(\text{Current})$ and the voltage applied for the thin film of KNN deposited over a p- type Si. There is an asymmetry of the branches showing a diode effect, since for positive voltages the current is greater than for negative voltages and does not show a photoresponse effect. Even for UV lighting there are small changes in the current, which is quite associated with the variability in measurements (dark, visible, and ultraviolet light for each sample), rather than a photoresponse of the system [\[41\]](#).

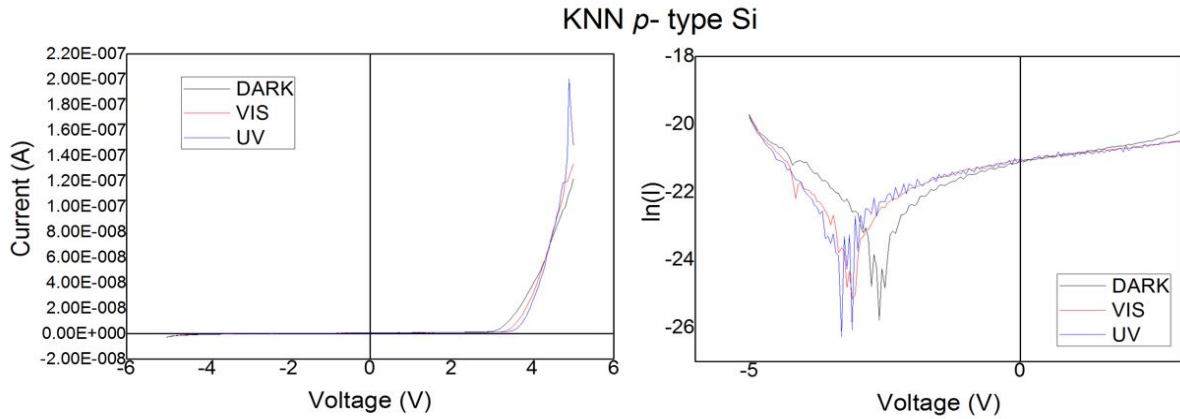


Figure 4.31: Current-Voltage for KNN/p- type Si.

4.2.1.2 KNN(2)/ITO/glass-75W 10min(x5)-650°C 60min O_2

A thin film was obtained by the growth of KNN over the ITO/glass substrate. As Figure 4.32 shows there is a uniform color after the heat treatment carried out at 650°C for 60 minutes in a tubular oven in O_2 atmosphere.

The XRD pattern of Figure 4.32 shows the presence of the principal phase $K_{0.5}Na_{0.5}NbO_3$ and the coexistence of the precursor components: sodium and potassium niobite. Also, the distinctive peaks of the ITO substrate were identified.

The ITO ($In_4Sn_3O_{12}$) can be visualized in the diffractogram, because the thickness is not homogeneous over the entire surface, which causes X-rays to have enough penetration to reach the substrate [66].

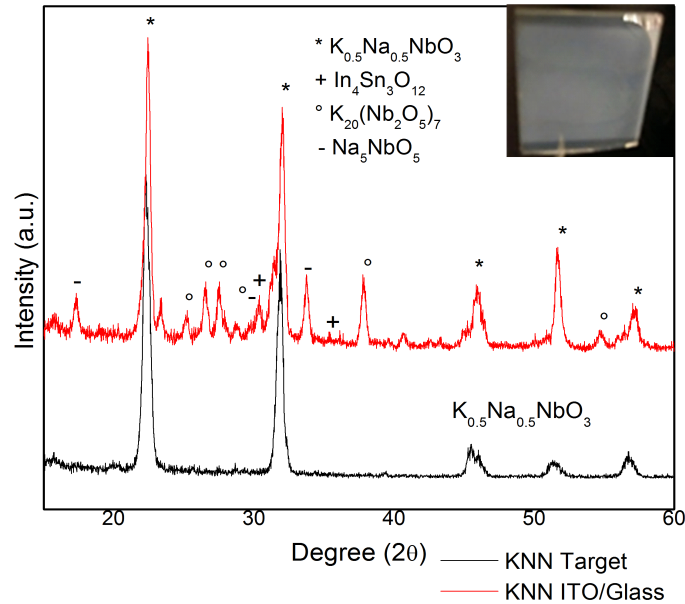


Figure 4.32: Film obtained after the heat treatment and XRD for KNN/ITO/glass sample deposited in 5 layers for 10 minutes, with a power of 75W, and sintered at 650°C for 60 minutes in an oxygen atmosphere.

Through profilometry, it was measured an average thickness and average roughness of 300nm and 0.027 μm , respectively. Figure 4.33 (a) and (b) show a 3D image of the material surface for the thickness and roughness obtained, respectively. In both of the cases it is notable that there are regions of higher growth which are identified by red zones.

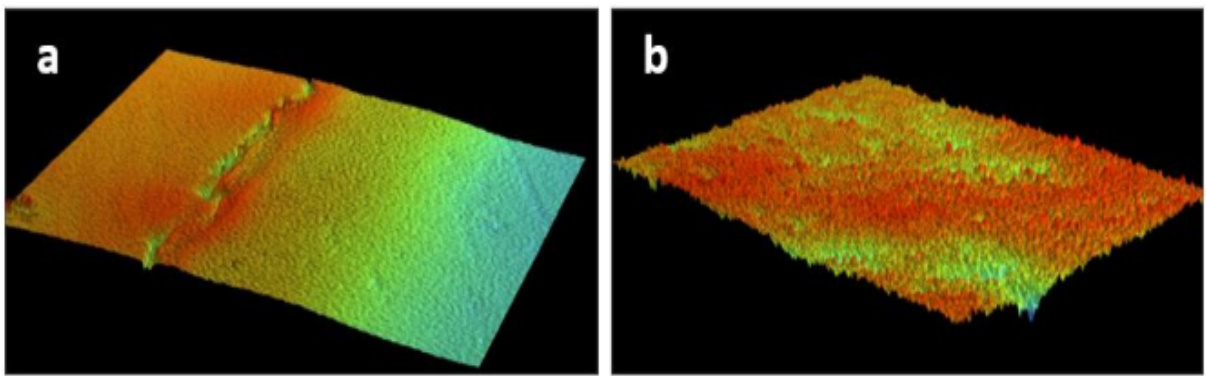


Figure 4.33: a)3D Thickness, and b)3D Roughness for KNN/ITO/glass

Figure 4.34 shows the ferroelectric characterization for the KNN/ITO/glass film. Initially, the film does not show a cyclic behavior. For this reason, a double polarization was applied but a characteristic curve of conductance was obtained.

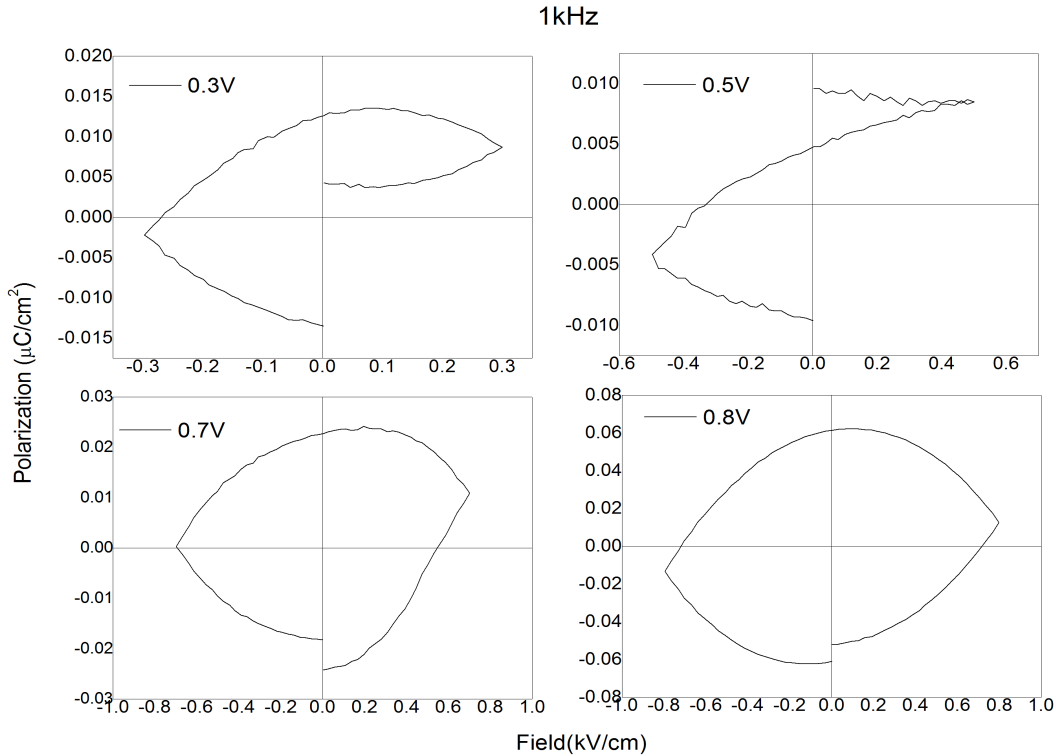


Figure 4.34: Ferroelectric hysteresis for KNN/ITO/glass. The period was 1ms(1000Hz).

The semiconductor characterization applied in the film of KNN/ITO, shows a photocurrent constant nearby to zero region, which increases until diode behavior is obtained, under dark, visible and ultraviolet light, where the current is higher at positive voltages than for negative voltages. As Figure 4.35 illustrates, the current response suffers only small changes in the three measurements, which could be related to the variability in measurements, rather than a photoresponse.

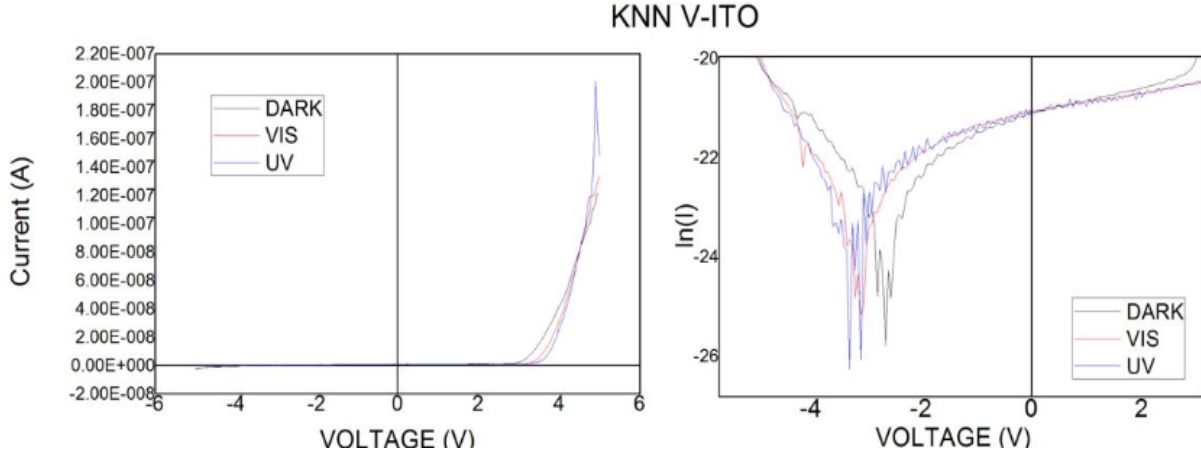


Figure 4.35: Current-Voltage for KNN/ITO/glass.

4.2.2 KNNCu0.5%mol - Chemical Formula 2

For the growth of thin films of KNN doped with 0.5% mol of copper, 2 targets were used, which were synthesized based on the stoichiometry of the chemical formula 2. The first KNNCu0.5% mol (1) and second KNNCu0.5% mol (2) targets had the $K_{0.5}Na_{0.5}NbO_3$ monoclinic phase as seen in Figure 4.26 and Figure 4.27.

4.2.2.1 KNNCu0.5%mol(1)/Pt/Si – 100W 90min- 600°C 30min O_2

Figure 4.36 shows a thin film of KNNCu0.5%mol deposited over silicon coated with platinum. The image shows the sample after the heat treatment, where a slight fracture is notable on the surface of the ferroelectric material. In addition, the film has color rings that are related to the different thicknesses of material growth.

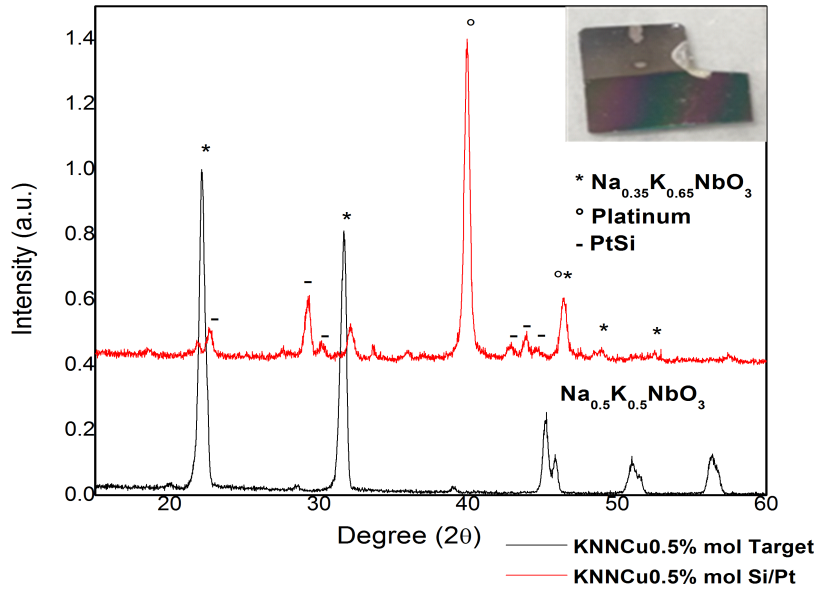


Figure 4.36: Film obtained after the heating treatment and XRD for KNNCu0.5%mol/Pt/Si deposited in 90 minutes, with a power of 100W, and sintered at 600°C for 30 minutes in an oxygen atmosphere.

The diffractogram in Figure 4.36 shows the presence of the main phase $Na_{0.35}K_{0.65}NbO_3$ without secondary phases, the other peaks being related to the substrate used. This phase was identified as PDF 77-0038 (monoclinic) by the PDF database of the JADE program, which has the following lattice parameters: $a=7.9751\text{\AA}$, $b=7.862\text{\AA}$, $c=7.9565\text{\AA}$, $\alpha=90^\circ$, $\beta=90.34^\circ$, and $\gamma=90^\circ$. Despite the presence of the phase $Na_{0.35}K_{0.65}NbO_3$ and the ferroelectric behavior, the sample does not present a photoelectric response and its surface does not be homogeneous.

4.2.2.2 KNNCu0.5%mol(1)/ITO/glass– 100W 90min- 600°C 30min

Figure 4.37 shows the thin film related to a KNNCu0.5%mol(1) grown over an ITO/glass substrate and annealed in a muffle at 600°C for 30 minutes. In the sample, a ring

zone is notable related to a different thickness, but in general, a homogeneous growth of the ferroelectric material is observed. In Figure 4.37, there is the diffractogram related to a $\text{KNNCu}0.5\% \text{mol}(1)/\text{ITO}/\text{glass}$, where it was identified the phase $\text{K}_{0.35}\text{Na}_{0.65}\text{NbO}_3$, accompanied by its precursors: sodium and potassium niobate.

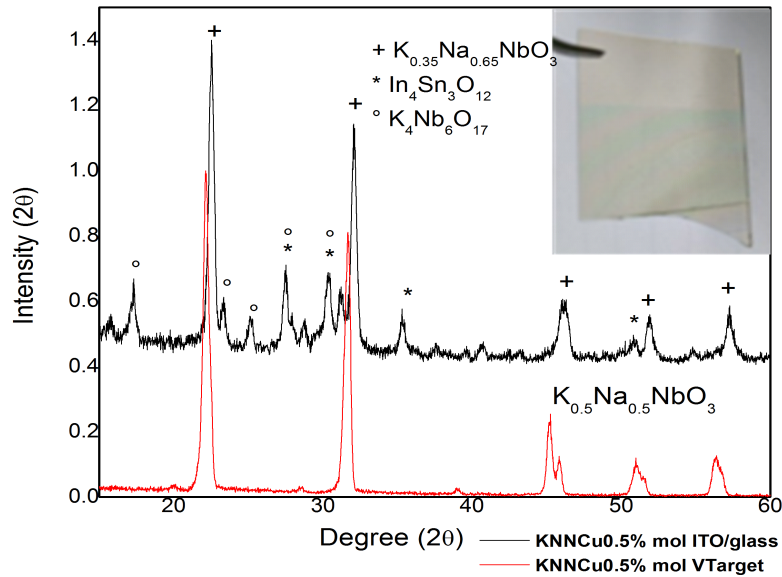


Figure 4.37: Film obtained after the heating treatment and XRD for $\text{KNNCu}0.5\% \text{mol}(1)/\text{ITO}/\text{glass}$ deposited for 90 minutes, with a power of 100W, and sintered at 600°C for 30 minutes.

Figure 4.38 illustrates a saturated I-V curve, where it was identified as an ohmic response of the material, which is characteristic of a linear relation between the voltage applied and the photocurrent produced. The measurement was carried out under dark and ultraviolet conditions, and in both of the cases, the response was the same according with the overlapping measurements.

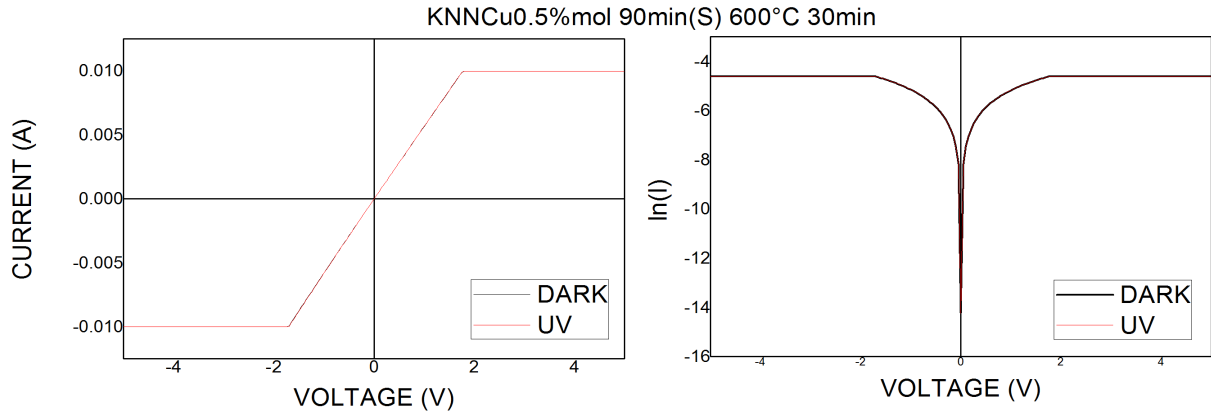


Figure 4.38: Current-Voltage for KNNCu0.5%mol/ITO/glass.

4.2.2.3 KNNCu0.5%mol(2)/ITO/glass – 75W-10min(x5) - 650°C 60min O_2

Figure [4.39](#) shows a film of KNNCu0.5%mol(2) grown over ITO/glass substrate via sputtering in 5 layers of 10 minutes with a power of 75W.

The samples were sintered in an oven with an O_2 atmosphere at 600°C for 60 minutes. The final film obtained look homogeneous. The phase identified through the PDF (Pattern Data File) database was the PDF - 61-0315 $K_{0.5}Na_{0.5}NbO_3$. The high reflection from the substrate $In_4Sn_3O_{12}$ is related to thickness of the substrate.

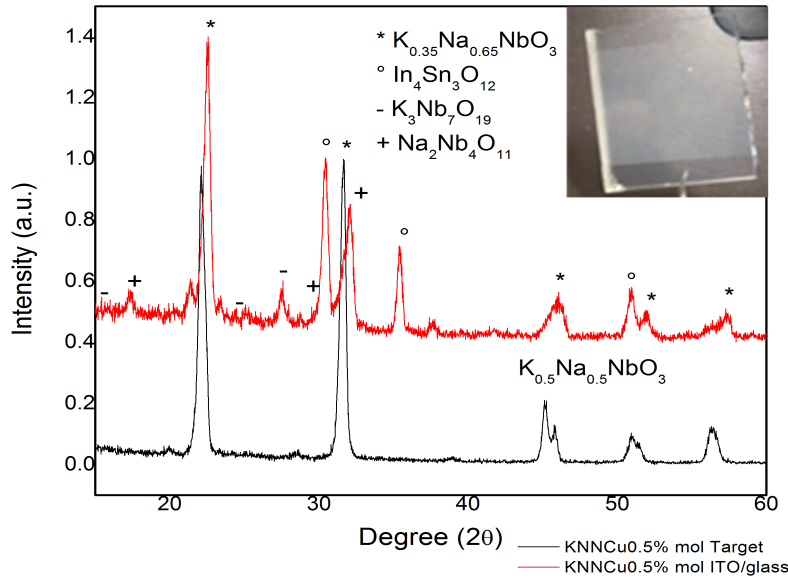


Figure 4.39: Film obtained after the heating treatment and XRD for KN-NCu0.5%mol(2)/ITO/glass deposited in 5 layers for 10 minutes, with a power of 75W, and sintered at 650°C for 60 minutes in an oxygen atmosphere.

Through profilometry, it was measured thickness of 300nm and average roughness of 0.025 μm . Figure 4.40 (a) and (b) show 3D surface images of thickness and roughness respectively. In both of the cases, it was obtained a homogeneous grain growth, despite having multiple phases illustrated previously in Figure 4.39

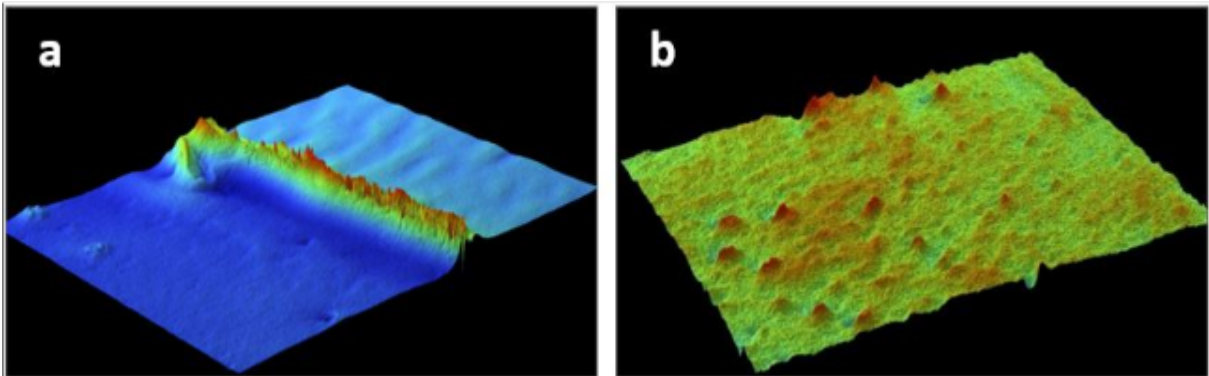


Figure 4.40: a) 3D Thickness and b) 3D Roughness for KNNCu0.5%mol(2)/ITO/glass.

The ferroelectric test shows a high conductance in the material which is illustrated in Figure 4.41. Film based on KNN/ITO/glass shows a resistance behavior characterized by a circle with the center near to the origin. The representative parameters are $P_r = 8.11\mu\text{C}/\text{cm}^2$ and $E_c = 5.70\text{kV}/\text{cm}$.

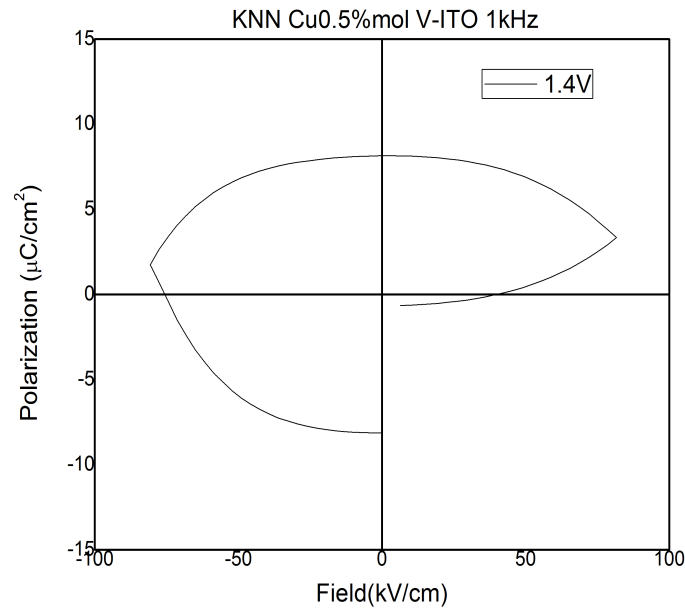


Figure 4.41: Ferroelectric hysteresis for KNNCu0.5%mol(2)/ITO/glass.

In Figure 4.42 is illustrated the I-V curve for KNNCu0.5%mol/ITO/glass, which shows a diode effect, the current is greater for positive voltages and for 4V the current shows a typical exponential growth of a diode. In this case the photoresponse effect is very clear, since the current increases upon UV light illumination. It can also be measured that for the external voltage equal to 0, there is a small current that constitutes a photovoltaic effect.

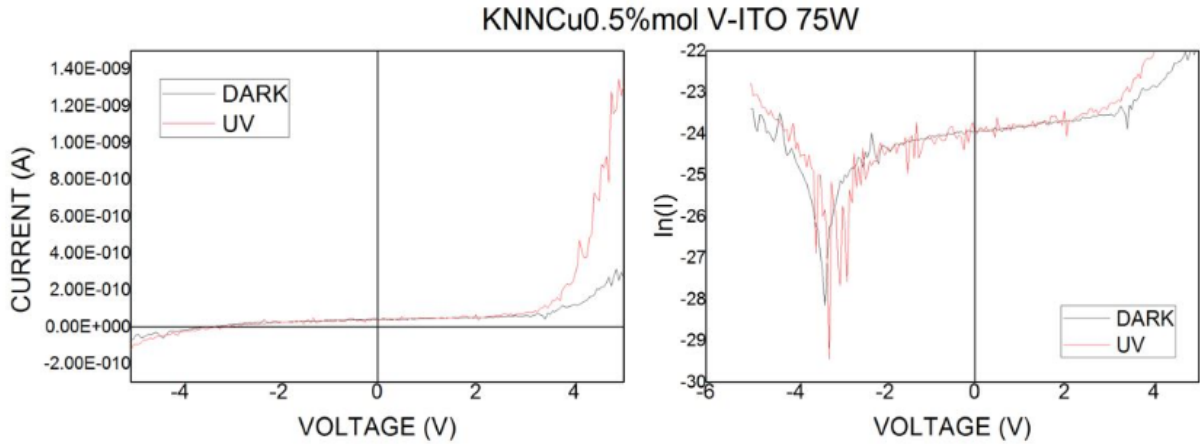


Figure 4.42: Current-Voltage for KNNCu0.5%mol/ITO/glass.

In the second graph ($\ln(I)$ vs Voltage(V)), the current shows a minimum in the current around 3V both in darkness and under UV illumination, this indicates that there is an internal field that the external voltage has to counteract to bring the resulting field equal to 0. If this internal field, produced by remnant polarization of the ferroelectric film, is inverted with external polarization, then it would add to the field due to the Schottky barrier and the photoresponse effect should be greater, as well as the photovoltaic effect [67].

4.2.2.4 KNNCu0.5%mol(2)/p- type Si – 75W 10min(x5)- 650°C 60min O_2

Figure 4.43 shows the thin film related to a KNNCu0.5%mol(2) grown over a silicon p- type Si substrate and annealed in a muffle at 650°C for 60 minutes in an oxygen atmosphere. In the sample, it is notable a ring zones that are related to a different thickness, but in general, there is a homogeneous growth of the ferroelectric material. As the diffractogram illustrates, the $K_{0.5}Na_{0.5}NbO_3$ phase is present in the film as verified by the comparison with the target diffractogram.

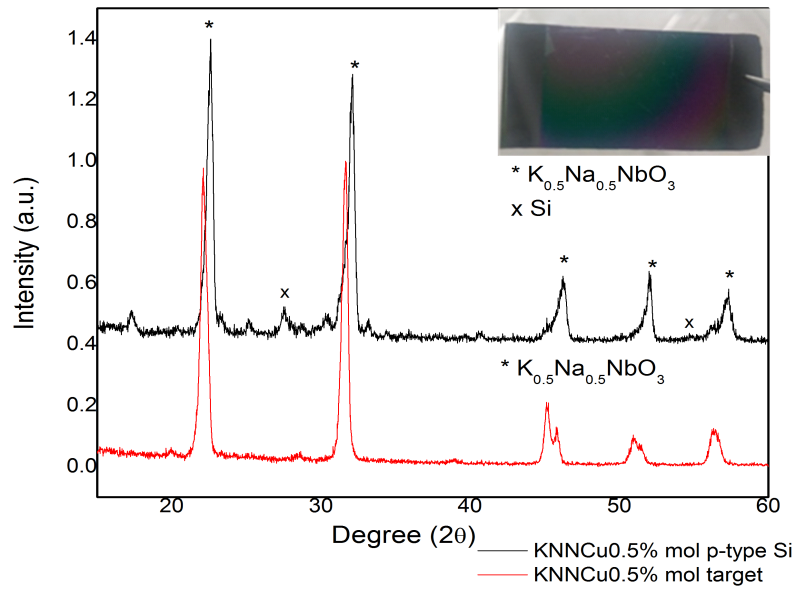


Figure 4.43: Film obtained after the heating treatment and XRD for KNNCu0.5%mol(2)/p- type Si deposited in 5 layers for 10 minutes, with a power of 75W, and sintered at 650°C for 60 minutes in an oxygen atmosphere.

Through profilometry, it was measured a thickness of 50nm and an average roughness of 0.049 μ m. This thickness is low compared with other films discussed before. Figure 4.44 (a) and (b) are 3D images from the surface material related to the thickness and the roughness, respectively.

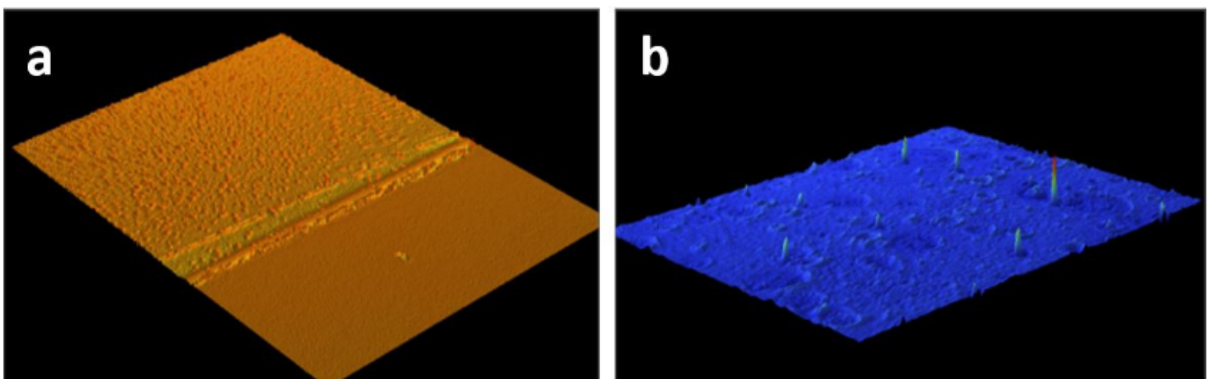


Figure 4.44: a) 3D Thickness and b) 3D Roughness for KNNCu0.5%mol(2)/p-type Si

For the ferroelectric test of the films $\text{KNNCu}0.5\% \text{mol}(2)/\text{p-type Si}$ it was measured in two contacts of Au ($r=1\text{mm}$). Figure 4.45 shows the first measurement which is developed in the range from 1V(1kHz) to 9V(100Hz). From the first measurements, there is a tendency to a cyclic behavior, but to have more defined results, double polarization cycles were applied. It was obtained a double hysteresis loop as can be seen in the measurement at 6.4V for 250Hz, which is signal of an antiferroelectric phase. At this point, it was obtained a $P_r = 5.23E - 4\mu\text{C}/\text{cm}^2$ and an $E_c = 2.78E - 1\text{kV}/\text{cm}$. As the voltage and period increased, the hysteresis curves showed a ferroelectric behavior up to 9V for 10ms, with a $P_r = 1.46E - 3\mu\text{C}/\text{cm}^2$ and an $E_c = 2.11\text{kV}/\text{cm}$. From this value, the hysteresis cycle begins to widen and indicates that at higher voltages a charge leakage already occurs. Moreover, it can be deduced the coexistence of the ferroelectric and antiferroelectric phases for this film, because there is a characteristic shape of a ferroelectric material with a slight narrowing in the center.

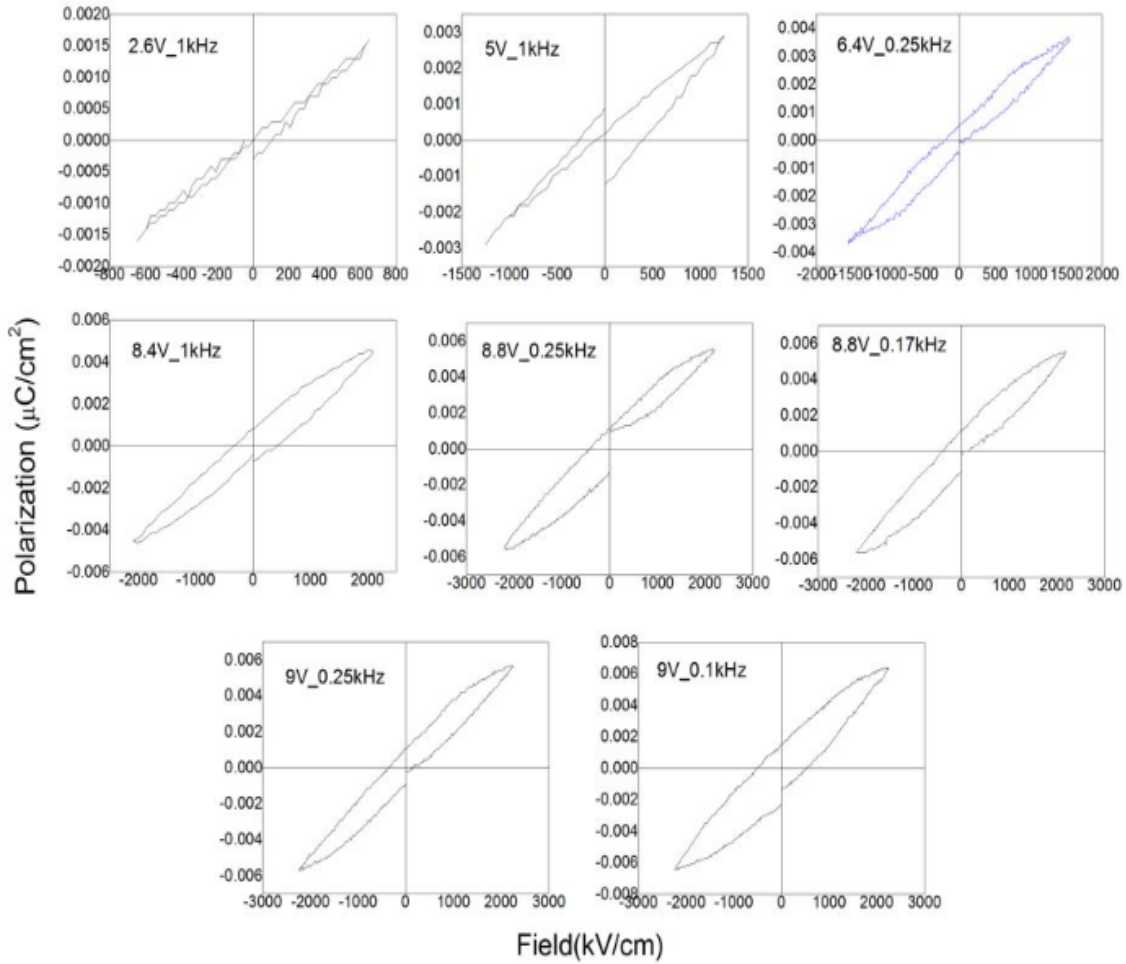


Figure 4.45: Ferroelectric hysteresis for KNNCu0.5%mol(2)/ p- type Si (contact 1). 1ms(1000Hz), 4ms(250Hz), 6ms(166.66Hz), and 10ms(100Hz)

In the second measurement related to another Au contact from the same film, it was observed in Figure 4.46 a ferroelectric phase, which was obtained by the application of a double polarization. This test was realized from 1.7V (1kHz) to 9V(0.53Hz). For the P-E loop at 9V(0.55hHz), it was defined as a ferroelectric loop with a value of $P_r = -3.73E - 3\mu C/cm^2$ and an $E_c = -1.51E - 2kV/cm$. At this point, there is a low presence of charge at the beginning because the cycle does not start at the origin. From the following measurement of 9V for 0.53hHz, conductance and the presence of charge leak were observed .

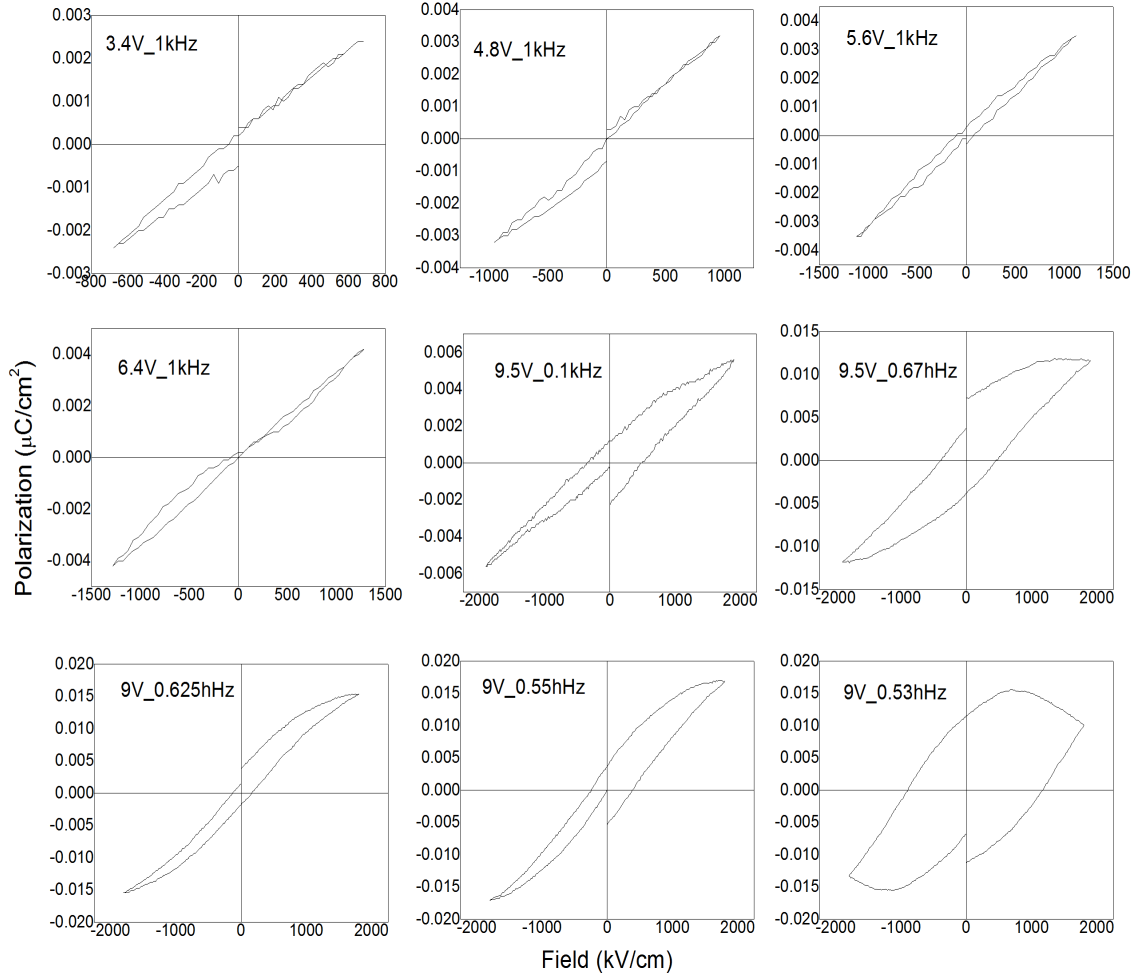


Figure 4.46: Ferroelectric hysteresis for KNNCu0.5%mol(2)/p- type Si (contact 2).

Figure [4.47](#) illustrates the I-V curves for the thin film of KNNCu0.5%mol/ p-type Si. In the first place, it was characterized by the photocurrent of the sample under dark, visible and ultraviolet light. The curve (a) and (b) show a diode behavior, which is caused by Schottky barriers due to the asymmetric contact in the ferroelectric thin film. In this case the substrate was doped with silicon on one side and metal on the other side. As the figure (a) illustrates, the current for positive voltages is greater than for negative voltages, however, the changes under illumination is minimal, meaning this sample does not show photocurrent response. Nevertheless, when the sample is polarized at room temperature with a battery of 9V for 5 minutes, interesting behaviors are noticeable. The

photocurrent was measured again under the same conditions. In the I-V curve (c) there is an ohmic behavior under visible and ultraviolet light, but in the dark conditions, there is a diode effect with a low current when the circuit is closed and a zero-external voltage. This behavior could be related to an internal field with low current, circulating when the circuit is closed. The fact that the current is minimum for V close to 1 volt, indicates that due to the presence of the internal field, an external voltage has to overcome so that the total field is 0 and the current has a minimum, which in this case is practically 0.

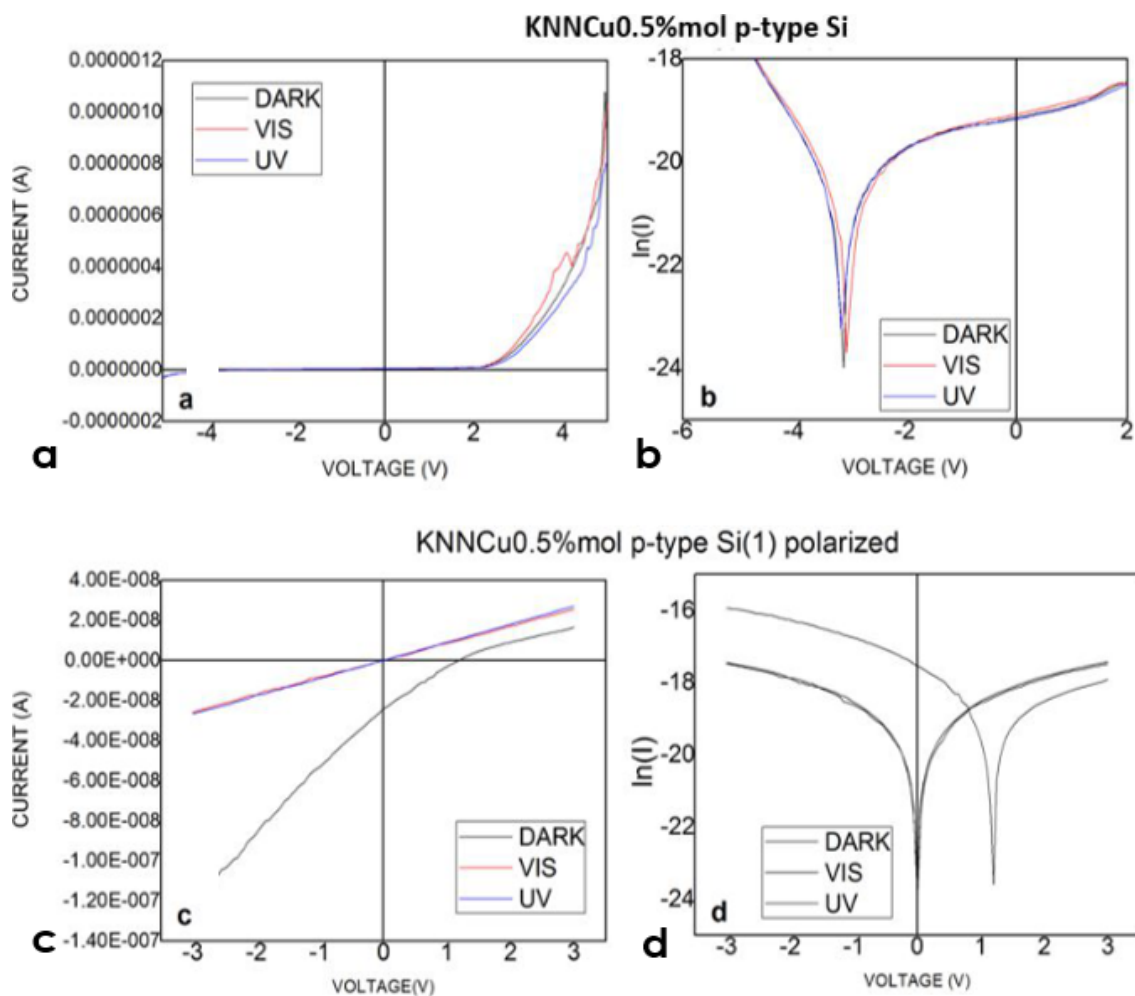


Figure 4.47: Current-Voltage for KNNCu0.5%mol(2)/p- type Si and polarized

4.2.3 KNNCu1%mol - Chemical Formula 2

For the processing via sputtering of thin films of KNN doped with copper in 1% mol, KNNCu1%mol(1) target was used. XRD shows the presence of $K_{0.5}Na_{0.5}NbO_3$ (PDF 61-0315) monoclinic phase as seen in Figure 4.26

4.2.3.1 KNNCu1%mol(1)/ITO/glass– 100W 90min- 600°C 30min O_2

The thin film of KNNCu1%mol(1)/ITO/glass obtained by sputtering at 100W during 90 minutes was sintered at 600°C for 30 minutes in an oxygen atmosphere and the final film is shown in Figure 4.48 which seems homogeneous.

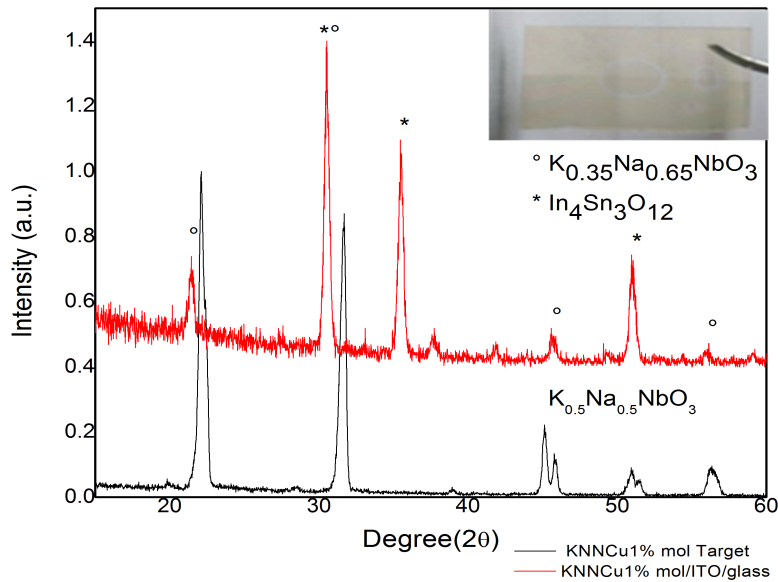


Figure 4.48: Film obtained after the heating treatment and XRD for KNNCu1%mol(1)/ITO/glass deposited for 90 minutes, with a power of 100W, and sintered at 650°C for 60 minutes in an oxygen atmosphere.

The diffractogram shows the presence of PDF 77-0038 $K_{0.35}Na_{0.65}NbO_3$ monoclinic phase, which has a displacement compared with the $K_{0.5}Na_{0.5}NbO_3$ phase from the target. The displacement could be explained based on the cell parameters. For the $K_{0.5}Na_{0.5}NbO_3$ phase, their related values are: $a=4.00462\text{\AA}$, $b=3.94464\text{\AA}$, $c=4.002\text{\AA}$, and for $K_{0.35}Na_{0.65}NbO_3$ phase: $a=7.9751\text{\AA}$, $b=7.862\text{\AA}$, $c=7.9565\text{\AA}$. The greater structure of cell with have a displacement to the left size as we can see in the figure [4.48](#).

For the thin film sample of $KNNCu1\%mol(1)/ITO/glass$, the ferroelectric measurement was developed in the range of 0.3V to 0.5V for the minimum period of 1ms(1kHz), where a resistance behavior was obtained in all of the P-E loops as Figure [4.49](#) illustrates.

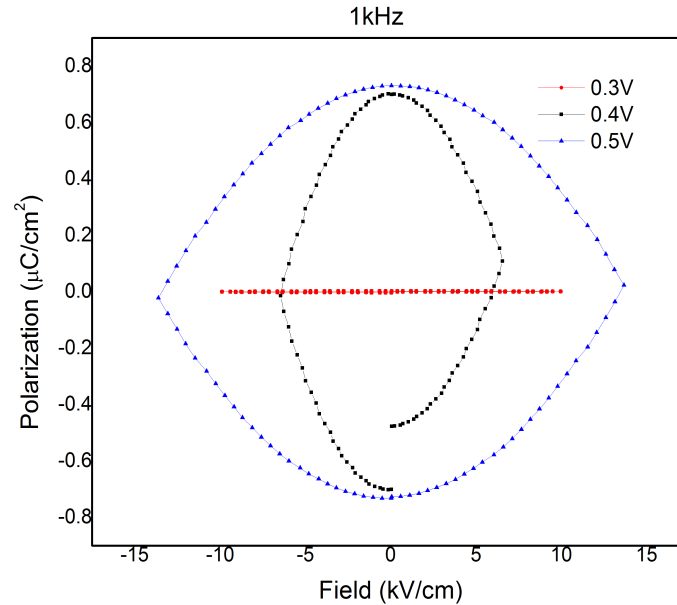


Figure 4.49: Ferroelectric hysteresis for $KNNCu1\%mol(1)/ITO/glass$

Figure [4.50](#) illustrates the resultant I-V curves for the sample $KNNCu1\%mol/ITO/glass$, where it was identified an ohmic response of the material, showing a linear relation between the voltage applied and the photocurrent produced. The measurement was carried out under dark, visible light and ultraviolet light, and in all of the cases, the response was the same, that there are not photoresponse.

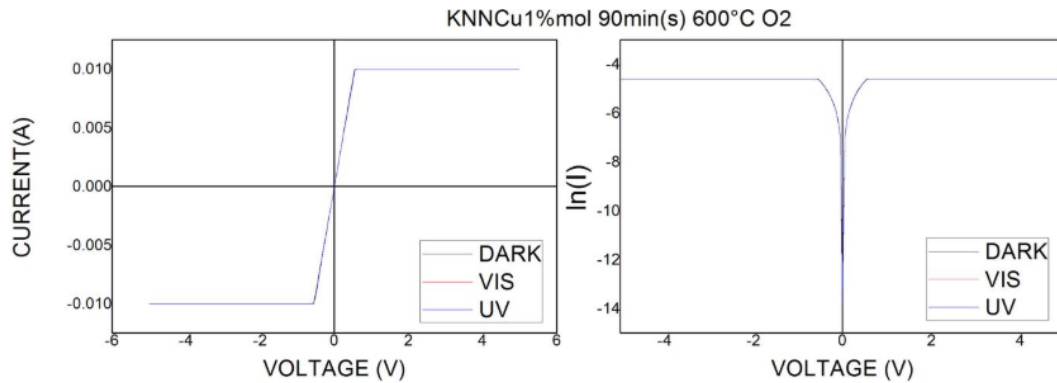


Figure 4.50: Current-Voltage for KNNCu1%mol/ITO/glass.

4.2.3.2 KNNCu1%mol(1)/ITO/quartz– 50W 10min(x5)- 650°C 60min

The thin film of KNNCu1%mol(1)/ITO/quartz was grown with a power of 50W in 5 layers of 10 minutes and the sintering treatment consisted of 650°C for 60 minutes encapsulated

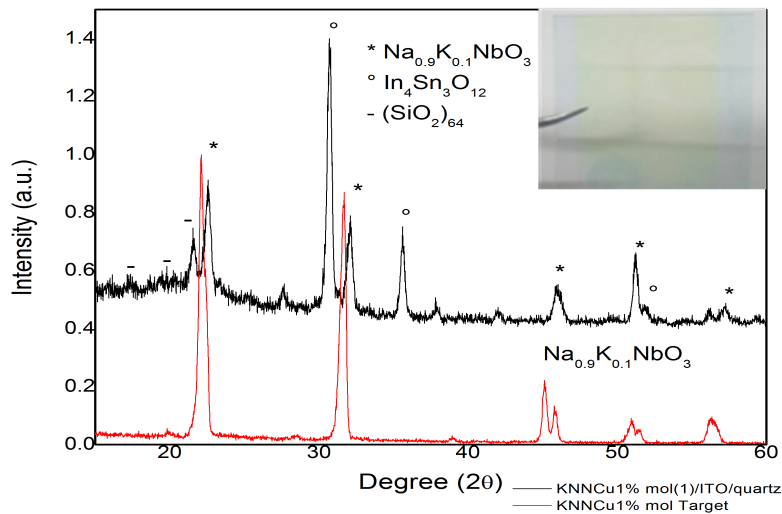


Figure 4.51: Film obtained after the heating treatment and XRD for KNNCu1%mol(1)/ITO/quartz deposited in 5 layers for 10 minutes, with a power of 50W, and sintered at 650°C for 60 minutes .

As Figure 4.51 shows, the final film was homogeneous after the thermic treatment and it presents the PDF 74-2025 $Na_{0.9}K_{0.1}NbO_3$ phase according to its diffractogram. The following lattice parameters: $a=7.8782\text{\AA}$, $b=7.792\text{\AA}$, $c=7.8632\text{\AA}$, $\alpha=90^\circ$, $\beta=90.479^\circ$, and $\gamma=90$ are obtained.

The profilometry measurement, give us an average thickness of 70nm. Figure 4.52 represents a 3D image related to the surface area of the film after the sintering treatment applied. It is notable a homogeneous growth in almost all of the surface material.

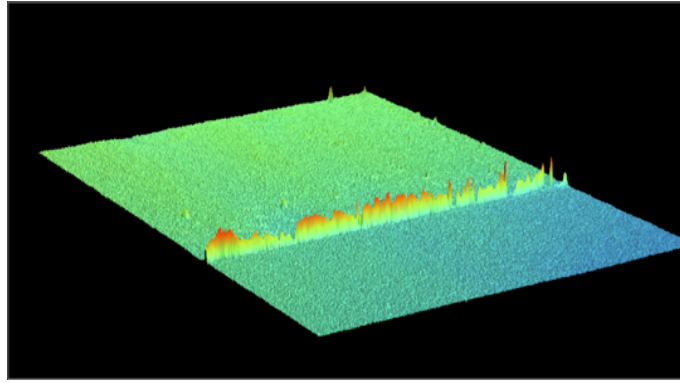


Figure 4.52: Thickness 3D image for $KNNCu1\%mol(1)/ITO/quartz$.

Besides the homogeneous growth, this film presents good results according to XRD and profilometry, the ferroelectric test did not show a representative ferroelectric property. The sample measured consisted of $KNNCu1\%mol/ITO/quartz$ and its related P-E loops obtained, as illustrated in Figure 4.53. The measurement was taken from 1V to 7V with a frequency of 200Hz, in which a double polarization was applied. Finally, the behavior of the P-E curves seems to tend to a relaxor behavior, including with voltage increase or double polarization cycle the behavior remained as the loops in Figure 4.53. The loops are characteristic of materials with low grain size in the scale of nanometers.

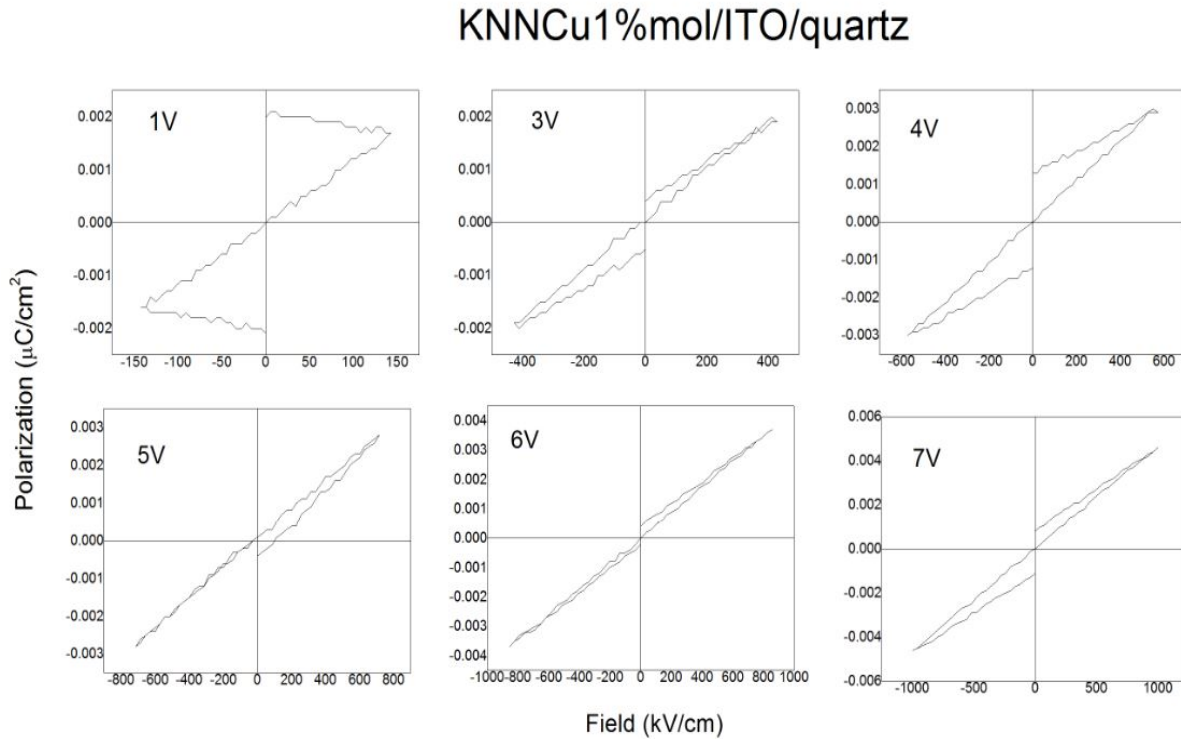


Figure 4.53: Ferroelectric hysteresis for KNNCu1%mol(1)/ITO/quartz. Period: 1ms(1000Hz).

Figure [4.54](#) shows the I-V curves for the thin film KNNCu1%mol/ITO/quartz measured under three different conditions: dark, visible light and ultraviolet light. The graph illustrates a linear relation between the applied voltage and the current produced, which is characteristic of an ohmic response. The absence of photoresponse occurs for the three measurements as we can see in the overlapped lines.

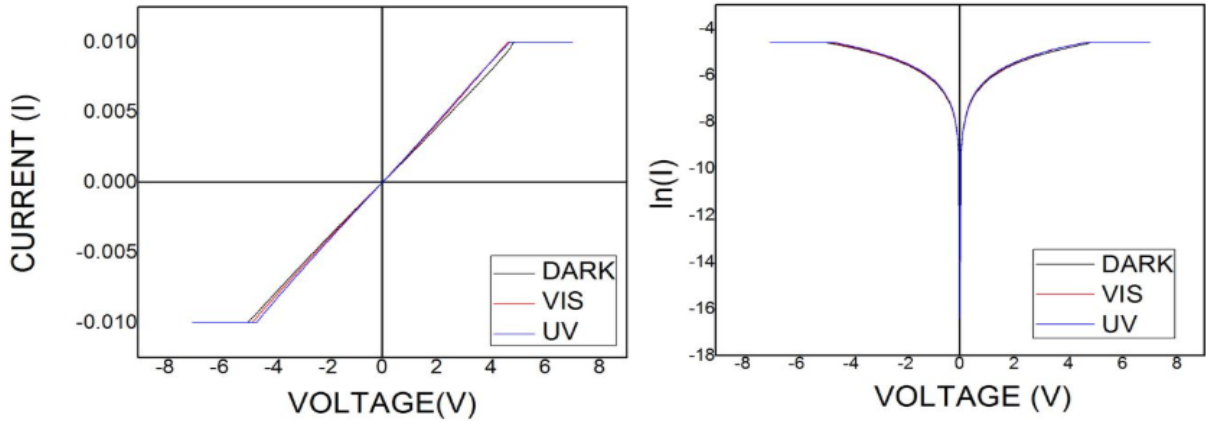


Figure 4.54: Current-Voltage for KNNCu1%mol(1)/ITO/quartz.

4.2.3.3 KNNCu1%mol(1)/ITO/glass– 75W 10min(x5)- 700°C 60min

The sample of KNNCu1%mol(ITO)/glass was obtained through sputtering with a related power of 75W. The growth was developed by layers, in 5 periods of 10 minutes, and after that, the film was sintered at 700°C for 60 minutes in an oxygen atmosphere. The sample was subjected to a higher temperature because in previous samples sintered at 600-650C there was the presence of precursors (sodium and potassium niobates) of the desired phase. Based on that, higher temperature or a longer sintering period could be required. In this case the ITO/glass substrate did not stand the highest temperature and broke. However, it presents the principal phase of $K_{0.5}Na_{0.5}NbO_3$ as the diffractogram shown in Figure 4.55. The presence of precursors, sodium niobite and potassium niobite, are also notable as identified in the XRD results. In the diffractogram, the characteristic peaks of the ITO ($In_4Sn_4O_{12}$) can be observed, despite the fact that the deposited film has a considerable average thickness of 700nm. The penetration range of X-rays is less than the thickness of the film, however it is visible since the thickness is not homogeneous over the entire surface [66].

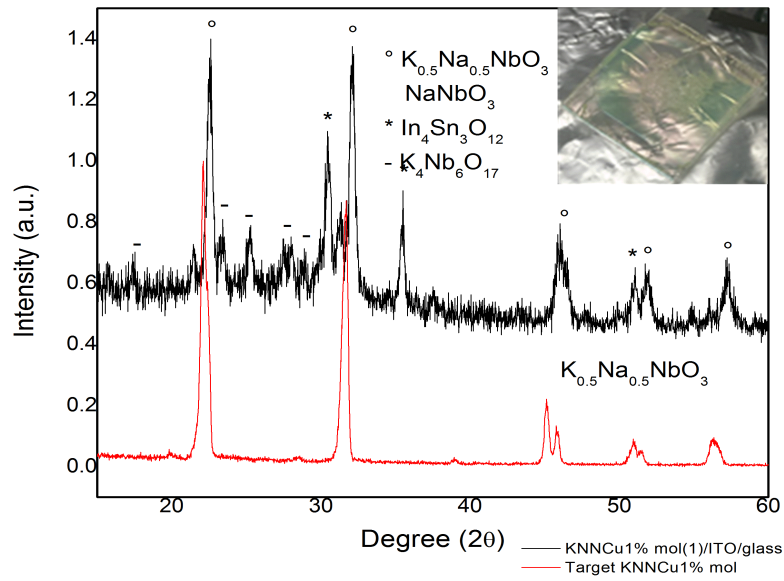


Figure 4.55: Film obtained after the heating treatment and XRD for KN-NCu1%mol(1)/ITO/glass deposited in 5 layers for 10 minutes, with a power of 75W, and sintered at 700°C for 60 minutes.

Through profilometry, it was measured an average thickness of 700nm for the film of KNNCu1%mol(1)/ITO/glass. Figure 4.56 presents a 3D image of the surface material, where the film presents a series of waves that are caused by the high temperature at which the material was sintered, which could affect the precision of the thickness value obtained previously.

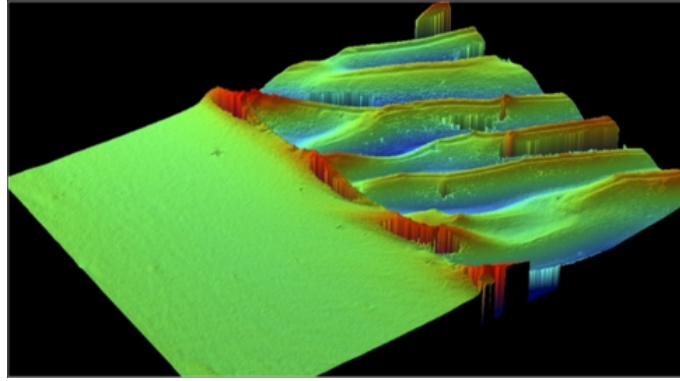


Figure 4.56: Thickness 3D image for KNNCu1%mol(1)/ITO/glass.

Figure 4.57 shows the P-E loops obtained for KNNCu1%mol(1)/ITO/glass, which was tested in the range of 1V(1000Hz) to 9V(40Hz). Through the application of double polarization, a cyclic behavior was obtained, which is more defined in the measurement at 9V for 0.63hHz, with a $P_r = -2.46E-31C/cm^2$ and an $E_c = 2.26kV/cm$. From this point, the ferroelectric phase change to resistance, which could be noted in the measurement at 9V for 0.55hHz.

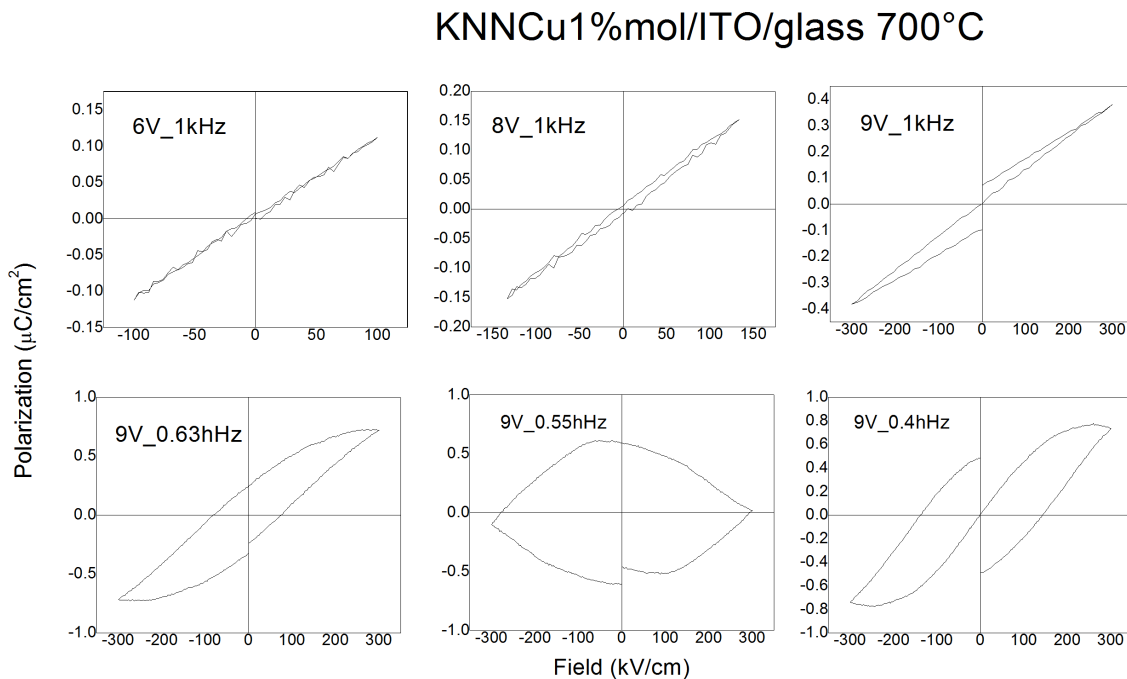


Figure 4.57: Thickness 3D image for KNNCu1%mol(1)/ITO/glass.

In the Table 4.6 there is a summary of the values of saturation polarization (P_S), remnant polarization (P_r), and coercitive field (E_c) for all of the bulk samples. The most representative sample are KNN/p- type Si, KNNCu0.5%mol(2)/p- type Si, KNNCu1%mol(1)/ITO/quartz, and KNNCu1%mol(1)/ITO/glass, because they have shown ferroelectric behavior.

Thin film samples	Ps ($\mu\text{C}/\text{cm}^2$)	Pr ($\mu\text{C}/\text{cm}^2$)	Ec (kV/cm)
KNN(2)p- type Si – 75W 10min(x5)-650°C 60min O ₂ (9V 200Hz)	0.0671	0.0033	0.3781
KNNCu0.5%mol(2) /p-type Si – 75W 10min(x5)-650°C 60min O ₂ (6.4V 250Hz)	0.0037	0.0005	0.3052
KNNCu0.5%mol(2) /p- type Si – 75W 10min(x5)-650°C 60min O ₂ (9V 100Hz) (C1)	0.0064	0.0015	521.5454
KNNCu0.5%mol(2) /p- type Si – 75W 10min(x5)-650°C 60min O ₂ (9V 100Hz) (C1)	0.0170	0.0037	385.1929
KNNCu1%mol(1)/ITO/quartz– 50W 10min(x5)-650°C 60min (9V 1000Hz)	0.0037	4.40E-6	0.2616
KNNCu1%mol(1)/ITO/glass– 75W 10min(x5)-700°C 60min (9V 62.5Hz)	0.7233	0.2466	74.9308

Table 4.6: Summary of hysteresis results for thin films samples.

Taking into account the characterization of thin films, it could be seen how for p-type Si substrates it was obtained a single main phase, while for the rest of substrates (glass/ITO, quartz/ITO, and Si-Pt coated), secondary phases are obtained. For the ferroelectricity measurements, the presence of a ferroelectric behavior was evidenced mainly in the KNN/p-type Si, KNNCu0.5%(2)/p-type Si, and KNNCu1% mol/ITO/glass samples. The ferroelectric behavior was obtained through a double polarization, which helped reorient the electric dipoles. These same samples were characterized by current-voltage to measure the photoresponse generated under different conditions (dark, visible, and ultraviolet), and most of them showed a diode behavior with low photocurrent response.

The ceramic bulk $K_{0.5}Na_{0.5}NbO_3$ lead-free system was synthesized via conventional method. The system was doped with copper in 0.5% and 1%mol and compared with the pure ferroelectric system KNN. Moreover, there was a variation related to the sintering process, verified by XRD, which allow to conclude that long time of sintering is not required for the obtention of the perovskite structure. This structure with different phases was found in the three systems (KNN, KNNCu0.5%mol, and KNNCu1%mol) obtained with different processing conditions (time of sintering and encapsulation conditions). Densification characterization by Archimedes method probes that all the bulk samples keep over 90% in relation with the relative density $4.51g/cm^3$. SEM characterization showed that the reduction of the time of sintering in bulk reduces the incipient fusion and improves the formation of grains structure. The main characterization is the ferroelectric test, where the P-E loops show that the system doped in 0.5%mol has an antiferroelectric behavior, while the pure system and the system doped in 1%mol keep their ferroelectric behavior. The temperature dependence was studied by impedance, where the transition temperatures were obtained around $215^\circ C$ and $415^\circ C$, which are related to the orthorhombic-tetragonal and tetragonal-cubic transitions respectively. The second temperature was related to the

Curie temperature, where the material loss its ferroelectric properties and a paraelectric arrangement is produced in the material.

In the case of thin films, the method used was sputtering with a radiofrequency power. For the cathodic erosion, the obtention of targets of the systems KNN, KNNCu05%mol, and KNNCu1%mol was needed. The growth was developed with different powers and times. The substrates used for the sputtering included ITO/glass, ITO/quartz, silicon Pt coated, p- type Si. The sintering treatment was carried out for 30 or 60 minutes and in most cases with an atmosphere of oxygen. The thin films were measured through XRD, and then characterized those who present the perovskite structure. The principal phase found was $K_{0.5}Na_{0.5}NbO_3$ with a low presence of secondary phases in some cases. For the followed characterization, it was needed the deposition of Au contacts to develop the semiconducting and ferroelectric test. The samples of KNN(2)/p-type Si, KNNCu0.5%mol(2)/p-type Si, KNNCu1%mol/ITO/quartz, and KNNCu1%mol/ITO/glass showed ferroelectric phase, highlighting the thin films deposited on the p- type Si substrates. Finally, the ferroelectric films show a low photoresponse effect through the semiconductance characterization.

5.1 Recommendations

To perform scanning of intermediate concentrations of copper doping, where new concentrations could be found for the KNN ceramic system, with the objective to find alternative concentrations that show antiferroelectric phase.

To vary the conditions of cathodic erosion or sintering over p- type Si substrate, because it shows better results compared with the ITO/glass and Si-Pt coated. In that sense, the cleaning process process was particularly important because it influences the obtention of a correct growth.

To reduce the times of milling and sintering for bulks samples, because the required phase can be easily obtained and at the same time the incipient fusion is avoided.

Perform sintering, the films obtained through RTA because it is not needed longer periods of temperature. To characterize through the impedance test the films that resulted in the ferroelectric phase.

To improve the processing of films, to reduce the secondary phases, an alternative is to heat the substrate during the growth process in the erosion chamber, or a subsequent heat treatment in a controlled oxygen atmosphere.

To obtain films with good ferroelectric properties, to polarize the films, establishing an internal electric field, with which the photogeneration of the hollow electron pair will be separated obtaining a good photovoltaic effect.

APPENDIX A

CRYSTALLITE SIZE FWHM ESTIMATION FIGURES

A.1 KNN, KNNCu0.5%mol, and KNNCu1%mol sintered for 1 hour at 1100°C - Encapsulated

Sample	2 θ	hkl	FWHM	XS (Å)
KNN	22.1493	100	0.5230 (0.0059)	247 (4)
	31.6320	110	0.5539 (0.0043)	205 (3)
	45.2188	200	0.5147 (0.0116)	225 (6)
	45.9004	020	0.4719 (0.0323)	262 (19)
KNNCu0.5%mol	22.2237	100	0.6122 (0.0088)	181 (4)
	31.6796	110	0.5483 (0.0061)	208 (3)
	45.2208	200	0.4373 (0.0155)	306 (12)
	45.8614	020	0.4911 (0.0259)	244 (14)
KNNCu1%mol	22.2089	100	0.5783 (0.0037)	200 (2)
	31.6645	110	0.4942 (0.0025)	254 (2)
	45.2089	200	0.3953 (0.0051)	398 (6)
	45.8655	020	0.4145 (0.0081)	347 (8)

Table A.1: Values of 2θ , FWHM, and XS, for the crystallographic reflections at (100), (110), (200), and (020), for the samples of KNN, KNNCu0.5%mol, and KNNCu1%mol sintered 1 hour at 1100°C.

A.2 KNN, KNNCu0.5%mol, and KNNCu1%mol sintered for 3 hours at 1100°C - Encapsulated

Sample	2 θ	hkl	FWHM	XS (Å)
KNN	22.0945	100	0.5306 (0.0044)	239 (3)
	31.5801	110	0.5816 (0.0034)	189 (2)
	45.2277	200	0.7869 (0.0086)	121 (2)
KNNCu0.5%mol	22.1350	100	0.5017 (0.0059)	274 (3)
	31.6354	110	0.5355 (0.0032)	217 (2)
	45.1987	200	0.5429 (0.0078)	206 (4)
	45.9162	020	0.4050 (0.0194)	369 (19)
KNNCu1%mol	22.1330	100	0.5200 (0.0053)	250 (4)
	31.6467	110	0.4994 (0.0021)	249 (2)
	45.2425	200	0.4454 (0.0073)	294 (6)
	45.9343	020	0.3176 (0.0144)	1000 (?)

Table A.2: Values of 2 θ , FWHM, and XS, for the crystallographic reflections at (100), (110), (200), and (020), for the samples of KNN, KNNCu0.5%mol, and KNNCu1%mol sintered 3 hours at 1100°C.

A.3 KNN, KNNCu0.5%mol, and KNNCu1%mol sintered for 4 hours at 1100°C - Without encapsulation

Sample	2 θ	hkl	FWHM	XS (Å)
KNN	22.1494	100	0.5250 (0.0033)	245 (3)
	31.6320	110	0.5544 (0.0025)	204 (2)
	45.2189	200	0.5142 (0.0066)	225 (4)
	45.8910	020	0.4694 (0.0184)	265 (11)
KNNCu0.5%mol	22.2248	100	0.6057 (0.0038)	184 (2)
	31.6794	110	0.5475 (0.0027)	209 (2)
	45.2216	200	0.4348 (0.0067)	310 (6)
	45.8610	020	0.4868 (0.0112)	247 (7)
KNNCu1%mol	22.2089	100	0.5784 (0.0037)	200 (2)
	31.6646	110	0.4941 (0.0025)	255 (2)
	45.2090	200	0.3955 (0.0051)	397 (6)
	45.8656	020	0.4139 (0.0081)	348 (8)

Table A.3: Values of 2 θ , FWHM, and XS, for the crystallographic reflections at (100), (110), (200), and (020), for the samples of KNN, KNNCu0.5%mol, and KNNCu1%mol sintered 4 hours at 1100°C.

APPENDIX B

CRYSTALLITE SIZE PLOTS

B.1 KNN Sintered 1 hour at 1100°C - Encapsulated

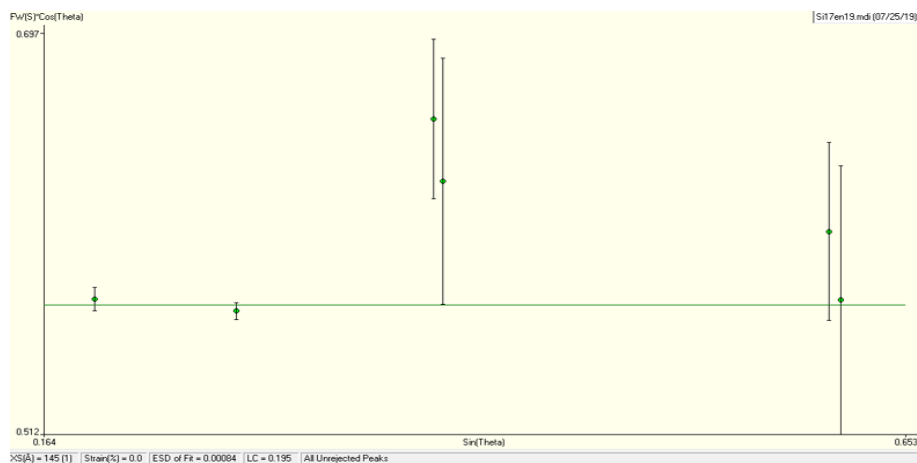


Figure B.1: XS estimation for the sample KNN sintered 1 hour at 1100°C - Encapsulated.

B.2 KNNCu0.5%mol Sintered 1 hour at 1100°C - Encapsulated

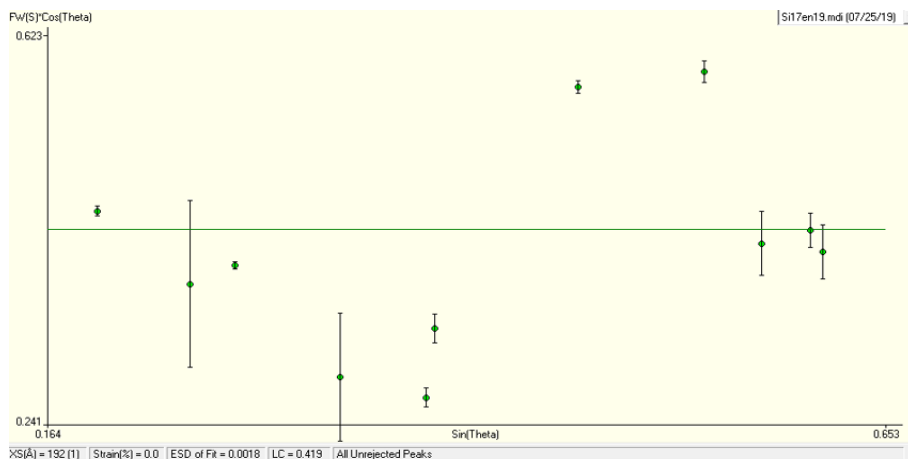


Figure B.2: XS estimation for the sample KNNCu0.5%mol sintered 1 hour at 1100°C - Encapsulated.

B.3 KNNCu1%mol Sintered 1 hour at 1100°C - Encapsulated

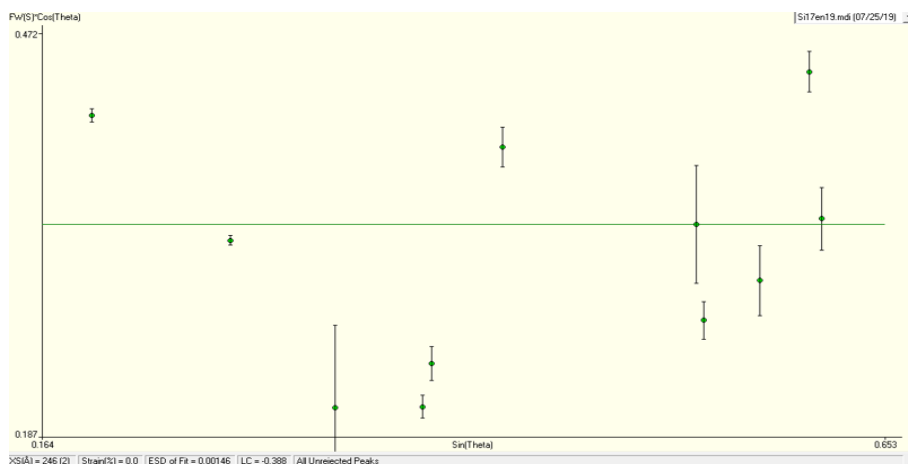


Figure B.3: XS estimation for the sample KNNCu1%mol sintered 1 hour at 1100°C - Encapsulated.

B.4 KNN Sintered 3 hours at 1100°C - Encapsulated

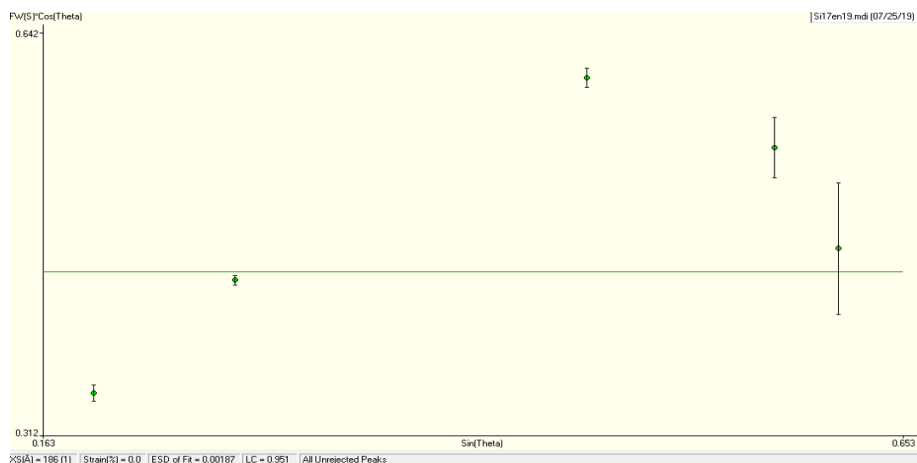


Figure B.4: Heating ramp for calcination stage, the heating treatment was carried out at 900°C for 4 hours, with a heating rate of 5°C per minute and a cooling rate of 7°C per minute.

B.5 KNNCu0.5%mol Sintered 3 hours at 1100°C - Encapsulated

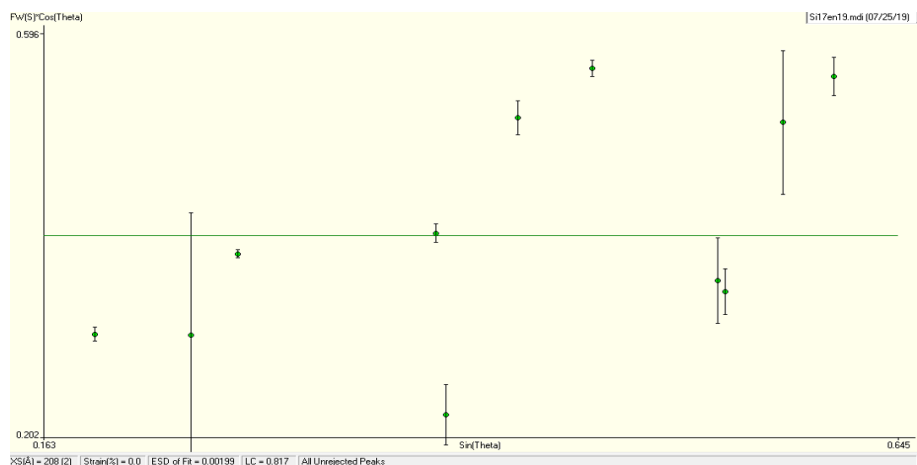


Figure B.5: XS estimation for the sample KNNCu0.5%mol sintered 3 hours at 1100°C - Encapsulated.

B.6 KNNCu1%mol Sintered 3 hours at 1100°C - Encapsulated

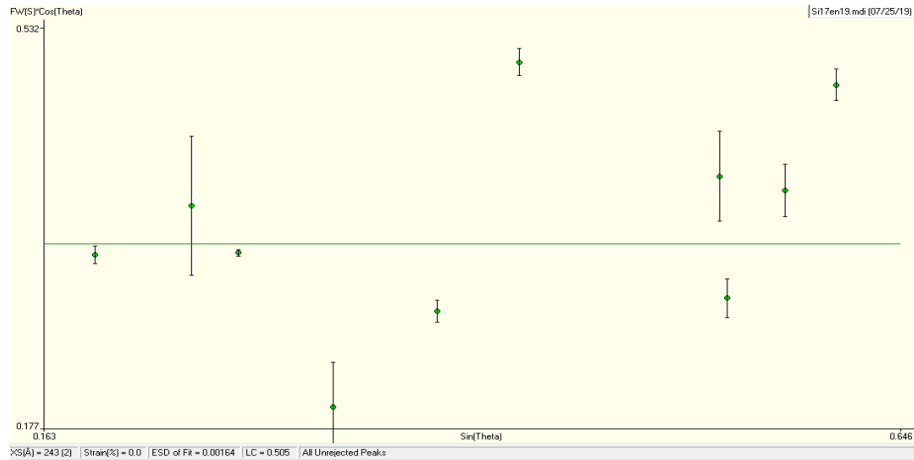


Figure B.6: XS estimation for the sample KNNCu1%mol sintered 1 hour at 1100°C - Encapsulated.

B.7 KNN Sintered 4 hours at 1100°C - Without encapsulation

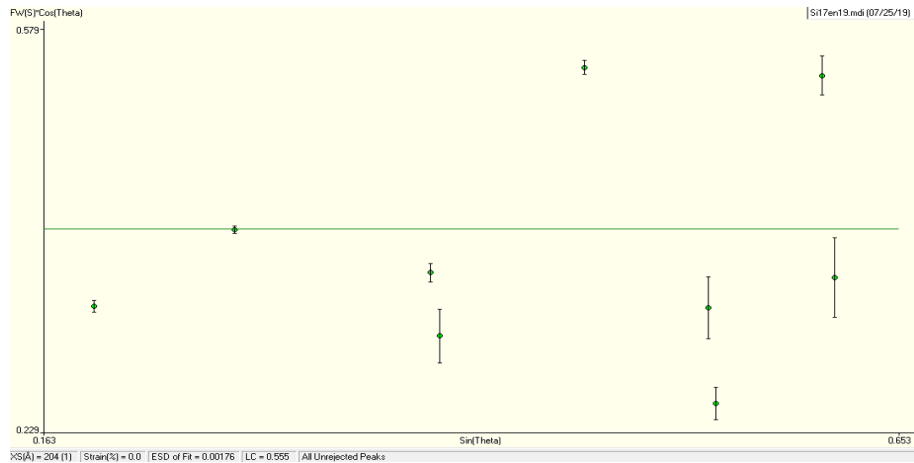


Figure B.7: XS estimation for the sample KNN sintered 4 hours at 1100°C - Without encapsulation.

B.8 KNNCu0.5%mol Sintered 4 hours at 1100°C - Without encapsulation

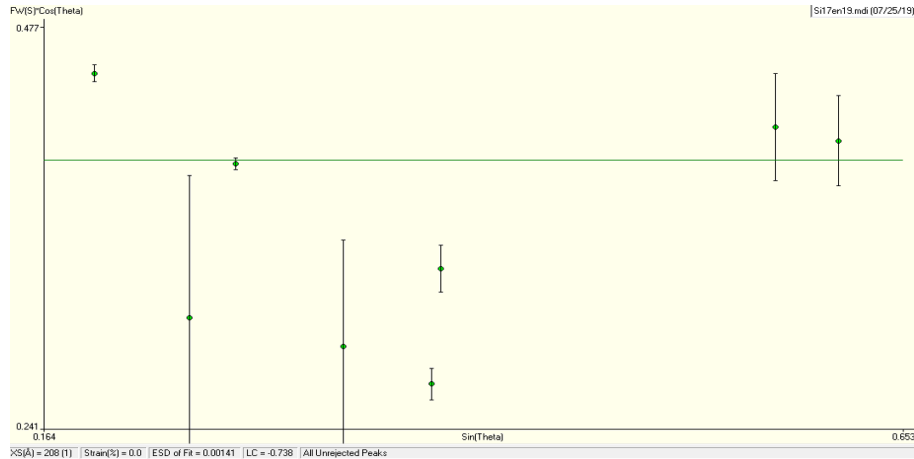


Figure B.8: XS estimation for the sample KNNCu0.5%mol sintered 4 hours at 1100°C - Without encapsulation.

B.9 KNNCu1%mol Sintered 4 hours at 1100°C - Without encapsulation

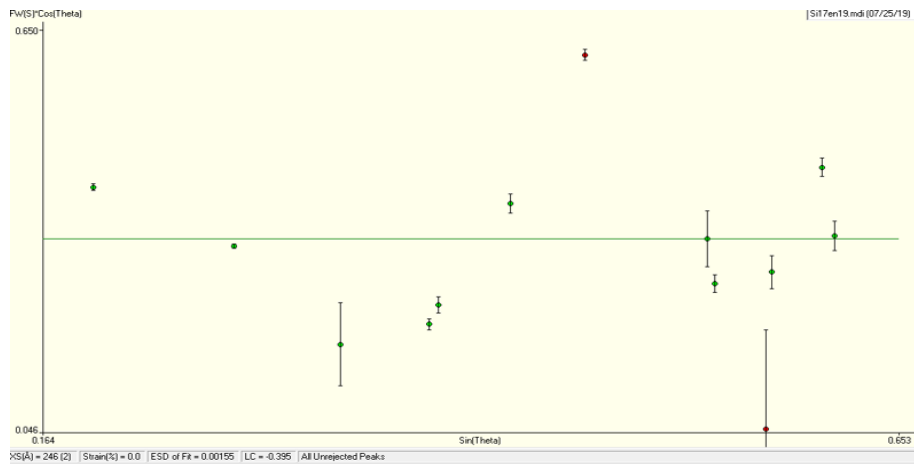


Figure B.9: XS estimation for the sample KNNCu1%mol sintered 4 hours at 1100°C - Without encapsulation.

BIBLIOGRAPHY

- [1] A. Bain and P. Chand. Ferroelectrics- principles and applications. *Wiley-VCH*, 2017.
- [2] P. Kumaria; R. Raia; S. Sharmab; M. Shandilyaa; and A. Tiwaric. State-of-the-art of lead free ferroelectrics: A critical review. *Advanced Materials Letters*, 6:453–484, 2015.
- [3] E. Alkoy an M. Papila. Microstructural features and electrical properties of copper oxide added potassium sodium niobate ceramics. *Ceramics International*, 3:1921–1927, 2010.
- [4] M. Kosec; B. Malič; A. Benčan; T. Rojac. Knn-based piezoelectric ceramics. piezo-electric and acoustic materials for transducer applications. *Springer*, pages 81–102, 2008.
- [5] L. Jin; F. Li; and S. Zhang. Chiral molecular films as electron polarizers and polarization modulators. *American Ceramic Society*, 97:1–27, 2014.
- [6] A. Chauhan; S. Patel; R. Vaish; and C. Bowen. Anti-ferroelectric ceramics for high energy density capacitors. in materials. *Materials*, 8:8009–8031, 2015.

- [7] R. Steinhausen; C. Pientschke; A. Kuvatov; H. Langhammer; A. Movchikova; and O. Malyshkina. Modelling and characterization of piezoelectric and polarization gradients. *Journal of Electroceramics*, 20:47–52, 2008.
- [8] G. Haertling. Ferroelectric ceramics: History and technology. *Journal American Ceramic Society*, 82:797–818, 1999.
- [9] A. Spierings; M. Scheinder; and R. Eggenberger. Comparison of density measurement techniques for additive manufactured metallic parts. *Rapid Prototyping Journal*, 17:380–386, 2011.
- [10] E. Rocha. Introducción a los materiales cerámicos. *UAM Azcapotzalco*, 1st Edition, 2005.
- [11] O. García. Estudio de las propiedades relajadoras de sistemas plzt. 2012.
- [12] P. Littlewood. Physics of ferroelectrics. 2002.
- [13] A. Moulson and J. Herber. Electroceramics: Materials, properties, applications. *John Wiley Sons*, 2003.
- [14] J. B. Goodenough. Electronic and ionic transport properties and other physical aspects of perovskites. *Institute of Physics Publishing*, 67:1915–1993, 2004.
- [15] K. Wang and J. Li. Analysis of crystallographic evolution in (na,k)nbo3-based lead-free. *Applied Physics Letters*, 91, 2007.
- [16] R. López; F. González and M. Catrejón. Lead-free ferroelectric ceramics with perovskite structure. *Ferroelectrics - Material Aspects*, pages 305–330, 2011.
- [17] D. Lin; K. Kwok and H. Chan. Double hysteresis loop in k0.5na0.5nbo3 cu-doped lead-free piezoelectric ceramics. *American Institute of Physics*, 90, 2007.
- [18] C. Bedoya. Crecimiento y caracterización eléctrica y estructural de películas delgadas de $bi_x ti_y o_z$ producidas mediante magnetron sputtering. *Universidad Nacional de Colombia Facultad de Ingeniería, Departamento de Mecánica y Mecatrónica*, 2013.

- [19] G. Rikken and E. Raupach. Materials science and engineering- an introduction. *John Wiley Sons, Inc*, 8th Edition, 2010.
- [20] K. Chi. Dielectric phenomena in solids with emphasis on physical concepts of electronic processes. *Elsevier Academic Press*, pages 4652–4655, 2004.
- [21] J. Ravez. Ferroelectricity in solid state chemistry. *Comptes Rendus de l'Academie des Sciences Series IIC Chemistry*, 3:267–283, 2000.
- [22] W. Barsoum. Fundamentals of ceramics. *Institute of Physics Publishing*, 2003.
- [23] Edited by M. Lallart. Ferroelectrics - applications. *InTech*, 2011.
- [24] Y. Xu. Ferroelectric materials and their applications. *Elsevier Science Publishers*, 1st Edition, 1991.
- [25] Li; X. Wang P. Zhao; H. Wang; L. Wu; L. Chen; Z. Cai; L. High [U+2010] performance relaxor ferroelectric materials for energy storage applications. *Advanced Energy Materials*, 9:1803048, 2019.
- [26] A. Blázquez-Castroa; A. García-Cabañes; and M. Carrascosa. Biological applications of ferroelectric materials. *Applied Physics Review*, 5:041101, 2018.
- [27] C. Cui; F. Xue; W. Hu; and L. Li. Two-dimensional materials with piezoelectric and ferroelectric functionalities. *2D Materials and Applications*, 2:18, 2018.
- [28] R. Dorey. Microstructure–property relationships: How the microstructure of the film affects its properties. *Ceramic Thick Films for MEMS and Microdevices*, 4:85–112, 2012.
- [29] C. Obregón. Análisis, diseño y caracterización de sensores piezoeléctricos ultrasónicos libres de plomo, en película delgada. 2013.
- [30] M. Wegrzyn. Sodium potassium niobate based piezoelectric ceramics. *University of Manchester*, 2012.

- [31] X. Hao; J. Zhai; L. Kong; and Z. Xu. A comprehensive review on the progress of lead zirconate-based antiferroelectric materials. *Progress in Materials Science*, 63:1–57, 2014.
- [32] S. Abhinay. Effect of dispersant and binder on fabrication of bzt0.5bct piezoelectric wafers by tape casting technique. *DEPARTMENT OF CERAMIC ENGINEERING NATIONAL INSTITUTE OF TECHNOLOGY*, n.d.
- [33] C. Kittel. Theory of antiferroelectric crystals. *Physical Review*, 82:729–732, 1951.
- [34] M. Bengisu. Engineering ceramics. *Springer*, 2001.
- [35] D. Richerson and W. Lee. Modern ceramic engineering: Properties, processing, and use in design. *CRC Press*, 3rd Edition, 2003.
- [36] K. Kao. Dielectric phenomena in solids with emphasis on physical concepts of electronic processes. *Elsevier Academic Press*, 2004.
- [37] K. Shibata; R. Wang; T. Tou; and J. Koruza. Applications of lead-free piezoelectric materials. *MRS Bulletin*, 43:612–616, 2018.
- [38] J.Ge; D. Remiens; X. Dong; Y. Chen; J. Costecalde; F. Gao; F. Cao; and G. Wang. Enhancement of energy storage in epitaxial pbzro3 antiferroelectric films using strain engineering. *Applied Physics Letters*, 105:112908, 2014.
- [39] M.Vopson; G. Caruntu; and X. Tan. Polarization reversal and memory effect in anti-ferroelectric materials. *Scripta Materialia*, 128:61–64, 2017.
- [40] D. Zhao;I. Katsouras; K. Asadi; W. Groen; P. Blom; and D. de Leeuw. Retention of intermediate polarization states in ferroelectric materials enabling memories for multi-bit data storage. *Applied Physics Letters*, 108:232907, 2016.
- [41] Y. Yuan; Z. Xiao;B.Yang; and J. Huang. Arising applications of ferroelectric materials in photovoltaic devices. *Journal of Materials Chemistry A*, 2:6027, 2014.

-
- [42] K. Butler; J. Frost; and A. Walsh. Arising applications of ferroelectric materials in photovoltaic devices. *Energy Environmental Science*, 17:838–848, 2015.
- [43] H. Liu; J. Zhong; C. Lee; S. Lee; and L. Lin. A comprehensive review on piezoelectric energy harvesting technology: Materials, mechanisms, and applications. *Applied Physics Reviews*, 5:041306, 2018.
- [44] K. Shibata; F. Oka; A. Ohishi; T. Mishina; and I. Kanno. Piezoelectric properties of (k, na)nbo3 films deposited by rf magnetron sputtering. *Applied Physics Express*, 1, 2008.
- [45] M. Avdeen; J.Jorgensen; and S. Short. Pressure-induced ferroelectric to antiferroelectric phase transition in pb0.99(zr0.95ti0.05)0.08nb0.2o3. *Physical Review B*, 73, 2006.
- [46] S. Ke; H. Huang; H. Fan; L. Zhou; and Wai Y. Antiferroelectric-like properties and enhanced polarization of cu-doped k0.5na0.5nbo3 piezoelectric ceramics. *American Institute of Physics*, 101, 2012.
- [47] K. Sakata and Y. Masura. Ferroelectric and antiferroelectric properties of (na0.5bi0.5)tio3-srtio3 solid solution ceramics. *Ferroelectrics*, pages 347–349, 1974.
- [48] Gu; I. Takeuchi; S. Kalinin; F. Xue; L. Liang; Y and L. Chen. Composition- and pressure-induced ferroelectric to antiferroelectric phase transitions in sm-doped bifeo3 system. *Applied Physics*, 106, 2015.
- [49] M. Sopicka. Introduction to mechanochemical processing. high-energy ball milling mechanochemical processing of nanopowder. *Woodhead Publishing Limited*, page 421, 2010.
- [50] W. Kingery. Introduction to ceramics. *Journal of The Electrochemical Society*.
- [51] J. Abella. Láminas delgadas y recubrimientos: preparación, propiedades y aplicaciones. *Solana e Hijos A.G*, 2003.

- [52] J. Reed. *Ceramics processing second edition. John Wiley Sons, Inc. (US)*, 1995.
- [53] L. Smart; and E. Moore. *Solid state chemistry- an introduction. Taylor Francis Group*, 2012.
- [54] ; E. Lifshin; P. Echlin; L. Sawyer;D. Joy; J. Goldstein; C. Lyman; D. Newbury and J. Michael. *Scanning electron microscopy and x-ray microanalysis. Kluwer Academic/- Plenum Publishers*, 2003.
- [55] A. Duparre; and S. Jakobs. *Combination of surface characterization. Optical Society of America*, 2011.
- [56] M. Lines; and A. Glass. *Principles and applications of ferroelectrics and related materials. Clarendon Press*, 1977.
- [57] A. Pérez; A. Mingorance; D. Tanenbaum; and M. Lira. *Metal oxides in photovoltaics: All-oxide, ferroic, and perovskite solar cells. The Future of Semiconductor Oxides in Next-Generation Solar Cells.*, 2017.
- [58] M. Nowak; B. Kauch; and P. Szperlich. *Determination of energy band gap of nanocrystalline sbsi using diffuse reflectance spectroscopy. Review of Scientific Instruments*, 80:046107, 2009.
- [59] S.Abdullahi; S. Güner; Y. Koseoglu; I. Musa; B. Adamu; and M.Abdulhamid. *Simple method for the determination of band gap of a nanopowdered sample using kubelka munk theory. Journal of the Nigerian Association of Mathematical Physics*, 35:241–246, 2016.
- [60] A.Escobedo; E. Sánchez; and U. Pal. *Use of diffuse reflectance spectroscopy for optical characterization of un-supported nanostructures. Revista Mexicana de Física*,, pages 18–22, 2007.
- [61] Cichang; S.Cheng ; Y. Chen; Huang and G. Chen. *Characterization of sns films prepared by constant-current electro-deposition. Thin Solid Films*, pages 96–100, 2006.

- [62] M. Matsubara; T. Yamaguchi; K. Kikuta; and S. Hirano. Sintering and piezoelectric properties of potassium sodium niobate ceramics with newly. *The Japan Society of Applied Physics*, 44:258–263, 2015.
- [63] E. Hollenstein; M. Davis; D. Damjanovic; and N. Setter. Piezoelectric properties of li- and ta-modified $(\text{k}0.5\text{na}0.5)\text{nbo}_3$ ceramic. *Applied Physics Letters*, 87:182905 – 182905–3, 2005.
- [64] Y. Saito; H. Takao. Piezoelectric properties of li- and ta-modified $(\text{k}0.5\text{na}0.5)\text{nbo}_3$ ceramic. *Ferroelectrics*, 338:17–32, 2008.
- [65] O. García; A. Peláiz; J. Guerra; M. Mendoza; F. Calerón; and D. Hall. Influence of the a and b vacancies on the dielectric and structural properties of the plzt 8/60/40 ferroelectric ceramic system. *Physica B*, 406:1622–1626, 2011.
- [66] A. Broadhurst; K. Rogers; T. Loweb; and D. Lane. Determination of depth-dependent diffraction data: a new approach. *Acta Crystallographica Section A: Foundations and Advances*, A61:139–146, 2005.
- [67] T. Raymond. The physics and chemistry of the schottky barrier height. *Applied Physics Reviews*, 1st Edition, 2013.